



## DIPLOMARBEIT

# Development of a smart sensor solution for non-invasive in-vivo determination of human skin viscoelasticity based on elastic wave propagation

ausgeführt am Institut für  
Angewandte Physik  
der Technischen Universität Wien

unter der Anleitung von  
**Ao.Univ.Prof. Dr. Martin Gröschl**

in Kooperation mit dem  
Austrian Institute of Technology  
Biomedical Systems

**DI Andreas Oberleitner**  
**Christoph Matoschitz, Msc.**

durch  
**Konrad Leskovar**

Vienna, May 13,  
2019

---

Unterschrift StudentIn

# Acknowledgement

I would like to express my sincere gratitude to my supervisor Ao.Univ.Prof. Dr.techn. Martin Gröschl for supporting and giving me the opportunity to pursue my master's thesis at the Institute of Applied Physics at the Vienna University of Technology.

I would also like to thank the Austrian Institute of Technology, AIT, for the collaboration and especially, Dipl.-Ing. Andreas Oberleitner and Christoph Matoschitz, Msc for their great support and continuous guidance throughout this work.

I would further like to thank Michael Reiter from Kubo Tech Ges.m.b.H for providing various rubber materials.

Finally, I particularly like to thank all my friends and family members for their great support over the past years.

# Abstract

The skin is the largest and most versatile organ of the human body. It serves as protection against external influences and loss of endogenous substances, contains our tactile and temperature senses, regulates the temperature of the body and plays a significant role in our social life.

The achievement of this multifunctional tasks is a result of the complex structure as well as the physicochemical regime of the skin, in which the supreme layer, the stratum corneum plays the most significant role. The mechanical properties of the skin are affected directly by the natural chronobiological aging, as well as by external chemical and physical influences and depends on the site of the body investigated. Especially the viscoelasticity is a major characteristic for many cosmetic and clinical applications and can directly be used in combination with the hydration and PH-value for determination of the skins condition and its ability to achieve the important protection as well as its regulatory responsibilities.

Current measurement methods used for determining the viscoelasticity of the human skin are linked to unhandy tabletop units and are only applicable by pre-instructed professionals. The measurement results of the available appliances are only arbitrary values for comparison but cannot deliver any physical relevant values. Nowadays, via the extensive distribution of smartphones capable of near field communication (NFC) as well as Bluetooth low energy communication (BLE), smart sensor solutions represents an easy, fast and handy way to measure human health data like the skin viscoelasticity. Especially smart sensor solutions for health data acquisition becoming more and more important in a world where “smart wearables”, “lifelogging” or “quantified self” plays a snowballing role.

The aim of this master thesis is to develop a novel smart sensor solution based on elastic wave propagation for determination of the skin’s viscoelasticity and anisotropy. The power for the reusable sensor solution is meant to be supplied by a small battery or via the NFC interface of the smartphone or tablet applied. This is as well used for receiving and evaluating the desired values which subsequently can be monitored, compared and shared with others or passed to a healthcare system or the personal dermatologist.

# Kurzfassung

Die Haut ist das größte und vielseitigste Organ des menschlichen Körpers. Sie dient als Schutz vor externen Einflüssen, Verlust endogener Substanzen, beinhaltet unsere Tast- und Temperatursensoren, reguliert die Temperatur des Körpers und spielt auch in unserem sozialen Leben eine entscheidende Rolle.

Die Bewerkstelligung dieser vielseitigen Aufgaben resultieren aus der komplexen Struktur wie auch aus den physikochemischen Eigenschaften der Haut, wobei in dieser Hinsicht dem Stratum Corneum die größte Bedeutung zukommt. Die mechanischen Eigenschaften der Haut werden direkt durch die natürliche chronobiologische Alterung, wie auch durch externe chemische und physikalische Umwelteinflüsse verändert und sind an unterschiedlichen Körperstellen verschieden. Speziell die Viskoelastizität ist ein wesentlicher Parameter der Haut, welcher direkt in Kombination mit Hautfeuchte und dem Haut-PH-Wert für die Ermittlung des Hautzustandes und ihrer Fähigkeit, wichtige Schutz- und regulatorischen Aufgaben zu erfüllen, in vielen kosmetischen und klinischen Anwendungen zur Diagnose herangezogen wird.

Aktuelle Messmethoden zur Ermittlung der Viskoelastizität der menschlichen Haut sind an unhandliche Tischgeräte gebunden, welche nur von instruiertem Fachpersonal bedient werden können. Die resultierenden Messergebnisse dieser Messgeräte werden nur in Arbiträreinheiten angegeben, um Messungen zwischen unterschiedlichen Probanden vergleichen zu können, jedoch liefern sie keine Elastizitäts- bzw. Viskoelastizitätswerte in physikalischen Einheiten. Durch die umfassende Verbreitung von Smartphones bzw. Tablets welche die Nahfeldkommunikation (NFC) wie auch die Bluetooth-Niedrigenergie-Kommunikation (BLE) unterstützen, repräsentieren smarte Sensorlösungen heutzutage eine einfache, schnelle und handliche Möglichkeit um menschliche Gesundheitsdaten wie z.B. die Viskoelastizität der Haut zu messen. In einer Welt in der sich “smart wearables”, “lifelogging” und “quantified self” wie ein Schneeballeffekt verbreiten spielen smarte Sensorlösungen für die Ermittlung von Gesundheitsdaten eine immer wichtigere Rolle.

Ziel dieser Masterarbeit ist die Entwicklung einer neuen Sensorlösung, basierend auf elastischer Wellenpropagation zur Ermittlung der Viskoelastizität und Anisotropie der Haut. Die Energie der wiederverwendbaren Sensorlösung soll über eine kleine eingebaute Batterie, oder über die NFC-Schnittstelle des verwendeten Smartphones bzw. Tablets zur Verfügung gestellt werden können. Zusätzlich sollen die Messdaten an ein über NFC oder BLE angekoppeltes Gerät zur weiteren Aufarbeitung der ermittelten Daten übertragen, wie auch darauf visualisiert werden. In weiterer Folge können diese Messdaten mit Messwerten anderer Hautstellen bzw. anderer Nutzer verglichen und über soziale Medien geteilt, oder an das Gesundheitssystem/ den Dermatologen zur weiteren Untersuchung übermittelt werden.

# Table of contents

1. Introduction.....	7
1.1. Motivation.....	7
1.2. The human skin.....	10
1.3. Specification for development of the sensor solution .....	19
1.4. Hypothesis.....	20
1.5. Evaluation and summary over various measurement methods .....	20
1.6. Characterization of piezoelectricity .....	29
2. Materials and Methods.....	32
2.1. Development process of the smart sensor solution .....	32
2.2. Sensor Solution .....	34
2.3. Measurement setup .....	44
2.4. Evaluation of the measurement signal .....	45
2.5. Phantoms.....	48
2.6. In-vivo measurements .....	52
3. Results.....	55
3.1. Sensor Solution .....	55
3.2. Phantoms.....	64
3.3. In vivo measurements .....	68
4. Discussion.....	77
4.1. Sensor Solution .....	78
4.2. Evaluation of the measurement signal .....	81
4.3. Composition of the sensor solution.....	82
4.4. Phantoms.....	82
4.5. In-vivo measurements .....	84

5. Outlook .....	87
5.1. How the sensor solution is planned to operate.....	87
5.2. Next steps.....	88
6. Conclusion .....	89
7. References.....	91
7.1. Bibliography .....	91
7.2. Table of figures .....	100
8. Supplementary .....	103

# 1. Introduction

## 1.1. Motivation

The skin is the most versatile organ of the human body and achieves various, even critical requirements. It serves as a mechanical and pathogenic barrier, regulates the temperature of the body and protects the underlying tissue from loss of endogenous substances. These functions are achieved via the extensive structure of the skin and its physicochemical characteristics. The outermost dermal layer, the stratum corneum plays the most significant role of the multilayered skin and is renewed every 4-6 weeks by migrating cells from inner layers. The properties of the skin in correlation with the elasticity and humidity are influenced directly by the chronobiological aging and exogenic physical and chemical influences and vary with the position examined on the body. Via determination of these parameters, the condition of the skin can be accessed which plays a snowballing role in terms of clinical and scientific dermatology as well as in cosmetics. As an example, the number of publications<sup>1</sup> where “skin elasticity” is mentioned increased exponentially in the last couple of years.

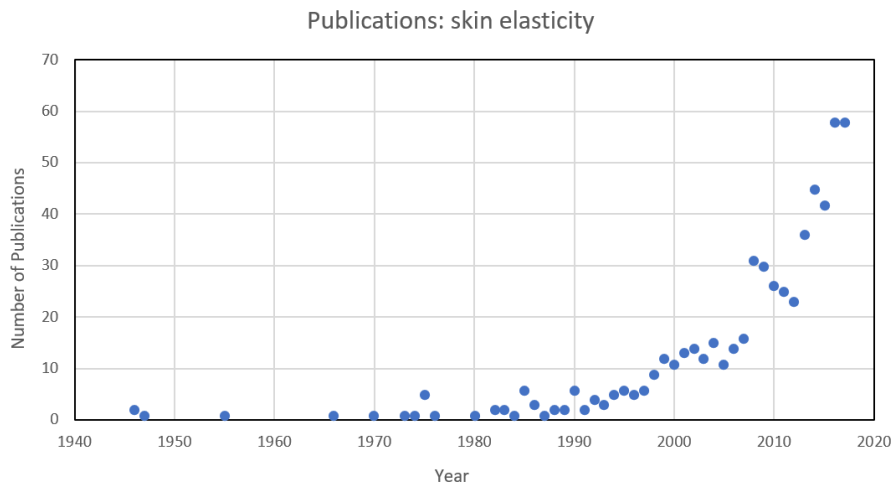


Fig. 1: Timeline of publications per year, where “skin elasticity“ is mentioned [1]

In surgery the information about the skins anisotropy helps surgeons to place the cut in the right direction to the skin lines of tension, because scars cut parallel to both the Langer as well as the Kraissl dynamic lines, heal most rapidly [2]. In clinical diagnosis, for example, the decrease of the skin hydration as well as skin elasticity is a characteristically epiphenomenon for atopic dermatitis and psoriasis. Particularly, the prevalence of atopic dermatitis is increasing in the industrialized countries and shows up for 5-20% of

<sup>1</sup> Source: <https://www.ncbi.nlm.nih.gov/pubmed/>

children and 1-3% of adults and it is assumed that it is induced by the modified environment and the overreacting hygiene awareness. Like seen in the graph below, the number of publications<sup>2</sup> where “atopic dermatitis” is mentioned increased exponentially in the last couple of years.

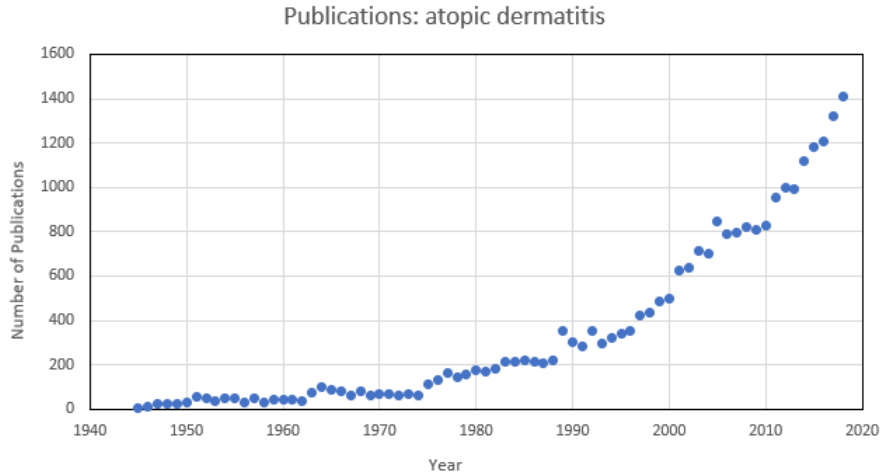


Fig. 2 Timeline of publications per year, where „atopic dermatitis“ is mentioned [1]

Another scope of application is in skin cancer diagnosis, where the stiffness of the tumorous skin area features an increasing Young modulus compared to its surrounding tissue [3]. For these reasons, the information about the elastic properties of the skin are important for treatment of many skin diseases as well as early self-diagnosis.

The possibility of smart data acquisition and *in situ* monitoring of human health data like the skin elasticity gets more and more important in a world where “lifelogging”, “quantified self” and “smart wearables” play a significant role. This trend is too well seen in the number of publications<sup>3</sup> about “wearables”:

<sup>2</sup> Source: <https://www.ncbi.nlm.nih.gov/pubmed/>

<sup>3</sup> Source: <https://www.ncbi.nlm.nih.gov/pubmed/>



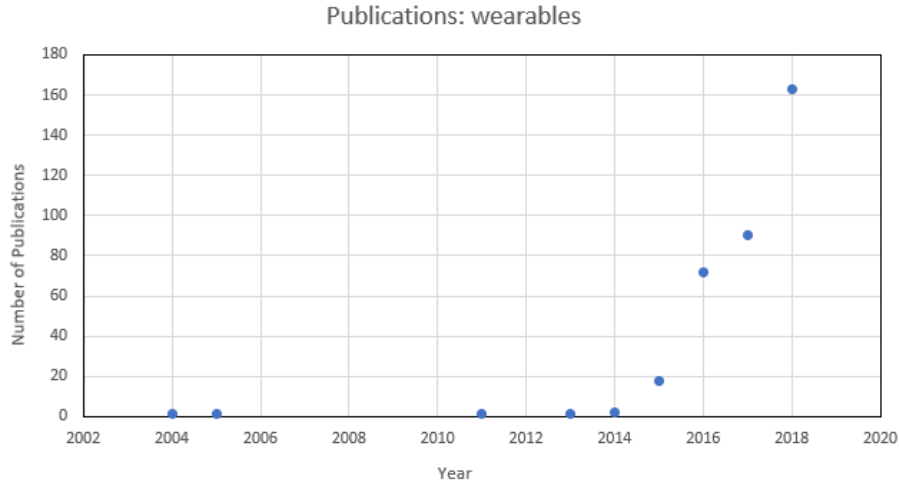


Fig. 3.: Timeline of publications per year, where „wearables“ is mentioned [1]

For example, IDTechEx published in 2015 that the wearable technology market in the health sector will grow by three times within the following 9 years <sup>4</sup>. As well in dermatology and cosmetics, this area of subject is of very high importance, thus it can be used in dermatological therapies, curative studies and during treatment of various cosmetics. In differential diagnosis and medical therapy monitoring the so-called tele-dermatology as “electronic distance medicine” serves as an improvement of Medicare. Current measurement equipment for determination of the human health data like skin elasticity are linked to unhandy and expensive tabletop units and are only applicable by pre-instructed professionals. The available measurement appliances only show arbitrary values which are only comparable using the same measurement instrument, and no physical elasticity values are available. Nowadays, smart and cheap sensor solutions represent an easy, fast and handy way to measure human health data like the skin viscoelasticity. While cheap and smart sensors for heart rate, blood pressure or blood oxygen monitors are available on market, smart sensors for skin data have hardly been explored.

<sup>4</sup> [http://ec.europa.eu/newsroom/document.cfm?doc\\_id=40542](http://ec.europa.eu/newsroom/document.cfm?doc_id=40542)

## 1.2. The human skin

### 1.2.1. Structure of the skin

The human skin is composed of three different layers. The topmost layer is the epidermis, briefly connected to the underlying dermis which is linked to the fatty hypodermis or as well the so called subcutis.

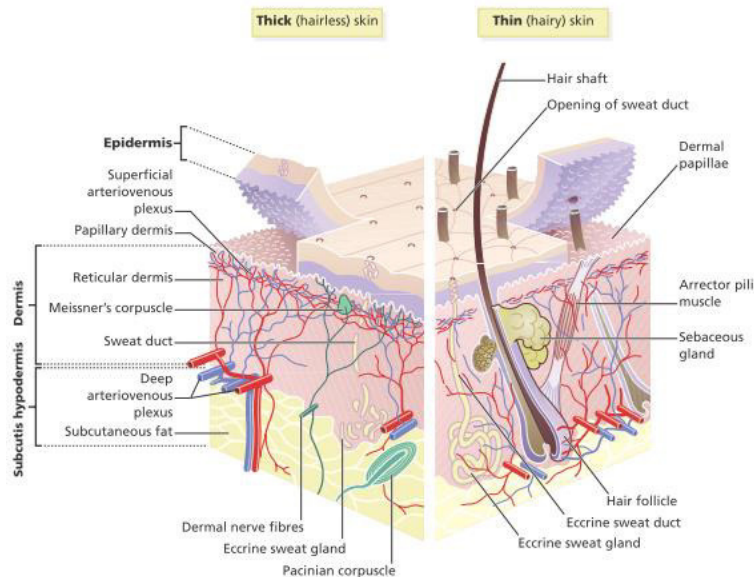


Fig. 4: Three-dimensional image of the human skin; on the left side thick hairless skin is presented like appear on the hands and soles, while on the right side the thin and hairy skin is illustrated [4].

#### 1.2.1.1. Epidermis

The topmost layer of the epidermis, called stratum corneum, consists of piled-up layers of flattened dead keratinocytes, filled with keratin and acting as a hardened squamous epithelium featuring a thickness of about  $15\mu\text{m}$ . It behaves as protection against penetration of potentially harmful matter, oxidative and UV-light of the beneath lying tissue, and prevents the loss of endogenous substances and interstitial fluid from within the body [5], [6], [7]. The underlying layers are made by 90% of moving outward keratinocytes and 10% “symbiotic cells” (which are Langerhans cells, melanocytes, Merkel cells and T-Lymphocytes) [6]. Keratinocytes are formed in the lowermost, the basal layer of the epidermis by division, and later start to move outwards, to differentiate into a horn cell of the stratum corneum [8]. This cell cycle, called keratinization, takes 4-6 weeks in time, meaning, that the topmost layer of the skin is renewed almost every month [9]. The thickness of the epidermis in total measures between 0.1mm on the eyelids to 1mm on the

palms and soles [4]. The epidermis is naturally wrinkled and serves the second most part for the skins viscoelasticity capacity [10].

### 1.2.1.2. Dermis

The layer beneath the epidermis and directly connected to the bottom side of the basal layer, consists of two sublayers, the papillary and the reticular dermis. It is mostly composed of collagen and elastin fibrils, which are hold in place by a ground substance. It contains a lot of irregularities like blood and lymph vessels, nerve endings and hair follicles as well as sebaceous and sweat glands. The papillary layer only represents 10% of the total thickness of the dermis serving the topmost layer connected directly to the epidermis. On the junction, the epidermis penetrates the papillary dermis, leading to the structure of the skin which is well seen on the finger tips [6]. The dermis layer serves the most part for the skins viscoelasticity and is naturally contracted, featuring a thickness of approximately 1mm [10].

### 1.2.1.3. Hypodermis

The lowest layer of the skin which acts as link to the underlying muscles, bones and organs, is basically made of adipose tissue and behaves like a protective cushion and an insulating coat for the body. It as well contains a minimum of collagen fibers and the thickness can range from 1 to 50mm [6].

## 1.2.2. Skin mechanical function

The skin is in total an inhomogeneous, anisotropic, non-linear viscoelastic material under prestress in vivo [6].

The major part of the elastic behavior and tensile strength of the skin is featured by the dermis which is a felting of wavy coiled collagen bundles as well as elastin fibers which are naturally contracted. These fibers are lying in the ambient of the viscose ground substance. The tightness and expansibility of the skin is mostly given by the collagen bundles, while the elastin fibers are responsible for the rebounding of the skin to its initial position [11]. The ground substance transmits the major part of the viscose ability of the skin [10]. In comparison, the overlying epidermis is more rigid and naturally wrinkled due to the naturally contracted dermis layer. The superficial layer of the epidermis, the stratum corneum is the most resistant part of the skin represented by horny skin cells, very firm, but pliable [10].

### 1.2.2.1. Total skin mechanical behavior

The properties of the skin as an elastic material is subject to mechanical laws. In general, the elasticity of linear solid materials are described by the Young's modulus which specifies the relation between stress

$$\sigma = \frac{F}{A} \text{ and strain } \varepsilon = \frac{\Delta l}{L_0} \text{ [12]:}$$

$$E = \frac{\sigma}{\varepsilon} \tag{1}$$

The rigidity of a material is described by the modulus of rigidity, hereafter called shear modulus. For linear elastic isotropic solids, the shear modulus  $\mu$  and the Young's modulus  $E$  are linked via:

$$\mu = \frac{E}{2(1 + \nu)} \tag{2}$$

where  $\nu$  is the Poisson's ratio defined by the relation between transverse strain to axial strain [13].

In general, the elastin and collagen fibers are expected as linear elastic materials, but the skin shows a non-linear stress-strain curve under applying uniaxial tension. In the first phase, when the collagen bundles start to unfold only the elastin fibers are responsible for the linear stress-strain relation. In the second phase, the collective straightening of the collagen bundles leads to a non-linear behavior, when in the third phase all collagen bundles are fully stretched the relation gets linear again [6].

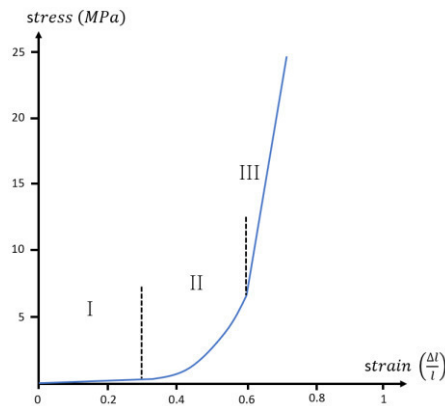


Fig. 5: The stress-strain relation of the skin is divided into three phases, described in the paragraph above. The stress ( $\sigma$ )/strain ( $\frac{\Delta l}{l}$ ) relation is given in equation (1) [6]

From the mechanical point of view the description of these three phases are illustrated on a sudden and sustained creep test. In the primary phase it shows an immediate, pure elastic extension. Then a variable creep and finally a constant creep takes place [14]. After the constant creep phase, which is below a strain of 25% an irreversible deformation will follow leading to a painful rupture of the skin [10]. These three

phases without rupture of the skin are scientifically proposed in an analog mechanical model shown in Fig. 6.

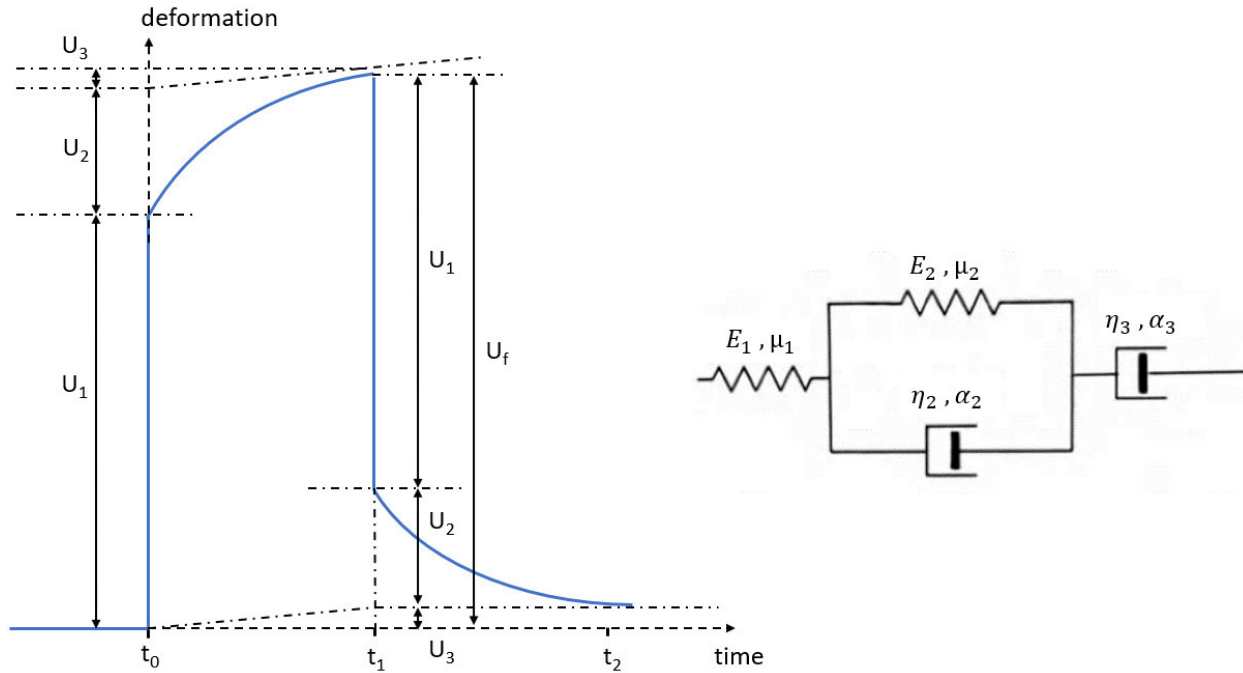


Fig. 6: Mechanical model for the behavior of the skin when at  $t_0$  the skin is elongated via a constant force and at  $t_1$  the force is released and the starts to relax;  $U_1$ : immediate deformation (totally elastic),  $U_2$ : viscoelastic deformation,  $U_3$ : late deformation (entirely viscous),  $U_f$ : total deformation of the skin,  $E_1, \mu_1$ : elasticity and shear modulus of the immediate deformation phase,  $E_2, \mu_2, \eta_2, \alpha_2$ : elastic modulus, shear modulus, damping ratio and damping coefficient of the viscoelastic deformation phase,  $\eta_3, \alpha_3$ : damping ratio and damping coefficient of the entirely viscose phase [14]

The immediate extension is represented by a spring, following hook's law. While the variable creep is shown by a dashpot in parallel to a spring connected in serial to the first phase. The third phase, constant creep acts like a dashpot in serial to the first two stages. This model is a combination of the Maxwell model and Kelvin-Voigt-Model connected in series and known as the Burgers model of viscoelasticity [15].

In literature several methods were developed to measure the viscoelastic behavior of human skin, whereat each method issues its own arbitrary measurement value. For each measurement method an individual customized theoretical model was published which describe the non-linear behavior of viscoelastic materials like skin, because the mechanical properties of the skin cannot result of the raw data from a measurement method, since the data depend on the device and the method likewise [10].

### 1.2.2.2. Mechanical anisotropy of the skin

The collagen bundles as well as the elastin fibers grow into a predefined direction, resulting in an anisotropy of the skin shown by the Langer-lines [6]. The resistance to traction of the skin is predominating, and the excised skin shrinks more and has a minimum extensibility, in this direction. Therefore, it is an anisotropy of prestress of the skin. Thus, the elastic modulus varies with the direction of measurement on the skin and shows it's maximum in the Langer lines axis [10]. When Langer-lines describe the orientation of collagen fibers, the direction of maximum resting skin tension are described by Kraissl-dynamic-lines. The knowledge of both are important for surgery. Thus, scars cut parallel to both lines, heal most rapidly [2].

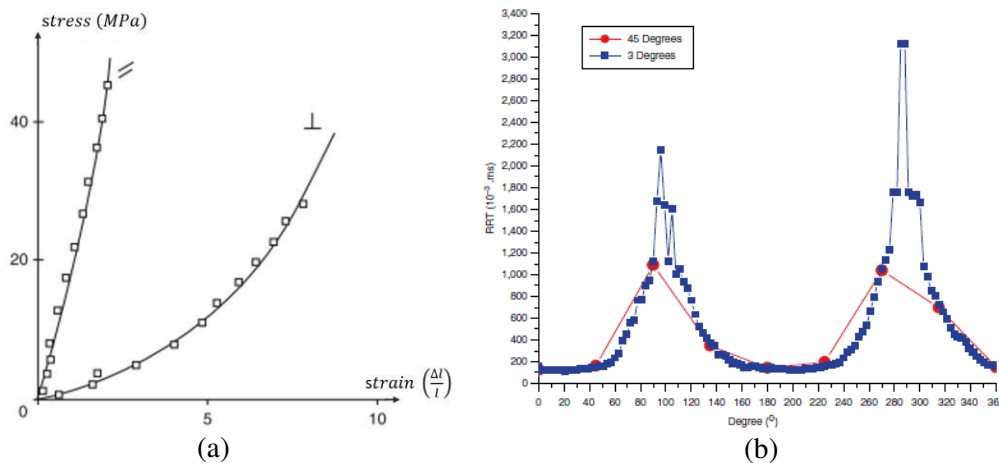


Fig. 7 a) Stress-strain relation of the skin parallel and orthogonal to the Langer-lines measured using the method of “uniaxial elongation”, the x-axis shows the relative elongation  $\left(\frac{\Delta l}{l}\right)$  and the y-axis the stress ( $\sigma$ ) applied to the skin [14]; b) Anisotropy of the skin, measured using the elastic wave propagation method (Reviscometer) [16]

### 1.2.2.3. Viscosity of the skin

The viscosity of the skin is mediated by the resistance of the collagen as well as elastin fibers they experience, while moving through the ground substance of the dermis [6]. Viscous deformation only take place, if skin encounters stress levels during more than brief time periods which are normally not occur. In the image above (Fig. 6), the viscoelastic phase is described by the parameter  $U_b$  when the total viscous phase is shown by the parameter  $U_c$  [10].

### 1.2.2.4. Wave propagation in skin

In soft tissues like skin different types of elastic waves can propagate. Starting with the invention of ultrasound in the late 1950ies where compressional elastic waves were used for imaging of soft tissues of

the human body, three decades later it was found that shear as well as Raleigh surface waves propagate in skin, which as well were considered for tissue investigation [17].

In ultrasound imaging compressional (longitudinal) waves are used to investigate human tissue. The motion of a wave is described by the wave equation. For simplification a linear elastic, isotropic and homogenous material is assumed. Then the wave equation for compressional waves is given by [18], [19]:

$$\rho \frac{\partial^2}{\partial t^2} u_i(x, t) = (\lambda + \mu) \frac{\partial^2}{\partial x_i \partial x_k} u_k(x, t) + \mu \frac{\partial}{\partial x_k} \frac{\partial}{\partial x_k} u_i(x, t) \quad (3)$$

Here  $\lambda$  and  $\mu$  are the lame-constants,  $\rho$  is the density of the material,  $u_i$  is the displacement vector,  $x_i$ ,  $x_k$  is the spatial vector in two individual directions and  $t$  is the time. The lame-constant  $\mu$  is the shear modulus which is given in formula (2), and  $\lambda$  show the following relationships with the Young's modulus  $E$ :

$$\lambda = \frac{E}{(1 + \nu)(1 - 2\nu)} \quad (4)$$

Where  $\nu$  is the Poisson's ratio.

With these relationships between the lame coefficients and the E-Modulus the wave equation can be written using a semi-inverse approach:

$$\frac{\partial^2}{\partial t^2} u_i(x, t) = \frac{E(1 - \nu)}{\rho(1 + \nu)(1 - 2\nu)} \frac{\partial^2}{\partial x_i^2} u_i(x, t) \quad (5)$$

Then, the compressional wave-velocity  $c_c$  is given by:

$$c_c = \sqrt{\frac{E(1 - \nu)}{\rho(1 + \nu)(1 - 2\nu)}} \quad (6)$$

The Poisson ratio is assumed to be around 0.5 in most soft tissues as well as in skin, which is the condition for incompressibility. The compressional wave speed is too mediated by the compressibility and the density of the tissue, which are defined by the short-range molecular interaction and water, that serves the main component of soft tissues. Therefore, the wave velocity of compressional waves in soft tissue and skin is around 10% equal to the one of water and lies in the range between 1450 – 1800m/s [17], [20].

The usage of shear waves in medical diagnostics started to find acceptance in the 1990ies, because around this time, it was approved by the society of medical imaging, that mechanical waves in soft tissues can propagate with phase velocities 100 times slower than sound in air, which was felt to be surprisingly slow for the investigators.

For simplification the above-mentioned Burge's model is reduced to the general Kelvin-Voigt-model which is commonly used in literature for characterization of human soft-tissue, shown in the figure below.

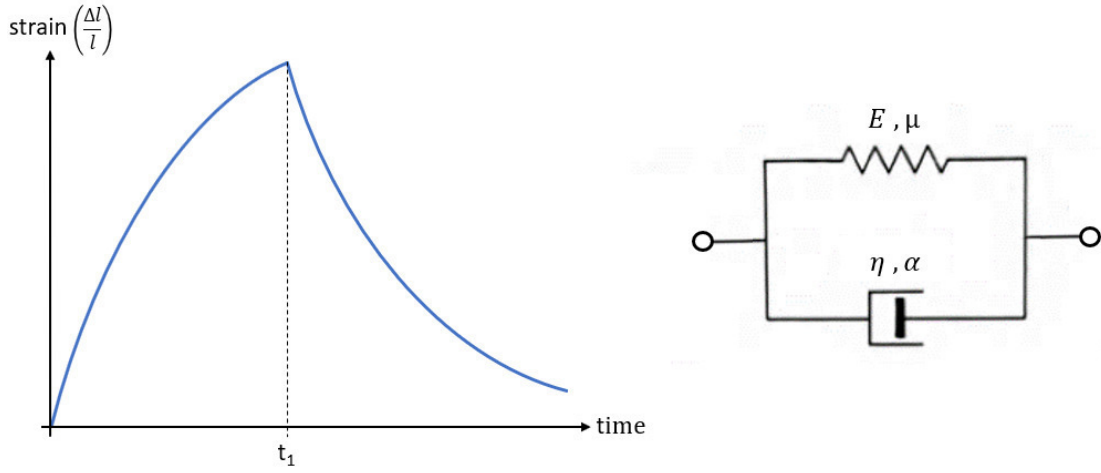


Fig. 8: Schematic representation of the Kelvin-Voigt-model,  $E, \mu$  are the elastic modulus and the shear modulus, and  $\eta, \alpha$  are the damping ratio and the damping coefficient of the model [21];

The phase velocity of shear waves depends on the shear modulus  $\mu$ . The wave equation for shear waves is, under assumption of the Kelvin-Voigt-model, given by [22]:

$$\frac{\partial^2}{\partial t^2} u_i(x, t) = \frac{\mu}{\rho} \frac{\partial^2}{\partial x_i^2} u_i(x, t) \quad (7)$$

And the phase velocity of shear waves  $c_s$  can then be calculated using formula (2) to:

$$c_s = \sqrt{\frac{\mu}{\rho}} = \sqrt{\frac{E}{2\rho(1+\nu)}} \quad (8)$$

As a fact, that human skin behaves like a viscoelastic material rather than an elastic, this viscoelasticity can be incorporated in the shear wave calculation. Therefore, the wave number of shear waves, can be defined as a complex quantity [17]:

$$k = k_r + ik_i \quad (9)$$

$$k_r = \frac{\omega}{c_s}, k_i = \alpha_s \quad (10)$$

Where  $k_r$  is the real and  $k_i$  the imaginary part of the wave number,  $\omega$  is the angular frequency, and  $\alpha_s$  the damping coefficient which is calculated by [23]:

$$\alpha_s = \frac{\ln\left(\frac{A_1}{A_2}\right)}{\Delta l} \quad (11)$$



where  $A_1, A_2$  is the amplitude of the shear wave at distance 1, 2 from the sender respectively, whereat  $A_1 > A_2$  and  $\Delta l$  is the difference between these distances.

As a result, that the wave number is a complex quantity, the shear modulus as well gets a complex quantity:

$$\mu = \mu_1 + i\omega\mu_2 \quad (12)$$

Here  $\mu_1$  is the elastic, respectively storage modulus and  $\mu_2$  the loss or as well called viscous modulus, given by:

$$\mu_1 = \rho\omega^2 \frac{k_r^2 - k_i^2}{(k_r^2 + k_i^2)^2} \quad (13)$$

$$\mu_2 = -2\rho\omega \frac{k_r k_i}{(k_r^2 + k_i^2)^2} \quad (14)$$

Additionally, in comparison to the compressional waves, shear waves are polarized, which makes them sensitive to the anisotropy of the skin, an important feature for estimation of skin aging and applicable in surgery [13], [14]. Because of the viscoelasticity of tissue the shear waves propagating in it show dispersion, resulting in an increasing phase velocity with increasing frequency [17].

When the wavelength of the shear waves are approximately in the range of the thickness of skin, various modes of guided waves and surface waves can be excited in skin [17]. Surface waves are almost dominated by Raleigh waves, which too are used for tissue characterization [2], [17]. Rayleigh waves are as well as shear waves dispersive in heterogenous (layered) material and polarized, thus the skins anisotropy can be investigated too. In isotropic and homogenous materials, the surface wave speed of Raleigh waves  $c_R$  is given by [26]:

$$c_R \approx \frac{0.87 + 1.12\nu}{1 + \nu} \sqrt{\frac{E}{2\rho(1 + \nu)}} \approx \frac{1}{1.05} c_S \quad (15)$$

The depth of penetration of surface waves in skin is estimated via the following relation [27]:

$$z \approx \lambda = \frac{c_R}{f} \quad (16)$$

In literature, human tissues were investigated using several measurement methods, leading to different results for shear and bulk modulus. The variation of these modulus for different tissue types postulated in literature were collected and summed up by Sarvazyan et. Al., shown in Fig. 9 [28].

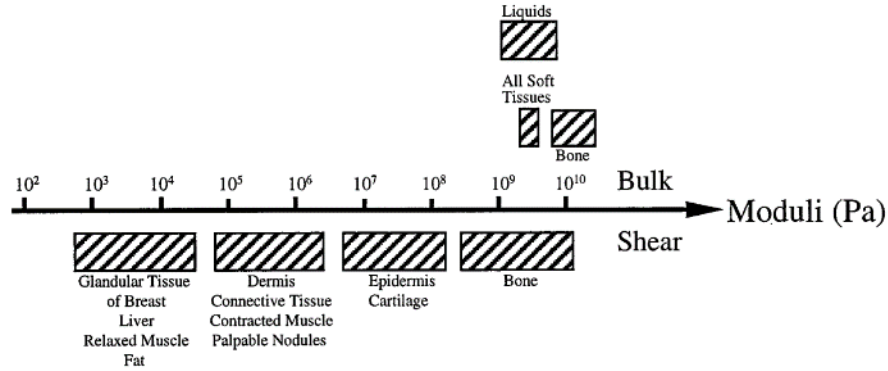


Fig. 9: Variation of the shear and bulk modulus of different materials and body tissues mentioned in literature are summarized and visualized as separated blocks for given tissue types [28].

### 1.2.3. Mechanical behavior of skin during ageing and moisturizing

During ageing the human skin changes its mechanical properties. As a fact, that the skin collagen content is growing from the birth to mid age, it decrease in postmenopausal women with a higher ratio [29], [9]. The skin gets thinner, stiffer, more dry, less flexible and more wrinkled in combination with poor wound healing with age and the anisotropy increase significantly, which is too well seen in the skin relief structure during aging [30], [16], [9]. But in research the behavior of the Young's modulus of skin during aging is highly debated. Even literatures using the same gold standard appliance for measurements of skin elasticity, like the Reviscometer from Courage&Khazaka face different results with growing proband age [24], [31]–[36]. Nevertheless, measurements with the suction devices like the Cutometer from Courage&Khazaka show decrease of the distensibility” (the arbitrary value  $U_f(R0)$ ) as well as “elasticity” (the arbitrary value  $U_r/U_f (R7)$ ) and increase of “viscoelasticity” (the arbitrary value  $U_v/U_e (R6)$ ) during aging. But this evaluated parameters are arbitrary values which provides information about the intrinsic skin parameters for comparison between different subjects, but doesn't represent any common physical elasticity values, therefore the parameters are written in quotation marks [36]–[47]. Measurement methods which evaluate the speed of the elastic wave in skin due to receiving the sent wave in various distances and not only the resonant running time from the sender to the receiver, show a significant increase of the phase velocity with ascending skin age, which means an increase of the Young's modulus with aging [48], [49].

There are many clinical and cosmetically procedures and treatments to make skin appearing younger and fresher. One way is moisturizing of skin. All moisturizers try to accomplish the same purpose, to increase the content of water in the stratum corneum. This can be achieved by preventing the evaporation of water from the skin or via increasing the involacy of the skins barrier through supply with fatty acids, ceramides,

cholesterol and taking control of the calcium gradient [9]. As a result, that the skin gets more humid with moisturizing, the resonant running time of the gold standard appliance Reviscometer increase slightly after a daily treatment with moisturizers. The application of hydrating moisturizers to skin as well can be detected in an increasing viscoelasticity value (the arbitrary value  $U_v/U_e$  (R6)) as well as increasing “distensibility” (the arbitrary value  $U_f$  (R0)) measured with the gold standard device of the suction method, the Cutometer [32], [50], [51].

### 1.3. Specification for development of the sensor solution

The basics for developing a smart skin elasticity sensor solution which is meant to be operated via NFC or BLE, must feature several boundary conditions. The later described methods can be compared to this boundary conditions, leading to favorable techniques for developing a novel smart sensor solution. The limits predefined are not hard boundary conditions, rather they describe guidelines containing tolerances.

- Small size:
  - The sensor solution should be of small size and flexible in order that various skin sites can be examined. Most frequent measuring sites are the volar forearm, followed by the cheek, dorsal forearm, forehead, abdomen and palm [24], [31]–[34], [36], [48], [50], [52]–[55]. That these sites can be investigated by the sensor, the dimensions of it should be within the following specified sizes:
    - 4x4cm surface
    - 5mm thickness
- Low current/power consumption:
  - It is preferred, that the power of the sensor solution is provided via the NFC interface and that no battery is necessary. If it is inevitable a small battery can be utilized.:
    - max. current: 3mA
    - Power: related to NFC/BLE energy harvesting
- Easy to use
  - the part of the body where the sensor is in use must not be poseyed, to ensure a simple usage on various skin sites of the body for the individual nescient customer.
  - requirements for skin preparation (e.g.: shave of hairs) and sensor preparation (e.g.: change of double-sided adhesive tape) appear in the required smartphone app.

- For investigation of the anisotropy via a uniaxial method, the angle of rotation will appear on the smartphone app (measured by means of the acceleration sensors provided by the smartphone).
- Fast in vivo measurement
  - <10 seconds (for one uniaxial measurement)
  - For investigation of the skin anisotropy under application of a uniaxial method, the accuracy of the value increase with the number of measured angles, thus the measured time increase according to it.
- Low cost of production
  - <1€/measurement: the sensor-solution must be reusable, or an extra low-cost version needs to be developed

## 1.4. Hypothesis

Under usage of low energy consuming piezoelectric bending transducers, one can build a smart sensor solution featuring a sender and minimum two receivers to inject elastic waves in skin and subsequently measure the stimulation time respectively the propagation speed as well as the damping coefficient. Wave propagation in soft tissue occurs via compressional, shear as well as surface waves, whereat compressional waves are negligible in the applied range of frequency. Via the measurement of the speed as well as the damping coefficient, the complex shear modulus of the skin *in vivo*, and thus the elastic and viscous modulus of the investigated tissue can be determined and monitored. By measurement of the angular elastic phase velocity distribution in skin the anisotropy and hence the preferential growing direction of the collagen as well as elastin fibers can be determined, which further can be utilized in surgery. Since the sensor solution is supplied via the NFC energy harvesting technology or connected over BLE the measured values, can directly be displayed on the employed smartphone or tablet as well as monitored and compared to other individuals or directly transmitted to the personal dermatologist for further diagnosis.

## 1.5. Evaluation and summary over various measurement methods

### 1.5.1. Evaluation

In past, several methods had been developed to access the mechanical properties of skin via noninvasive measurements in vivo. Some of the methods were enhanced by other investigators, however a few were not

successive and only mentioned by the author who invented the technique like the leverometry and the conformal piezoelectric system [14], [56], [57]. Thus, these techniques are not further described.

Using the enhanced methods, various techniques are utilized like: uniaxial stretching, torsion, suction, compression, elastic wave propagation. For these techniques, various tests could be performed in one or various of the below mentioned ways:

- creep test: a constant force is applied suddenly to the skin, and the deformation is measured over time
- progressive deformation test: an increasing stress is applied to the skin at a constant rate, and the resulting strain is measured
- relaxation test: a permanent deformation is applied to the skin, and the resisting force is measured over time
- dynamic test: an elastic wave is induced into the skin and the resonant running time, the phase velocity and damping coefficient can be measured. [10]

#### 1.5.1.1. Pressure based suction method

A partial vacuum is created in a small, hollow cylinder, featuring an inner diameter between 2-10mm, which causes a hemispherical deformation of the skin via suction, when at the same time the displacement of the investigated tissue is measured, using various physical techniques. Using this method, the creep as well as the progressive deformation test can be performed. There are various versions of this method postulated in literature in which four of them are commercially available. Via variation of the inner diameter of the suction device, various depth in skin can be investigated and therefore the mechanical properties of different layers can be examined.

In literature almost, the creep test is mentioned, and the resulting values of this test are compared. For the creep test a partial vacuum is applied during a predefined time, usually a few seconds, which is followed by a relaxation period, commonly set to the same time interval than the suction period, in which the skin starts to relax. After performing the preset suction/relaxation cycles the skin starts to retain to its initial position immediately, but incompletely. Full recovery of the skin requires a long time from a few minutes to several hours, shown by a residual deformation at the end of the test [10].

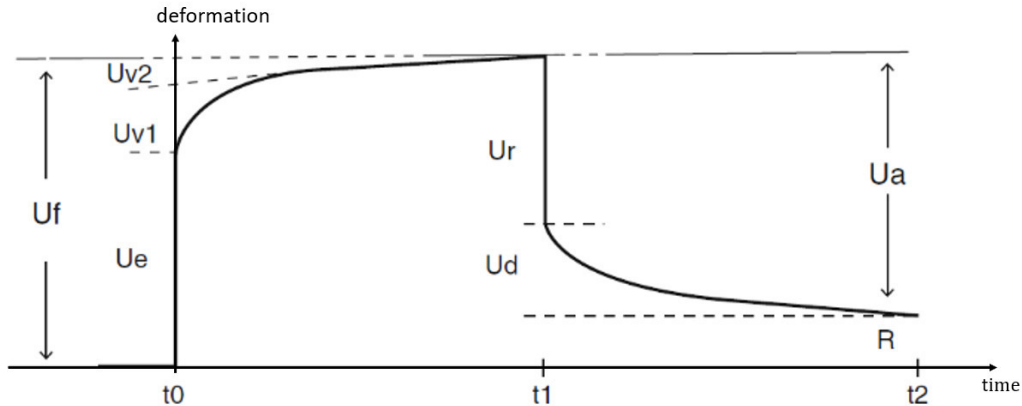


Fig. 10: Characteristic graph resulting from a creep test;  $U_e$ : immediate deformation (totally elastic),  $U_{v1}$ : viscoelastic deformation,  $U_{v2}$ : late deformation (entirely viscous),  $U_f$ : total deformation of the skin (skin distensibility),  $U_r$ : immediate recovery,  $U_a$ : late recovery,  $U_a$ : recovery at the end of the experiment,  $R$ : residual deformation at the end of the experiment,  $t_0$ : partial vacuum is applied to the skin,  $t_1$ : vacuum is released and skin starts to relax,  $t_2$ : end of the experiment [10]

The evaluated data are arbitrary values which provides information about the intrinsic skin parameters for comparison between different subjects but doesn't represent any common physical elasticity values.

Using this investigation method and via mathematical approximation a pseudo Young modulus, could be obtained delivering values around 0.1 – 0.4 MPa for various skin sites. To achieve these values A.O. Barel et al. used the Cutometer for measurements and estimated a skin thickness of 1.1mm for men and 0.9mm for women [42], [58], [59].

A recently developed and commercially available suction device built by Courage&Khazaka features a combination of the measurement of the skin elasticity as well as the anisotropy. The measuring probe is equipped with an 360° image recording system. The investigated skin area is sucked into a suction ring for several seconds and then released like described in the previously mentioned suction device. During the sucking and relaxing cycle, the built-in camera records the displacement leading to a circular 3D-Graph made by 360 single elasticity curves. Out of this data viscoelasticity as well as anisotropy data can be evaluated [60].

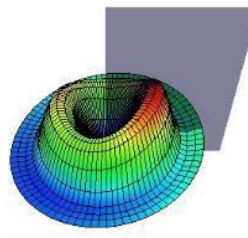


Fig. 11: Model of the deformed skin investigated by the commercially available "CutisScan CS 100", the asymmetric deformation of the model is based on the asymmetry of prestress of the skin [61]

### 1.5.1.2. Torsion method

A central disc is rotating inside a guiding ring, both stuck to the skin via a double-sided adhesive tape. A specific momentum is applied to the central disc, allowing it to rotate, while the unattached skin part between the disc and the ring is twisted tangentially, representing the counter torque. For investigation of the elasticity the torque as well as the rotation angle is recorded using various techniques. Using this method, the creep as well as the progressive deformation test can be executed [10].

In the creep test a predefined momentum is applied abruptly and the angle of the disc is recorded during time. After an initial fast rotating phase, a short creep phase follows. When the torque is switched off, the prestressed skin starts to relax, leading to a back rotation of the disc. The resulting curve looks similar like the one obtained by the suction method, shown in Fig. 10 [6].

Via variation of the distance between the central rotating disc and the guiding ring, different depths of the investigated tissue can be examined [10]. Using this measurement method, parameters that characterize elastic, viscoelastic and plastic properties of the skin can be evaluated [62].

The resulting data of the appliance are only arbitrary values which can be used for comparison between various test persons. Physical elasticity values, like the elastic modulus of the measured tissue can be approximated out of the arbitrary values using a theoretical model [59].

Using this method as well as the associated theoretical model, a Young's modulus between 0.4 – 1.2MPa for various skin sites were found. The thickness of the skin was evaluated by means of ultrasound [6].

### 1.5.1.3. Uniaxial elongation method

Two tabs are fixed on the skin and pulled apart, leading to a uniaxial load parallel to the skin surface. This type of mechanical testing is well known in material science and widely used. There are several diverse ways to perform this method, however only the uniaxial stretching is discussed. The most common is to attach two tabs using cyanoacrylate adhesive onto the skin, featuring a specific distance in between. Via this method the creep, progressive deformation as well as the relaxation test can be performed [6].

For the creep test a predefined force is applied abruptly between the two fixation points, which pulls the skin apart. The skin in between gets stretched immediately, followed by a slow viscous deformation. After a specific time, the force is withdrawn, and the skin retrieve whereat a slight skin deformation remains. The deformation versus time is measured. The resulting curve looks almost the same than for the suction and torsion method [10].

Using this method, the limits of the stretched area are not known, and therefore the approximation of the physical elasticity parameters from the measured arbitrary values are difficult to determine. Applying a finite element model to the possible stressed area allows to compute the deformation field over the total deformed area and thus the elasticity parameters can be approximated.

Via this method a Young's modulus between 4 – 20MPa for various skin sites were found [63].

Another way to perform this test, is called “gas-bearing-electrodynamometer”, where a small disc is adhered onto the skin and then moved forward and backward featuring a frequency around a few Hz. The stretching of the skin and the applied force is recorded and plotted, resulting in the following image:

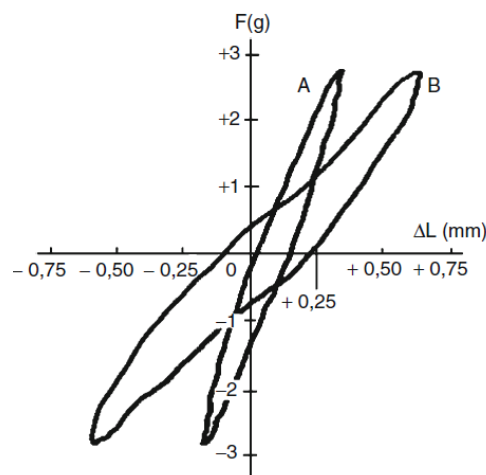


*Fig. 12: Graphs resulting via investigation of skin, using the gas bearing electro-dynamometer, F: force recorded due to stretching of the skin, ΔL: moving distance of the small disc adhered to the skin [10]*

Out of the image the stiffness of skin can be approximated via the steepness of the curve. The width of the ellipse is an indication for the capacity of the skin to subject passive deformation [10].

#### 1.5.1.4. Compressibility methods

##### Indentation

Indentation tests are a well-known method in mechanical engineering to evaluate the resistance of a material to deformation. An inelastic indenter of a specific ended shape like a plane ended cylinder, a half sphere, or a cone shaped tip is used to apply a given force or deformation to the skin [1]. It only can be performed on skin sites, where skin is directly attached to the underlying bone, like on the human forehead. Otherwise the compressibility of the subjacent muscle is measured along with the skin parameters [64]. In comparison to the before mentioned methods, in indentation mainly the capacity of the interstitial ground substance against motion is evaluated. This capacity depends on the viscosity of the ground substance and the gaps



between the meshwork of collagen fibers within the dermis. The vertical stretching of the collagen as well as elastic fibers are only involved by a slight percentage into the value evaluated by this method [65]. The test performed using Indentation is of creep type [10]. Nevertheless, elastic as well as the viscous properties can be accessed via the resulting loading and unloading cycle, given by a measuring loop shown in Fig. 13.

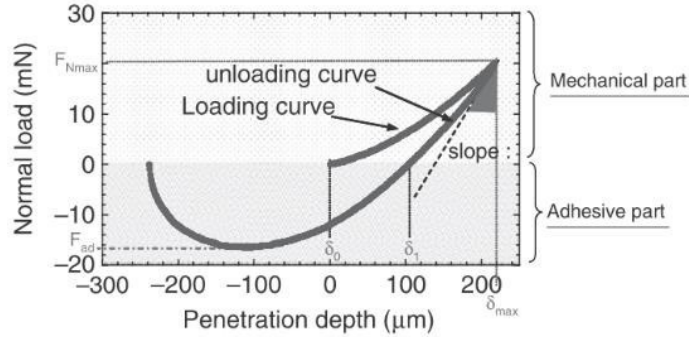


Fig. 13: Example of a loading and unloading curve examined via indentation of human skin,  $\delta_0$ : penetration depth at the beginning of the experiment, when normal load is 0mN;  $\delta_1$ : penetration depth during the unloading cycle when the normal load gets 0mN again,  $\delta_{max}$ : penetration depth at  $F_{Nmax}$  (maximal load),  $F_{ad}$ : minimal adhesion force during the unloading cycle [66]

Using this method a reduced Young's modulus of 8.3kPa, measured on the forearm and averaged over 20 women volunteers, results [66].

## Ballistometry

An object is dropped onto the surface of the skin applying a specific force. The recoil is measured during bouncing off the surface [16]. The primarily potential energy is released to kinetic- and finally transformed to deformation, heat or rebound-energy. The more energy transformed to rebound the higher the elasticity of the investigated tissue [10]. The main parameter of this method is the ratio of the rebound to the primary release height of the object:  $e = \frac{h_2}{h_1}$ . The depth of penetration to particular layers of the skin can be varied using different geometric sharpness of the dropped object [16]. The resulting values of this method are only of arbitrary nature, since the intrinsic skin parameters currently cannot be calculated from ballistometry experiments [10].

### 1.5.1.5. Wave propagation method

This method is based on elastic wave propagation in skin. Via an external vibrator or a sound transducer an elastic wave is induced into the skin and the response is measured using one or several receivers in a specific distance from the sender on the skin surface. The resonant running time represents the time delay between the wave sent and later received in a specific distance. Via measurement of the phase angle versus the

separation distance from the sender the wavelength at specific frequencies can be determined. Assuming, that the wave propagation in skin is uniaxial, the phase velocity can be calculated out of the product of the frequency and the wavelength [10][23]. A more accurate method uses two receivers placed in line but in different distances from the sending unit. Via the measurement of the time as well as the path length difference the phase velocity can be evaluated. Using this method, additionally the resonant running time to both receivers as well as the damping coefficient can be examined [23], [25], [67], [68].

In a theoretical analysis of an experimental procedure for determination of age related changes in skin it was suggested, that with frequencies below 1kHz the measured results strongly depend on the skin thickness, while at measurements with higher frequencies, influences by the thickness of the skin as well as subcutaneous fat was negligible [69]. In literature it is mentioned, that wave velocity seems to be proportional to the viscoelasticity, if acoustic waves in frequency range of 0.5-30kHz were applied [54]. Via stimulating soft tissue like skin using an elastic pulse or vibration, compressional waves, as well as shear and surface waves are generated. Since the frequency of the stimulation is in range between 1Hz-30kHz the wavelength of compressional waves measures 50mm-1500m, thus almost shear and surface waves are propagating in tissue in the mentioned frequency domain. However, in parts of the used frequency range the wavelength of the generated shear waves lie in range of the thickness of the skin, therefore additionally surface waves are excited [3], [17].

Several test setups for investigation human skin in vivo using elastic wave propagation had been developed, some of them are patent-registered and one of them is commercially available, the “Reviscometer”. All of them use excitation frequencies in range of several Hz to 30kHz and obtained wave velocities in range of 1 – 106m/s [24], [48], [54], [67], [70]–[72]. For comparative purposes measurement results obtained with one of the devices postulated, labeled as “viscoelastic skin analyzer”, featuring an excitation frequency of 5.6kHz are shown in Fig. 14 [54]. It is assumed, that the mean skin density is 1100kg/m<sup>3</sup> [67]. Via application of the above-mentioned formula (8) the mentioned wave velocity lead to shear modulus values in the range of 1.1kPa up to 12.4MPa.

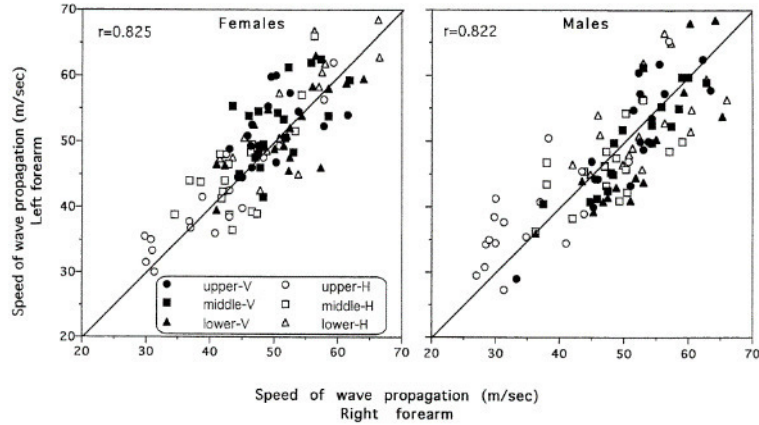


Fig. 14: Speed of wave propagation obtained on human skin in vivo; comparison between left and right forearm in healthy females and males; measurements were taken in vertical (V) and horizontal (H) direction [54]

Using this method, the shear elasticity and shear viscosity, as well as the anisotropy and resonant running time of the skin can be evaluated, see equation (13)(14).

The speed of sound shows a maximum, if measurements are taken in direction of the Langer-lines and shows it's minimum perpendicular to them. The definition of the Anisotropy of the skin is given by:

$$A = \frac{c_{min}}{c_{max}} \quad (17)$$

Here  $c_{min/max}$  is the minimum respectively the maximum of the phase velocity measured at one skin site, using different angles of measurement [10].

## 1.5.2. Summary

In general, methods which are based on mechanical stress of the investigated skin like the suction, torsion or uniaxial elongation method, are less suitable for developing a smart sensor solution according to the predefined guidelines, because they need a bigger amount of space as well as power than predefined in the guidelines.

In total, no method would perfectly fit the guidelines, however two methods could be used to establish a sensor solution:

- Indentometry method

Using this method under application of piezo biomorph elements, oscillating with its resonant frequency, equipped with tiny force sensing elements (Single Tact<sup>®</sup>, FSR<sup>®</sup>) and miniature strain

gauges on the piezo elements a sensor solution could be established fulfilling nearly the predefined guidelines [73]. But the main issue is, that the evaluated values are not elasticity values from skin but rather the capacity of the interstitial ground substance against motion. This too can be seen on the measured results obtained via this method, which are significantly lower than the values examined with the three excellent comparable methods (suction, torsion, uniaxial elongation).

- Wave propagation method

This method represents another possibility to establish a sensor solution which would fit the predefined guidelines, if piezo transducer elements are used. They are tiny, cheap in production and have a minimum power consumption. This method can be as well established uniaxial, thus the anisotropy of the skin can be examined excellently. The major disadvantage is, that the resulting values are more difficult to compare to the other methods mentioned, since no mechanical stress nor extensive strain is applied to skin. The resulting elasticity values show a wide range, since the propagation speed and examination depth depend on the investigation frequency.

Using the wave propagation method, the shear elasticity as well as the shear viscosity can be determined, and additionally, in comparison to indentometry, the anisotropy can be evaluated. Therefore, the wave propagation method seems more appropriate to develop a new smart skin elasticity sensor solution. In literature the two gold standard appliances for skin elasticity measurement, the Cutometer (suction method) and Reviscometer (wave propagation method) are well compared to each other that correlations between the individual measured arbitrary values can be proved. Especially the parameter  $U_f$  (total deformation of the skin) and  $U_a$  (recovery at the end of the experiment) of the Cutometer shows significant correlations to the arbitrary value RRT of the Reviscometer [35], [60].

### 1.5.3. Comparison of wave propagation method to the suction method

Both methods don't have anything in common, except that they attempt to obtain skins mechanical properties, thus in general a comparison of the measurement values between both methods must be treated with some caution. In literature it was assumed, that measurements of the viscoelasticity of more rigid skin areas are not possible with the Cutometer, and that sensing probes with small aperture are only measuring upper epidermal skin layers, when with bigger apertures properties of the dermis layer is investigated. Furthermore it was concluded, that the measurement of the speed of propagation of elastic shear waves in viscoelastic media is a more promising approach for investigation of skins mechanical properties [54]. Nevertheless, in literature comparison between the commercially available devices the Cutometer and the Reviscometer were investigated on human skin in vivo. The relation between both of the devices is highly

debated, in some publications no correlations were found between them, some mention a significant and robust correlation between the Cutometer values  $U_f$  (R0) and  $U_a$ (R8) and the running time of the Reviscometer, shown in Fig. 15 [35], [60], [74].

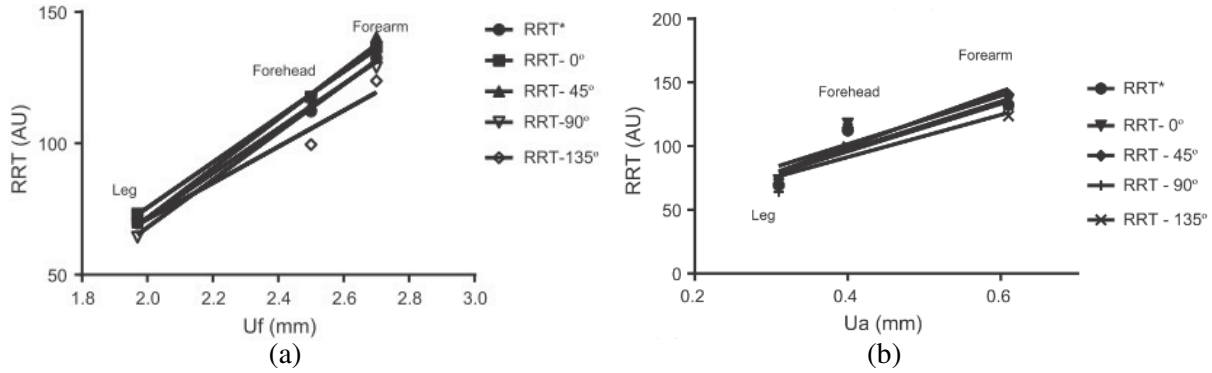


Fig. 15: comparison of the measurement results investigated using the gold standard appliance the Cutometer vs. Reviscometer; a) the distensibility ( $U_f$ ) measured with the Cutometer vs. the running time (RRT – 2mm distance) measured by the Reviscometer; b) the skin recovery ( $U_a$ ) measured with the Cutometer vs. the running time (RRT – 2mm distance) measured by the Reviscometer; Since the Reviscometer is an uniaxial measurement device various directions were investigated [60];

## 1.6. Characterization of piezoelectricity

When a dielectric material is placed within an electric field it undergoes changes in mechanical dimensions due to separation of the positive and negative charges and anharmonicity of the bonds within the material. This effect is the so-called electrostrictive effect and it is proportional to the square of the applied electric field. The mechanical deformation is independent of the polarization of the field and marginal for materials featuring a centrosymmetric lattice. For materials with a non-centrosymmetric lattice or similar structures (except the octahedral crystal class), there appears an additional asymmetric movement of the neighboring ions, thus the deformation is significant and directly proportional to the applied electric field. Therefore, dielectric substances featuring a non-centrosymmetric lattice or similar structures are so called piezoelectric materials [75].

The strain in these non-centrosymmetric materials is compressive or extensive depending on the polarization of the electric field subject to the material. The effect, that a material undergoes stress or strain as a result that it is subjected to an electric field, is called indirect piezoelectric effect. When piezoelectric materials are subject to external strain via applying pressure or stress to it, the charges inside the crystal get separated, thus an electric field across the material is generated. This effect is called the direct piezoelectric effect, exhibited as well by all piezoelectric materials.

If a piezoelectric material shows spontaneous polarization it is additionally called pyroelectric. But in common ambient conditions the spontaneous polarization itself cannot be observed, because they get compensated by free charges from the surroundings. But when temperature of a pyroelectric material is increased, the spontaneous polarization decreases, thus the effect can be measured via change in polarization.

Some pyroelectric materials as a subclass of piezoelectric materials show ferroelectric effects. Ferroelectric materials feature a hysteresis in polarization like ferromagnetic materials in magnetization do. Which means, that the spontaneous polarization can be reversed via applying an electric field in the inverse direction, and the spontaneous polarization shows saturation at a specific point. A closed loop hysteresis curve can be evaluated for each ferroelectric material as characterization of it. These materials as well feature a ferroelectric transition temperature where they lose the spontaneous polarization beyond this temperature and migrate from a ferroelectric to a paraelectric material.

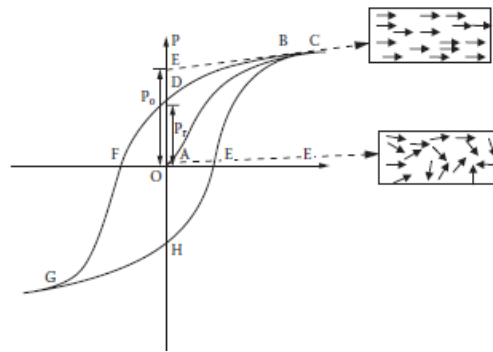


Fig. 16: hysteresis curve of a ferroelectric material, A...unpolarized material, ABC...polarization curve under application of a electric field in positive direction, C(P<sub>0</sub>)...saturation in positive direction, CDFG...polarization curve under polarization change using an electric field in the negative direction, D (P<sub>1</sub>)...remnant polarization in positive direction, GHEC.... polarization curve under polarization change using an electric field in the positive direction, H...remnant polarization in negative direction [75]

Consequently in ferroelectric materials a net remnant polarization can be generated via applying an adequate electric field. This process, where the ferroelectric domains inside the material start to get oriented inside the applied electric field is called poling.

The sensitivity of piezoelectric materials to both the direct and indirect piezoelectric effects are described by piezoelectric coefficients. There are two major piezoelectric coefficients/ constants describing the piezoelectricity in an individual material:

$$d = \left(\frac{\partial D}{\partial X}\right)_E = \left(\frac{\partial x}{\partial E}\right)_X \quad (18)$$

$d$  is the dielectric charge constant, describing the electric flux density  $D$  per unit of mechanical stress  $X$ .  $x$  is the mechanical strain.

$$g = -\left(\frac{\partial E}{\partial X}\right)_D = \left(\frac{\partial x}{\partial D}\right)_X \quad (19)$$

$g$  is the piezoelectric voltage constant, indicating the electric field  $E$  generated per unit of mechanical stress  $X$ .

As a result, that the electric flux density, the electric field, the mechanical stress and strain are all second rank tensors, the piezoelectric coefficients are third rank tensors. For simplicity a reduced matrix notation is used in the formulations, thus the piezo electric coefficients are represented by  $3 \times 6$  matrices allowing to describe four possibilities in direction of the piezoelectric effect. If equation (18) is simplified and written without the total differential it can be indicated like (under assumption of a constant electric field):

$$D_i = d_{ij}X_j \quad (20)$$

written in full dimensions:

$$\begin{pmatrix} D_1 \\ D_2 \\ D_3 \end{pmatrix} = \begin{pmatrix} d_{11} & d_{12} & d_{13} & d_{14} & d_{15} & d_{16} \\ d_{21} & d_{22} & d_{23} & d_{24} & d_{25} & d_{26} \\ d_{31} & d_{32} & d_{33} & d_{34} & d_{35} & d_{36} \end{pmatrix} \begin{pmatrix} X_1 \\ X_2 \\ X_3 \\ X_4 \\ X_5 \\ X_6 \end{pmatrix} \quad (21)$$

Out of this tensor four different possibilities of piezoelectric effect can be separated, depending on direction of displacement after application of an electric field in a specific way. The effect can be separated into the longitudinal, transversal, longitudinal shear and transversal shear direction, illustrated in the following graphic [75], [76]:

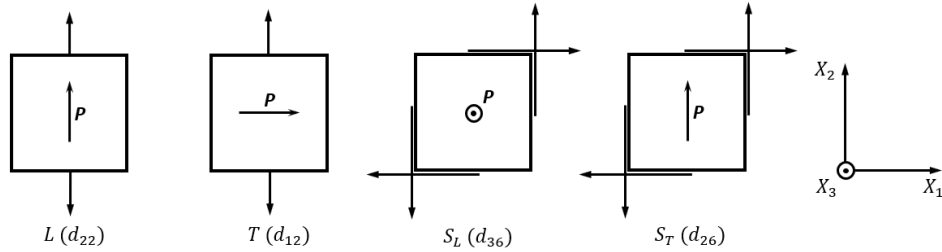


Fig. 17: The first index number of the coefficient indicates the direction of the electric field applied, when the second number specifies the direction of displacement (number 1-3)/ shear stress around an axis (4...around  $x_1$ , 5...around  $x_2$ , 6...around  $x_3$ ),  $P$  ...direction of Polarization,  $L$ ...Longitudinal displacement,  $T$ ...Transversal displacement,  $S_L$ ...Longitudinal Shear displacement,  $S_T$ ...Transversal Shear displacement [76]

## 2. Materials and Methods

### 2.1. Development process of the smart sensor solution

In general, for development of novel physical goods a process procedure methodology is beneficial to be generated in advance, that no step is neglected. Years ago, a high-level diagram for such a methodology was developed by the global design and innovation company IDEO. This diagram was employed and adapted for development of a smart skin elasticity sensor solution.

#### 2.1.1. General description of the development process

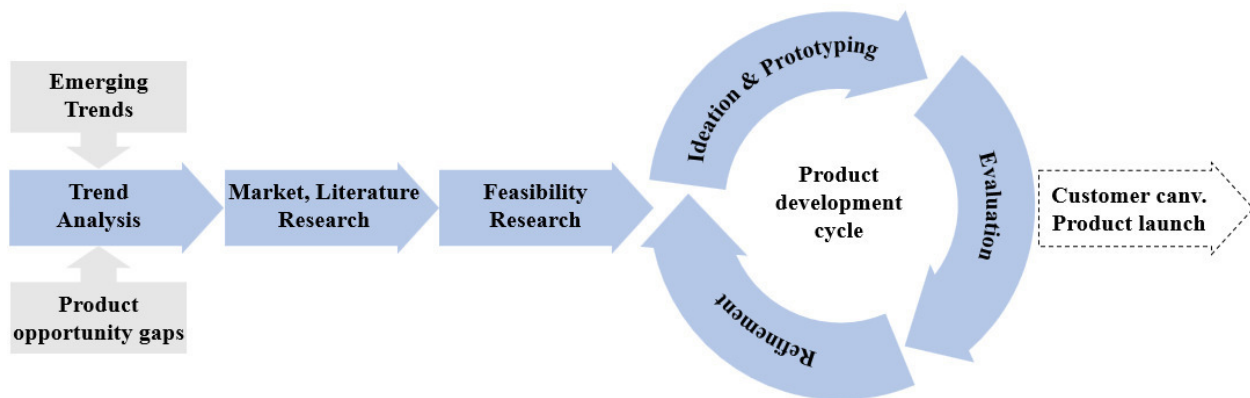


Fig. 18: Development process of a smart sensor solution

##### 2.1.1.1. Trend analysis

- Emerging Trends

In the last couple of years, the investigation of human skin especially of its elasticity gets more and more important, because skin is one of the most important organs of the human body protecting it from external influences and loss of endogenous substances. Via individual smart measurement sensor solutions an early recognition of the increasing skin illness like atopic dermatitis, psoriasis as well as tumorous skin can be fulfilled, rehabilitation can be applied sooner leading to an improving curability. Via the increasing market of tele-dermatology and electronic distance medicine, it is assumed, that medical consultation in most instances is not necessary.



- Product opportunity gaps

Nowadays, smart and cheap sensor solutions represent an easy, fast and handy way to measure human health data like the skin viscoelasticity. While cheap and smart sensors for heart rate, blood pressure or blood oxygen monitors are available on market, smart sensor solutions for skin data have hardly been explored.

### 2.1.1.2. Market, Literature research

Current measurement equipment for determination of the human health data like skin elasticity are linked to unhandy and expensive tabletop units. Several appliances for skin elasticity measurement are available on market like the Cutometer<sup>5</sup>, the DermaLab<sup>6</sup>, the CutiScan<sup>7</sup>, the Dermal Torque Meter DTM310<sup>8</sup> or the Ballistometer<sup>9</sup>, but nevertheless they are only applicable by pre-instructed professionals. Additionally, the available measurement appliances only show arbitrary values which are only comparable using the same measurement instrument, and no physical elasticity values are available. Although, various physical methods, like shown in 1.5.1 are developed to investigate elasticity of human skin, but only two of the mentioned methods fit the boundary conditions to develop a smart, low energy consuming and easy manageable sensor solution.

### 2.1.1.3. Feasibility Research

As a result, that for a bigger amount of stress or strain a big space as well as a quite amount of energy is necessary several methods are not applicable. Under usage of piezo elements two methods may be realized like shown in 1.5.2. As a result, that piezo elements are tiny, cheap in production and have a minimum power consumption they are predestinated for usage in this area.

### 2.1.1.4. Product development cycle

After literature research, marked analysis and feasibility-study a first prototype of a sensor solution was established and tested. During tests and evaluation of the results new ideas for improvement of the sensor solution comes up leading to refinement of the previous version and to literature research in new fields of focus for establishment of the next generation appliance. This cycle was run through several rounds till the results of measurement were satisfactorily and a correlation of the resulting measurement values with test

---

<sup>5</sup> <https://www.courage-khazaka.de/index.php/de/neuigkeiten/49-deutsch/produkte/wissenschaftlich/157-cutometer-d>

<sup>6</sup> <http://www.analyse-skin.com/dermatology/#elasticity>

<sup>7</sup> <https://www.courage-khazaka.de/index.php/en/products/scientific/273-cutiscan-e>

<sup>8</sup> <https://www.diastron.com/skin/>

<sup>9</sup> <https://www.diastron.com/skin/>

results from the gold standard appliance on human skin in vivo could be proven. A roadmap for a survey of the very beginning to the final sensor solution including some of the interim-versions are schematically depict in Fig. 19.

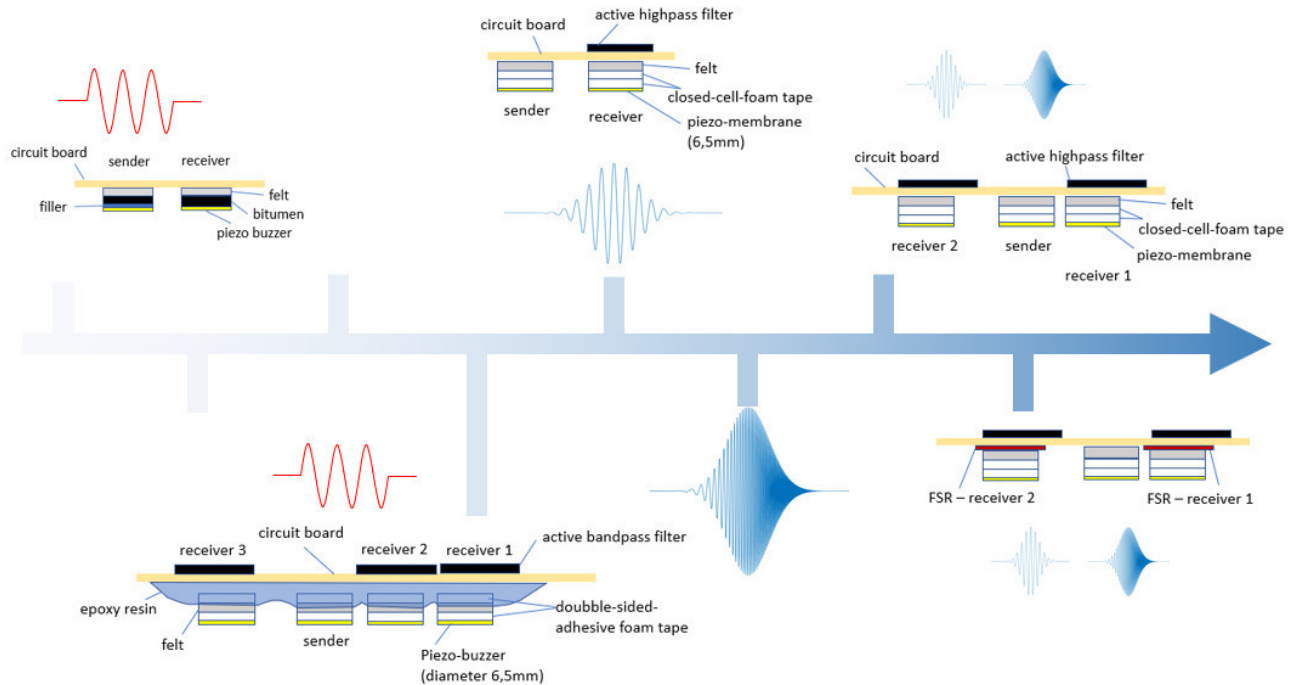


Fig. 19 Design-history of the sensor solution;

### 2.1.1.5. Customer canvassing and product launch

After achieving several goals of the previously defined boundary conditions and a reasonable correlation of the developed sensor solution in comparison to gold standard appliance is proved, the sensor solution is ready to be presented in front of prospective clients and customer acquisition can be initiated.

## 2.2. Sensor Solution

### 2.2.1. Selection and calculation of the appropriate sensor element

For establishing a small and smart sensor solution tiny piezo transducer featuring low energy consumption according to the guidelines as depicted in 1.3 are required. The resonant frequency of the elements must be in the range of 1-30kHz to exclusively induce shear or surface waves in human skin, like described in

1.5.1.5.. There are various shapes and designs of tiny piezo transducers to generate an elastic wave in skin. Most common designs are:

### 2.2.1.1. Piezo discs

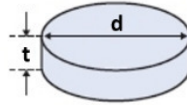


Fig. 20: schematic representation of a piezo disc featuring a diameter  $d$  and thickness  $t$  [77]

The oscillation occurs either in thickness or in radial direction of the disc, when the alternating voltage is applied on both flat sides of the disc. In this case the resonant frequencies are approximated to:

Oscillation of the thickness:

$$f_{R\_thk} = \frac{1}{2 \cdot t \sqrt{\rho \cdot s_{33}^D}} \quad (22)$$

Where  $t$  is the thickness of the disc,  $\rho$  the density and  $s_{33}^D$  is the elastic compliance at constant charge density.

Radial oscillation:

$$f_{R\_rad} = \frac{1}{\pi \cdot d \sqrt{\rho \cdot s_{11}^E}} \quad (23)$$

Where  $d$  is the diameter of the disc,  $\rho$  the density and  $s_{11}^E$  is the elastic compliance at a constant electric field [78].

### 2.2.1.2. Piezo rings/tubes

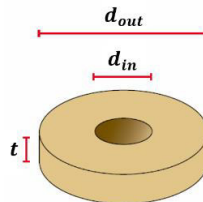


Fig. 21: schematic representation of a piezo ring or tube, featuring a thickness  $t$ , an outer diameter  $d_{out}$  and an inner diameter  $d_{in}$  [79]

The oscillation occurs in radial direction, thickness or wall-thickness of the ring, when the alternating voltage is applied on both flat sides of the ring. In this case the resonant frequency of the ring is approximated to:

Oscillation of the thickness:

$$f_{R\_thk} = \frac{1}{2t\sqrt{\rho \cdot s_{33}^D}} \quad (24)$$

Where  $t$  is the thickness of the disc,  $\rho$  the density and  $s_{33}^D$  is the elastic compliance at constant charge density.

Radial oscillation:

$$f_{R\_rad} = \frac{2}{\pi(d_{out} + d_{in})\sqrt{\rho \cdot s_{11}^E}} \quad (25)$$

Where  $d_{out}$  is the outer diameter and  $d_{in}$  is the inner diameter of the ring,  $\rho$  the density and  $s_{11}^E$  is the elastic compliance at a constant electric field.

Oscillation of the wall:

$$f_{R\_wall} = \frac{1}{(d_{out} - d_{in})\sqrt{\rho \cdot s_{11}^E}} \quad (26)$$

Where  $d_{out}$  is the outer diameter and  $d_{in}$  is the inner diameter of the ring,  $\rho$  the density and  $s_{11}^E$  is the elastic compliance at a constant electric field [78].

### 2.2.1.3. Piezo bending plates

Basic piezo bending plates consists of a three-layer composite, made of a piezo plate agglutinated onto a thin substrate, in general made of a thin metal plate. When a DC-voltage is applied, the piezo membrane contracts or expands, depending on the direction of the voltage applied. As a reason, that the piezo plate is glued onto the membrane, the whole structure bends up or down resulting from the expansion or contraction of the piezo plate.

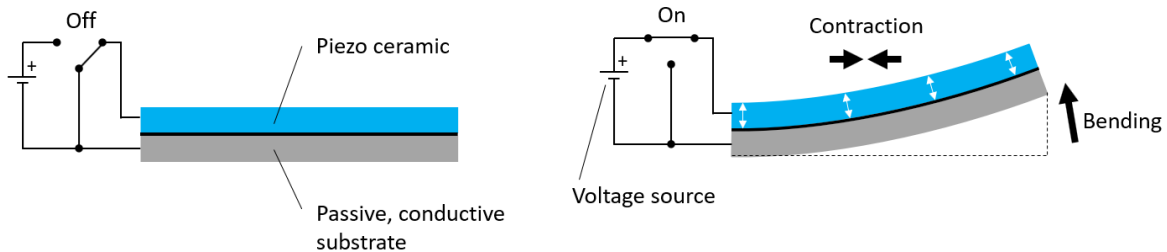


Fig. 22: schematic representation of a piezo bending plate agglutinated onto a passive, conductive substrate [80]

The oscillation happens due to bending vibration of the plate, when an oscillating voltage is applied. The resonant frequency is approximated to:

$$f_R = \frac{\alpha_n^2 \cdot t}{4 \cdot l^2 \sqrt{3\pi\rho \cdot s_{11}^E}} \quad (27)$$

Where  $\alpha_n$  is a non-linear correction coefficient and for the lowest oscillation mode  $\alpha_1 = 1.875$ ,  $t$  is the thickness,  $l$  the length,  $\rho$  the density and  $s_{11}^E$  is the elastic compliance at a constant electric field [81].

#### 2.2.1.4. Round Piezo bending elements

Round piezo bending elements consists of a three-layer structure, made of a smaller round piezo disc glued centrally on a bigger in general a circular metal membrane. When a voltage is applied between the top side of the piezo disc and the metal membrane, the piezo disc expands or contract in size depending on the polarization of the applied voltage. As a reason, that the piezo disc is glued onto the metal membrane the whole structure bends up or down like a bowl.

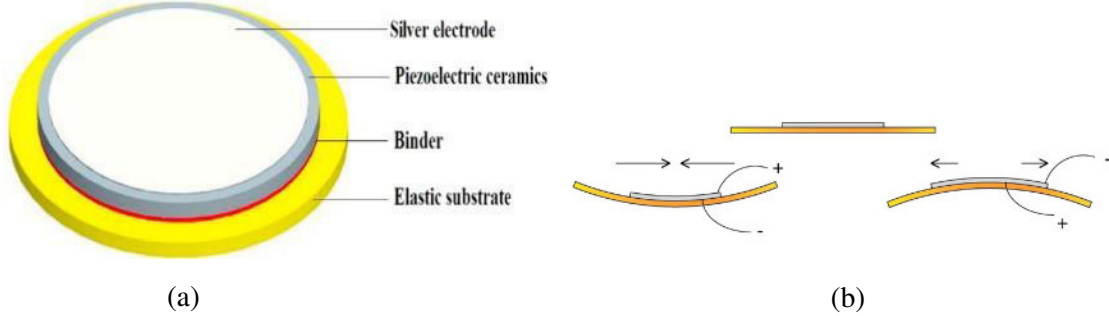


Fig. 23.: schematic representation of a round piezo bending element; a) composition of a round piezo bending element [82]; b) theory of operation [83]

The oscillation happens due to bending vibration of the plate, when an alternating voltage is applied on top and bottom of the big flat surface. Approximation of the resonance frequency of the round piezo bending membranes are done according to [84], [85]:

$$f_R = \frac{\alpha_n \cdot t}{2\pi r^2} \sqrt{\frac{E_{tot}}{12\rho_{tot} \cdot (1 - \nu_{tot}^2)}} \quad (28)$$

Where  $\alpha_n$  represents a vibration constant of the piezo membrane, depends on the number of the oscillation mode.  $t$  is the thickness of the three-layer structure,  $r$  the radius of the metal membrane,  $E_{tot}$  the mean Young modulus,  $\rho_{tot}$  the mean density and  $\nu_{tot}$  the mean Poisson ratio of the three-layer composite of the metal membrane, bonding glue and the piezo disc.

The mean Young modulus and the mean Poisson ratio of the two-layer structure, the piezo disc and the bonding epoxy resin is calculated via [86]:

$$E' = C_1 E_{PZT} + C_2 E_{bond} + \frac{C_1 C_2 E_{PZT} E_{bond} \cdot (v_{PZT} - v_{bond})^2}{C_1 E_{PZT} \cdot (1 - v_{bond}^2) + C_2 E_{bond} \cdot (1 - v_{PZT}^2)} \quad (29)$$

$$v' = \frac{C_1 v_{PZT} E_{PZT} \cdot (1 - v_{bond}^2) + C_2 v_{bond} E_{bond} \cdot (1 - v_{PZT}^2)}{C_1 E_{PZT} \cdot (1 - v_b^2) + C_2 E_{bond} \cdot (1 - v_{PZT}^2)} \quad (30)$$

Here  $E_{PZT}$ ,  $v_{PZT}$ ,  $E_{bond}$ ,  $v_{bond}$  are the Young modulus and the Poisson ration of the piezo material and the epoxy resin respectively. The constants are given by  $C_1 = \frac{h_{PZT}}{h_{PZT}+h_{bond}}$ ,  $C_2 = \frac{h_{bond}}{h_{PZT}+h_{bond}}$ , where  $h_{PZT}$  and  $h_{bond}$  is the thickness of the piezo material and the epoxy resin respectively. Subsequently the Young modulus of the three-layer structure is calculated using the same equations:

$$E_{tot} = C_3 E' + C_4 E_{mem} + \frac{C_3 C_4 E' E_{mem} \cdot (v' - v_{mem})^2}{C_3 E_{mem} \cdot (1 - v'^2) + C_4 E' \cdot (1 - v_{mem}^2)} \quad (31)$$

$$v_{tot} = \frac{C_3 v_{mem} E_{mem} \cdot (1 - v'^2) + C_4 v' E' \cdot (1 - v_{mem}^2)}{C_3 E_{mem} \cdot (1 - v'^2) + C_4 E' \cdot (1 - v_{mem}^2)} \quad (32)$$

Here  $E_{mem}$ ,  $v_{mem}$ , are the Young modulus and the Poisson ration of the membrane material. The constants are given by  $C_3 = \frac{h_{mem}}{h_{PZT}+h_{bond}+h_{mem}}$ ,  $C_4 = \frac{h_{PZT}+h_{bond}}{h_{PZT}+h_{bond}+h_{mem}}$ , where  $h_{mem}$  is the thickness of the metal membrane.

The mean density of the composite is finally approximated to:

$$\rho_{tot} = \frac{\rho_{PZT} r_{PZT}^2 h_{PZT} + \rho_{mem} r_{mem}^2 h_{mem} + \rho_{bond} r_{bond}^2 h_{bond}}{r_{PZT}^2 h_{PZT} + r_{mem}^2 h_{mem} + r_{bond}^2 h_{bond}} \quad (33)$$

Where  $\rho_{PZT}$ ,  $\rho_{mem}$  and  $\rho_{bond}$  is the density of the piezo material, the metal membrane and the epoxy resin respectively, and  $r_{PZT}$ ,  $r_{mem}$ ,  $r_{bond}$  is the radius of the three materials.

## 2.2.2. Filler/Backing Material

During operation of the sender, elastic waves are emitted from both the front and backside of the transducer membrane. As well the receiver may pick up waves from the two surfaces of the diaphragm. Both, the sender and receiver membranes are mounted on the same structure that the distance between them is fixed, and they are connected using cooper wires, which too can transmit elastic waves. Consequently, the elastic waves emitted from the sender may additionally propagate over the structure of the sensor solution, leading to inaccurate measurement results. Thus, backing material must be attached to the backside of the sender and receiver membrane respectively. In literature it was mentioned, that the backing material must feature enough acoustic attenuation to prevent reverberation, but if the attenuation is too high the sensitivity of the

sensor would be affected [87]. In ultrasonic applications the ceramic piezo transducer elements usually are backed by a metal epoxy-resin composite, matching the acoustic impedance of the transducer material [88], [89]. In lower frequency applications various other materials are mentioned like bitumen, hot melt glue, closed-cell foam which are used as backing material and cork, felt, elastomeric foam, fiberglass as vibration isolation [87], [90].

### 2.2.3. Probing Signals

For measurement of the phase velocity of elastic waves in the specimen a probing pulse as signal is necessary, thus the time delay between the send and received pulse can only be evaluated, if the same position of the wave can be recognized in both, the sent and received wave.

In literature various probing signals were published like a single pulse, a wave train overlaid by a  $\sin^2$ -function or a white noise source [23], [67], [68], [70].

Various of the probing signals mentioned in literature had been tested, but in all of them higher harmonics were included. Since shear waves show dispersion in human tissue, shown in 1.2.2.4., the higher frequent waves will propagate more fast in tissue, than the low frequent waves, leading to imprecise propagation time measurements. Therefore, a wave train pulse featuring a narrow frequency spectrum is required. As is well known, the frequency spectrum of a gaussian wave train is itself a gaussian function. Thus, a gaussian wave package was modelled using a homemade MATLAB script and uploaded to the arbitrary waveform generator using the “Agilent IntuiLink Waveform Editor”. The repetition rate of the signal sent by the waveform generator specifies the center frequency of the wave package. The repetition rate times 180 in this case yield to the center frequency of the wave package.

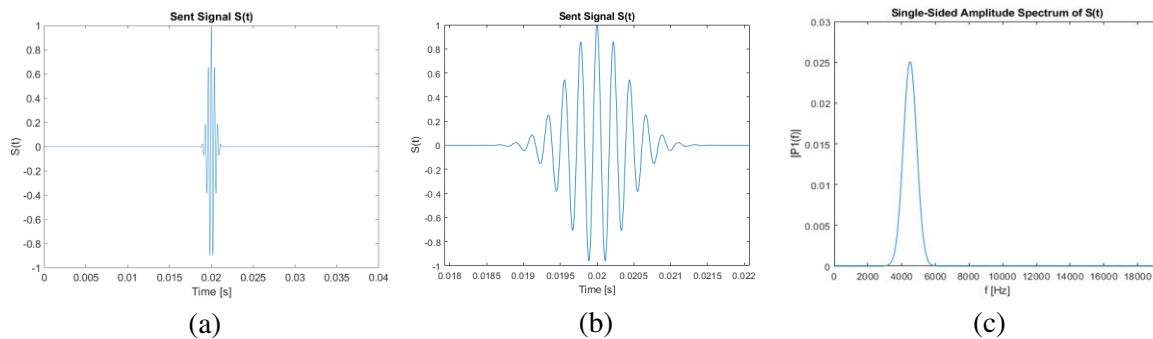


Fig. 24: Wave package modelled in MATLAB and uploaded to the frequency generator as arbitrary signal; a) full scale view of the signal; b) enlarged view of the signal; c) single-sided amplitude spectrum of the signal;

The bandwidth of the signal is given with the full width at half maximum which is  $\approx 940\text{Hz}$ .

## 2.2.4. Amplification and filtering of the received signal

As described in section 1.6 the charges in the piezoelectric disc gets separated due to external stress performed by the shear waves propagating on the connected tissue below. The separated charges lead to an electric field across the disc. As a fact, that the shear respectively surface waves propagating on the tissue measured are marginal, the strain performed onto the membrane and piezoelectric disc is minimal leading to a weak electric field. For accurate measurement of this low electric field generated by piezoelectric sensors an amplifier featuring a high input impedance is necessary. To prevent unnecessary conduction losses the amplifier circuit should be built next to the receiving piezo membrane [91], [92].

The receiving piezo membranes are directly laid and slightly pressed onto the skin surface in vivo. During the measurement process small low frequency vibrations caused by small movements of the person measuring as well as by the heartrate of the test person disturb the measurement process. Therefore, this low frequency noise must be filtered from the receiving signals. Additionally, the sensor solution is energized via a power supply and an arbitrary frequency generator both energized via the mains, featuring a frequency of 50Hz. Thus, this range of frequency additionally must be filtered from the received signals. As described above, the probing signal consists of a gaussian wave package featuring a narrow bandwidth, higher frequencies must not be filtered from the receiving signals, thus only an active high-pass filter for filtration of the low frequency noise is necessary. Since the amplitude of the signal is used for evaluation of the attenuation coefficient of the specimen the amplification factor of the active high pass filter must be equal over the entire frequency bandwidth of the measurement signal. A specific property of an amplifier is the unity gain bandwidth, which specifies the frequency whereat the open-loop voltage gain is dropped to 0dB. This critical frequency  $f_c$  of an amplifier is calculated by[93]:

$$f_c = \frac{f_{gbw}}{G} \quad (34)$$

Here  $f_{gbw}$  is the specific unity gain bandwidth of the applied amplifier and  $G$  is the desired gain. Since a high gain over a wide bandwidth is required, the use of two amplifiers in cascade or an amplifier featuring an extraordinary high  $f_{gbw}$  is necessary [93].

Since the input of the amplification circuit must feature a high input impedance an FET-amplifier has to be applied as pre-amplifier of the circuit. In general, non-inverting amplifiers feature a high input impedance in comparison to other circuits like the inverting amplifiers, thus the signal is directly connected to the high-resistance non-inverting input. An active high pass filter can be established out of the connection of a passive high pass in serial with a non-inverting amplifier.



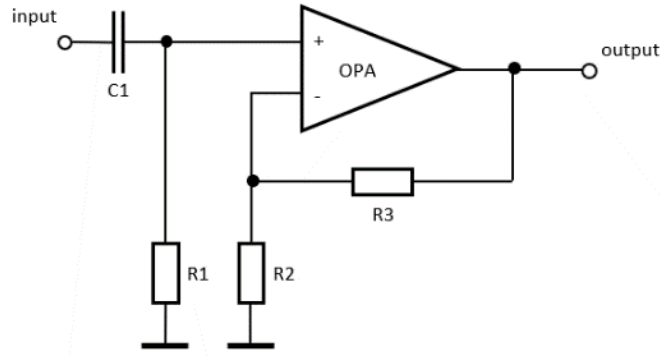


Fig. 25:non- inverting active high pass filter; OPA...operational amplifier

The gain of the non-inverting high pass filter is given as:

$$G = 1 + \frac{R_3}{R_2} \quad (35)$$

Calculation of the critical frequency of the circuit is done according to:

$$f_c = \frac{1}{2\pi \cdot R_1 C_1} \quad (36)$$

The frequency and phase response of the whole circuit is calculated by:

$$A = \frac{G \frac{f}{f_c}}{\sqrt{1 + \left(\frac{f}{f_c}\right)^2}} \quad (37)$$

$$\varphi = \tan^{-1}\left(\frac{1}{2\pi f R_1 C_1}\right) \quad (38)$$

As it is widely known, the frequency response of two filters connected in serial are multiplied and the phase response are summed up to obtain the values of the total circuit [94].

## 2.2.5. Composition of the sensor solution

According to the guidelines specified in 1.3 the sensor solution has restrictions in size. Additionally, the connection wires between the receivers and the individual related amplifiers must be as short as possible, as a result, that the unamplified signals are not influenced by inductive coupled parasitic signals.

For evaluation of the elasticity and the viscosity of the object measured the shear/surface wave speed as well as the damping length in the media is to be determined. Via measurement of the running time from the

sender to the receiver, the time of stimulation of the piezo sensor and the skin beneath must be considered. Thus, via application of one receiver only the running time including the stimulation time can be evaluated, shown in Fig. 26. Additionally, the initial amplitude of the wave injected by the sender is unknown and cannot be evaluated, neither by the signal amplitude nor by the deflection calculation of the piezo bending membrane, because the efficiency of injection is unknown and increase with ascending contact-pressure.

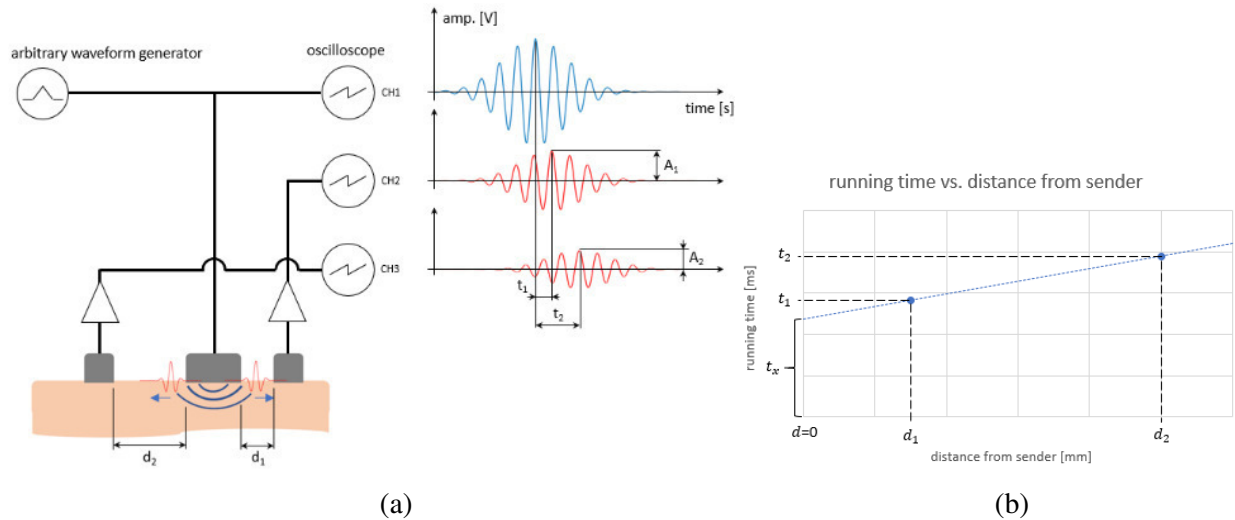


Fig. 26: fundamental composition and functionality of the sensor solution; a) principal functionality of the sensor solution; the blue colored oscillation represents the sent signal, and the red colored oscillations the received ones;  $d_1$ ,  $d_2$  ...distances between the sender and receiver 1, 2 respectively;  $t_1$ ,  $t_2$  ...running time of the signal from the sender to receiver 1, 2;  $A_1$ ,  $A_2$  ...maximal signal amplitudes observed on the receiver 1, 2; b)  $d_1$ ,  $d_2$  ...distances between the sender and receiver 1, 2 respectively;  $t_1$ ,  $t_2$  ...running time of the signal from the sender to receiver,  $t_x$  ...axis intercept of the running time, can additionally be interpreted as the stimulation time; like described above, if only one receiver is applied the stimulation time cannot be separated from the “raw” running time

Therefore, the running time as well as the amplitude of the elastic wave in the media between minimum two different distances must be evaluated leading to the fact that at least two receivers featuring a different distance to the sender are necessary.

A major advantage of the round piezo membrane is, that the sender emits a circular wave, if it is fabricated symmetrically and applied levelled onto the surface of the measured object. Thus, signals in all surface directions around the sender can be received. To prevent influence between two receivers via the arrangement of one after another one of the receivers is placed on the opposite side of the sender, both featuring different distances to the sending piezo membrane. Since the elements are not dotlike but rather have a specific dimension, the running time of certain areas of the testing tissue is evaluated, shown in figure Fig. 27. The higher the difference of the distance between the sender and both of the receiver the more accurate the speed can be evaluated, however the sensor solution has restrictions in dimension a maximal size is predefined in the guidelines 1.3.

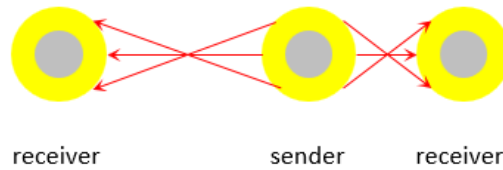


Fig. 27: Arrangement of sender and receiver elements, visualizing the disadvantage of the size of the sensors, leading to the fact, that the running time evaluated is not uniaxial, rather it results from a bigger angular range of the investigated material

To achieve good connection between the individual sensor element and the specimen, the sensor solution is laid onto the measurement object and slightly pressed against it. The more the sensors are pressed onto the specimen the harder the material gets due to compression and secondary dents start to arise at the position of the individual sensor. Additionally, the material in between the dents gets tensioned, leading to a rising modulus of elasticity and finally to wrong results of measurement.

During investigation of the sensor solution the variation of the amplitude of the receiving signal with different contact forces whilst measurement on human skin has been evaluated. Measurements had been executed at the thenar eminence and the volar forearm of a test person in vivo.

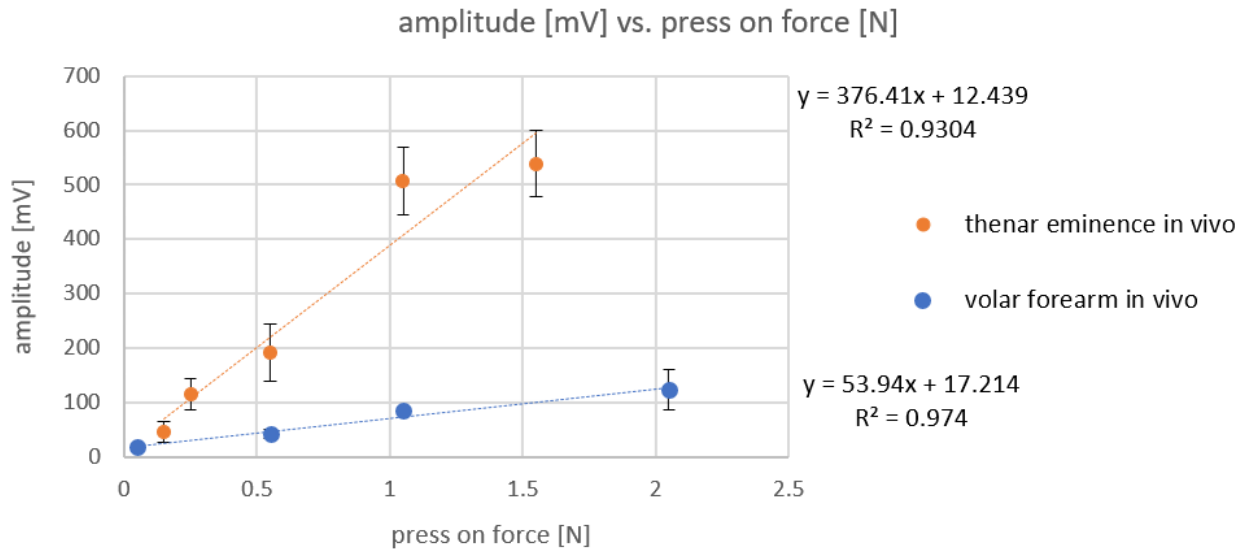


Fig. 28: variation of the amplitude of the receiving signal with variation of the contact pressure (press on force)

As seen in Fig. 28 the amplitude of the receiving signal increase with increasing contact force. Hence, the contact pressure must be known, that the amplitude of the received signal can be used for evaluation of the damping coefficient.

To find a compromise between the achievement of a sufficiently high amplitude of the measurement signal on the one side, but not a too high contact pressure causing skin hardening on the other side, it was found, that a force of approximately 500mN per sensor element is optimal.

## 2.3. Measurement setup

The testing setup by which all measurements presented in this thesis are performed, were established using a waveform generator, oscilloscope and a DC-power supply. The arbitrary waveform generator was used for generation of the sending signal and as supply of the trigger signal for the oscilloscope. Via the 4-channel digital storage oscilloscope, featuring an external trigger input, the visualization of the receiving signals and record of the measurements were performed. An additional DC power supply was necessary for supply of the amplification and evaluation circuit of the sensor solution:

	Waveform generator	Oscilloscope	DC power supply
Manufacturer	Agilent/Keysight	Agilent/Keysight	Agilent/Keysight
Type	33250A	DSO6014A	E3631A OE3
Serial number	MY40019994	MY45007916	MY40053816
Calibration expiry	06/2019	06/2019	06/2019

Table 1: Equipment used within the test setup

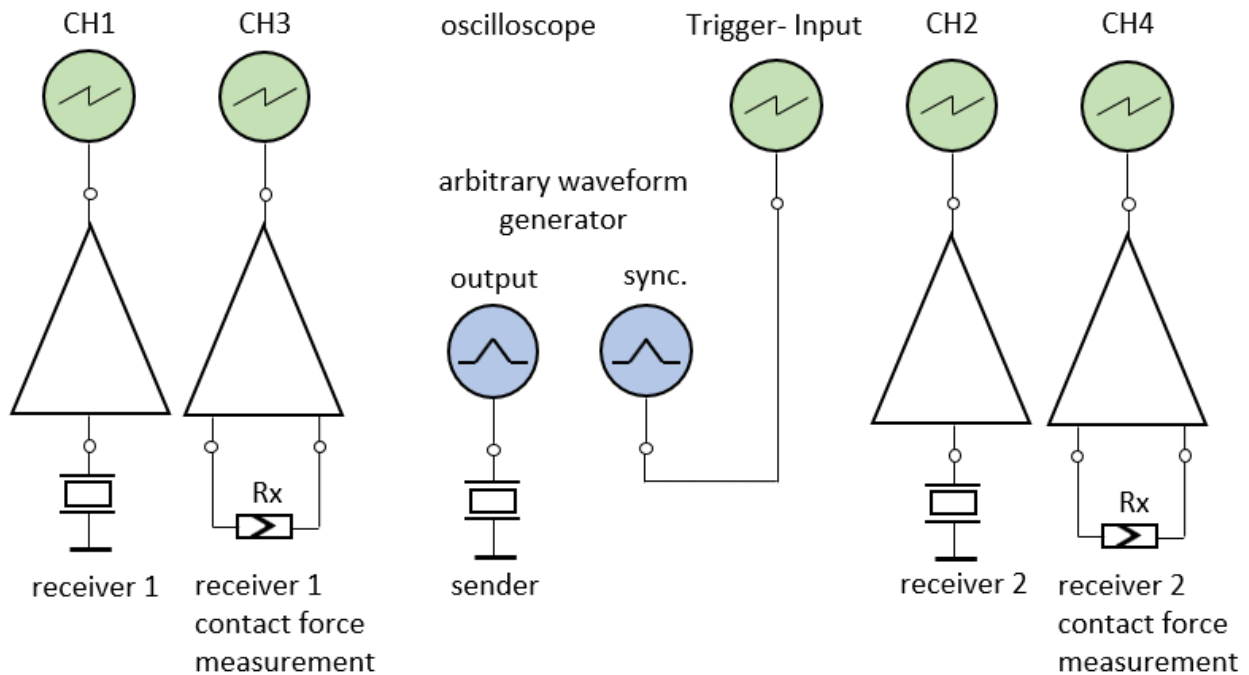


Fig. 29: schematic representation of the test setup; the sending signal was not registered on the oscilloscope, but it was later fit into the evaluation software, thus it was anyway generated by another MATLAB script; Rx...represents the force sensing resistor

As a result, that the piezo bending membranes which are directly laid onto the skin surface in vivo are straight connected to the ground potential of the setup, the whole setup had to be insulated from the mains

supply using an insulation transformer. Insulation of the whole setup including the final sensor solution was tested according to the technical standards for the safety and essential performance of medical electrical equipment IEC 60601-1 as well as to the technical standards of testing of medical electrical equipment and medical electrical systems IEC62353. The test certificates of the performed tests are added in the supplementary. Safety tests were performed using the electrical safety analyzer Rigel 288 shown in Table 2.

	Safety analyzer
Manufacturer	Rigel medical
Type	Rigel 288
Serial number	002062-28A-0930
Calibration expiry	04/2019

*Table 2: safety analyzer used for performing of the safety tests*

## 2.4. Evaluation of the measurement signal

Like shown in Fig. 29 the received and subsequently amplified signals as well as the associated contact force measurement signals of both receivers are visualized and recorded by the digital storage oscilloscope. As a result, that the oscilloscope only features 4 channels the sending-signal is not recorded. For evaluation of the running time and the amplitude of both receiving signals the visualized curves are converted to a \*.csv file and subsequently stored onto a USB-stick. These stored files are subsequently read by a homemade MATLAB-program for evaluation of the running time between the sender and each receiver as well as the amplitude and the contact pressure.

As a result, that human skin is a dispersive media the previously sent wave package may change its shape via induction and propagation in skin. Due to the narrow bandwidth of the wave package sent and that the wave-package does not difflence, it was assumed that the phase velocity is approximately equal to the group velocity. Caused by various unknown parameters sometimes the group velocity propagates slightly slower than the phase velocity, leading to slightly variable shapes of the received wave package. Thus, two methods had been elaborated for measurement of the running time.

The first method is based on the evaluation of the phase velocity via determination of the center maxima of the gaussian wave package. Since it was assumed, that the group velocity is slightly slower than the phase velocity the positive half-wave before the center maximum sometimes show the same height or is slightly higher than the center maximum. Therefore, a threshold of 80% of the maximal amplitude of the wave

package was calculated. Subsequently the first point of intersection between this threshold and the wave-package defines the positive half-wave directly before the center maximum of the wave-package.

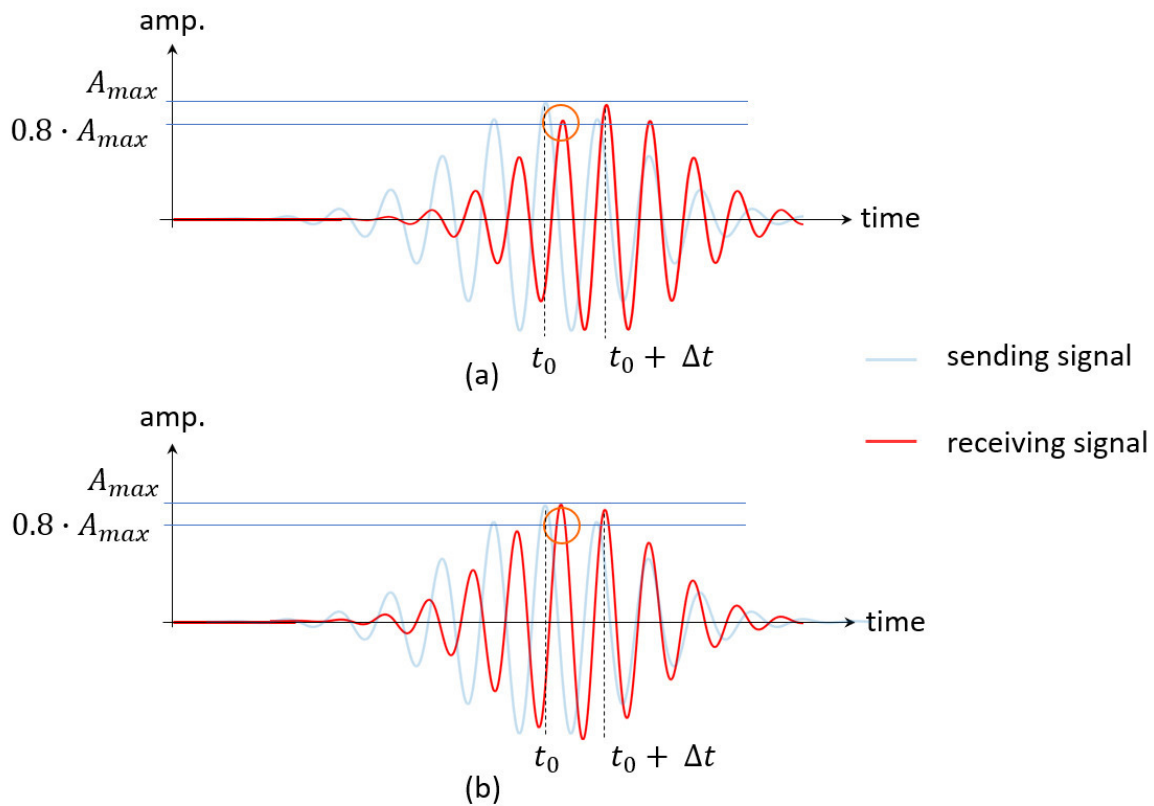


*Fig. 30: Method for evaluation of the running time from the sender to the individual receiver, via observing the center oscillation of the signal a) received wave have equal shape than the sent wave b) shape of the received wave is modified, the group velocity of the received wave is slightly slower than the phase velocity;  $t_0$  ...point in time when the wave was sent;  $\Delta t$  ...running time of the signal*

The second method is based on the determination of the running time of the wave group, via calculation of the envelope of the gaussian wave package. The running time is determined out of the time delay from the maximum of the envelope of the received wave group, to the maximum of the envelope of the sent wave group shown in Fig. 31.

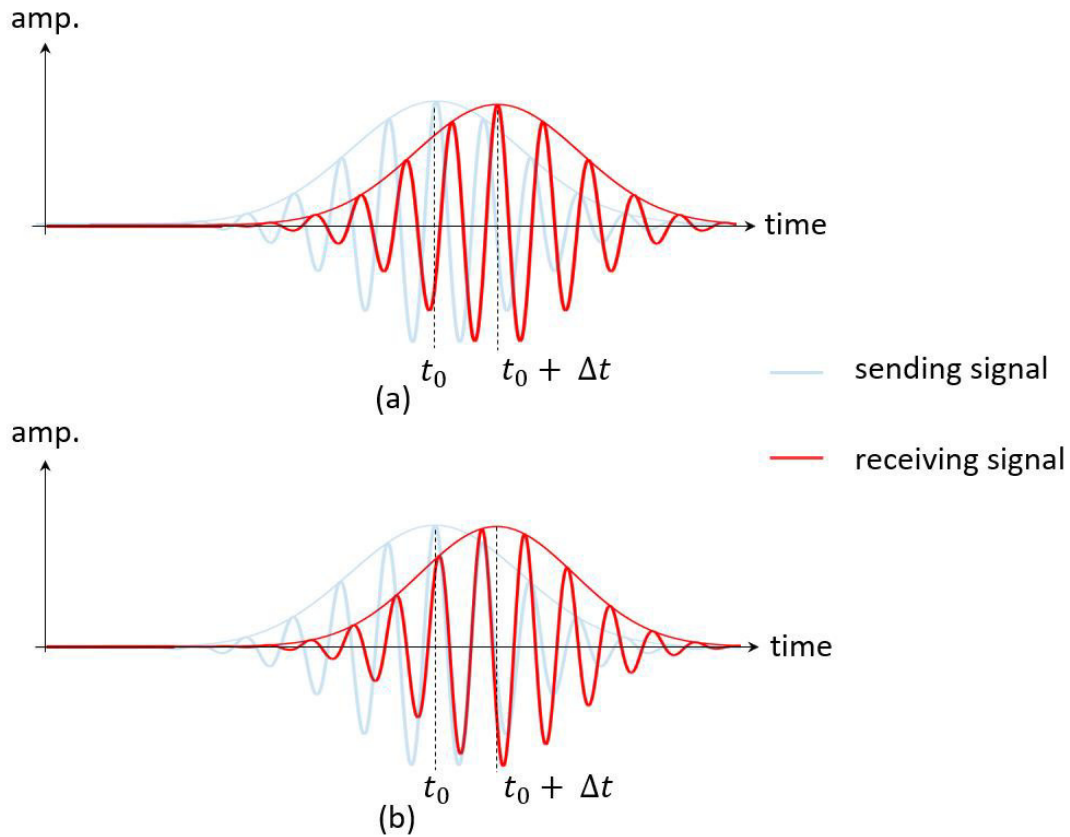


Fig. 31: Method for evaluation of the running time from the sender to the individual receiver, via observing the center of the gaussian wave package via calculation of the envelope of it; a) received wave have equal shape than the sent wave b) shape of the received wave is modified, the group velocity of the received wave is slightly slower than the phase velocity;  $t_0$  ...point in time when the wave was sent;  $\Delta t$  ...running time of the signal

The amplitude for evaluation of the damping coefficient is determined via the maximal amplitude without generation of the envelope of the received signal.

Calculation of the wave velocity is done according to the following equation:

$$c_s = \frac{d_2 - d_1}{t_2 - t_1} \quad (39)$$

Here  $d_1$ ,  $d_2$  and  $t_1$ ,  $t_2$  is the distance as well as the running time of the sender to receiver 1 respectively receiver 2. The damping coefficient is calculated according to equation (11).

## 2.5. Phantoms

Human skin is an inhomogeneous, anisotropic, non-linear viscoelastic material under prestress in vivo. Additionally, the elasticity of skin varies during time, after moisturizing and with differing water content. The interpretation of measurement results on skin in vivo presume previous knowledge about the measurement method and the sensor solution itself. Additionally, measurement values on skin can strongly vary during time, and with changing ambient conditions, although if the measurements are taken at the same skin position. Therefore, a material providing constant properties was necessary for previous tests of the sensor solution. Consequently, rubber materials featuring various shore hardness degrees represent a homogenous, isotropic medium featuring a constant elastic modulus. Additionally, production of skin phantoms featuring similar properties like skin were researched in literature, for collection of measurements under likewise and stable conditions.

### 2.5.1. Rubber phantoms

Rubber material like EPDM (ethylene propylene diene monomer rubber) are not as sensitive to the ambient condition like human skin in vivo and doesn't change its hardness during a short period of time. Therefore, rubber plates featuring a dimension of approximately 10x10cm and 5mm in thickness were used for a pretest of the sensor solution to verify that the resulting measurement values stay stable during various measurement cycles performed within several days. The characteristic values of the rubber plates used are listed in Table 3:

Type [95]	Shore A hardness	Density [kg/m <sup>3</sup> ] [95]	Poisson ratio [96]
101/EPDM 25	25 ±5	1000	0.499
001/AKD30	30 ±5	1030	0.499
002/E4580	50 ±5	1050	0.499
005/E9614	70 ±5	1220	0.499
008/E9575	80 ±5	1300	0.499

*Table 3: characteristic values of the rubber plates used as phantoms*

The hardness of polymers and rubbers are indicated by the shore hardness scales, which is measured using the shore durometer measurement tool, based on the indentation method. In literature an equation is given for approximation of the Young modulus out of the shore A hardness scales [97].



$$E = \frac{3F_0Y}{8p_0r} \quad (40)$$

Where  $F_0$  is the initial compressing spring force,  $p_0$  is the initial indenter protrusion,  $r$  is the radius of the indenter and  $Y$  is the dimensionless Young modulus given as:

$$Y = \frac{1 + Mi \cdot \frac{S}{100}}{1 - \frac{S}{100}} \quad (41)$$

Here  $Mi$  is the indenter stiffness (called mechanical indentability), introduced by Mix et. Al., and  $S$  is the shore Hardness reading on the durometer hardness scales [97].

For standardized hardness scales these parameters are predefined. For shore A hardness scales, the equation (40) changes to:

$$E = \frac{165(1+0.1364S)}{7.9(100-S)} \text{ [MPa]} \quad (42)$$

## 2.5.2. Self-made phantoms

For taking measurements on specimens like skin but isotropic in nature, manufacturing techniques for skin-mimicking phantoms imitating the various layers and featuring a similar viscoelastic behavior were researched in literature. Additionally, the skin phantoms must exhibit a resistant top layer, thus comparative measurements using the Cutometer can be applied without any rupture of the phantom material.

Several techniques, using various silicone products or biodegradable materials like agar or gelatin are postulated in literature [56], [98]–[108].

Result of the research lead to multilayered agar-gelatin skin mimicking phantoms according to the instruction of Chen et. Al., thus the shear modulus of each layer could be adjusted using higher respectively lower concentration of agar or gelatin [100]. Increase of mechanical strength of the top layer for Cutometer measurements is performed with addition of glutaraldehyde. Glutaraldehyde in this case is used as cross-linker between the collagen fibers of gelatin [85]. Additionally, the effect of concentration of agar and gelatin onto the alteration of Young modulus is well documented in this paper.

Comparison measurements were performed with:

	Cutometer
Manufacturer	Courage&Khazaka electronic GmbH
Type	440-33N
Calibration expiry	06/2019

*Table 4: Cutometer used for comparative measurements*

As container for the skin phantom a petri dish made of acrylic glass featuring a diameter of 145mm and a height of 21mm was utilized.

Several phantoms were produced, but various problems had to be faced, till a useful product was established. Some of the experienced difficulties were:

- The phantom except the epidermis layer must not be dried under a suction hood, thus the water within the layers vanish and they start to dry and contract.
- The BSA (bovine serum albumin) of the initial recipe from Chen et Al. was added to increase the attenuation of the compressional wave in the phantom. Since only shear or surface waves are measured this ingredient can be neglected.
- If more ethanol is added than written in the initial recipe the phantom is stable for several weeks without growing bacteria's or mushrooms
- While pouring out the liquid gelatin or agar solution into the petri dish it should be considered, that the surface is totally even without any gas inclusion and the border must completely be wetted by the liquid solution, thus no surface contraction occurs during gelling.

Weight measurements were performed on:

	Precession scales
Manufacturer	Acculab
Type	ATILON ATL-224-V
Serial number	25804870
Calibration expiry	11/2018

*Table 5: Scales used for weight measurement during production of self-made phantoms*

Best results were achieved using the following instructions:

Base Layer:

- 45.21g dist. water
- 4.206g gelatin
- 10ml ethanol

The water and gelatin were mixed at room temperature and stirred with a rotation speed of about 200rpm to be sure that only as less as possible air bubbles are mixed under the solution. The Petri dish was cleaned using alcohol to verify that it is hardly not contaminated. Finally, the base layer was poured to the empty base layer. Attention.: the gelatin solution must be heated to minimum 55°C for min. 2min to verify, that all the gelatin powder had been dissolved. After heating to 55°C the Ethanol was slowly added. After all gelatin smears vanished the solution was cooled to about 45°C when it was finally poured into the petri dish. The base layer got approx. 2h gelling time (not under the suction hood!!!!) till the hypodermis-layer was poured onto it.

Hypodermis Layer:

- 56.72 g dist. Water
- 0.233g agar
- 30.001g dist. Water
- 2.32g gelatin
- 30ml ethanol

The agar as well as the gelatin solution were mixed and heated apart, and finally commingled when both powders were fully dissolved in its own solution. It is recommended, that the magnetic stir bar only rotates very slowly in case that no air bubbles are generated. After mixing of both solutions in one container ethanol was added very slowly. Finally, when the solution was cooled down using a colt water bath to lower than 40°C under continuously stirring at 50rpm it was poured onto the fully gelled base layer. The hypodermis layer got approx. 2h gelling time (not under the suction hood!!!!) till the dermis-layer was poured onto it.

Dermis:

- 24.77g dist. Water
- 0.343g agar
- 7.92g gelatin
- ethanol

All three ingredients were mixed at room temperature. In this phase, it needs to be checked, that all the gelatin powder is soaked even a little with water, otherwise the remaining dry gelatin powder cannot be dissolved in the warm/hot solution. Subsequently the mixture is heated under constantly stirring at 70rpm to over 95°C for more than 2min to verify, that all the agar and gelatin powder has fully dissolved. After the solution was cooled down using a cold-water bath under constant stirring. When the temperature was below 60°C ethanol was added. Subsequently, the solution already featuring a temperature of approximately 50°C was poured onto the fully gelled hypodermis layer.

Half an hour later the dermis layer was fully gelled, and the epidermis layer could be placed on the top of the phantom.

Epidermis layer:

- 24.998g dist. Water
- 2.517g gelatin powder
- 25µl liquid glutaraldehyde

The two parts were mixed at room temperature and subsequently heated to over 55°C for more than 2 min. During heating 1ml glycerol was added using a pipette. After the gelatin powder was fully dissolved 25µl liquid glutaraldehyde was mixed in. Finally, the solution was poured on a previously cleaned Plexiglas plate. After a drying time of approximately of 1 day the ultrathin plastic like material was carefully separated from the Plexiglas plate and cropped into a round shaped disc featuring the same diameter than the petri dish to finally apply it onto the dermis layer of the skin phantom. During this process it has to be considered, that no air bubbles are trapped between the two layers.

## 2.6. In-vivo measurements

For verification of the functionality under real environment measurements were performed on various skin sites on male and female test persons. Comparative measurements were performed with the gold standard appliance, used for measurements of skin elasticity, the Cutometer MPA 580 (Courage & Khazaka Electronic GmbH, Cologne, Germany).

## 2.6.1. Measurements without moisture

Measurements had been taken on 16 healthy subjects (6 women and 10 men) in age between 26-56 years on both arms of each proband, except one man only was measured on the left arm. With respect to physiological variations the skin elasticity was investigated on four positions of each arm:

- On the volar forearm approximately 5cm before the elbow, representing a protected area from sun and daily hand wash treatment and in general the skin in this area is very smooth and pliable.
- The back of the hand between the index finger and the thumb, to incorporate smooth skin subjected to increased external influences due to sun exposure and daily treatment by washing hands or other actions
- The thenar eminence which in general is representing harder and thicker skin than on the previously mentioned positions
- On the side of the hand under the small finger, representing a combination skin of smooth skin from the back of the hand and hard skin from the hand inside.

### Bland – Altman plot and analysis

In literature the Bland-Altman Plot and Analysis is used for comparison of two measurement methods [109]. Therefore, for comparison of the two measurement methods, the gold standard appliance the Cutometer and the novel sensor solution a Bland-Altman Analysis was calculated. For application of this analysis tool both measurement methods must exhibit the same variable. Thus, for comparison the values obtained with the sensor solution are converted to Cutometer data. Hence, the obtained values of eight randomly chosen probands had been taken for calculation of the correlation equation between the two methods. Subsequently the quantified values of the remaining eight probands were used for calculation of the Bland-Altman Plot and Analysis. A test for distribution of the difference value of the two methods must be done in advance, that the Bland-Altman-Analysis can be applied. Thus, a Kolmogorov-Smirnov-test was performed under usage of a significance level of  $P < 0.05$  [110].

## 2.6.2. Measurements with moisture

Measurements had been taken on four subjects (1 woman, 3 men) in the age between 29 to 40 years on two skin sites on both arms.

- On the volar forearm approximately 5cm before the elbow, representing a protected area from sun and daily hand wash treatment and in general the skin in this area I very smooth and pliable.

- The thenar eminence which in general is representing harder and thicker skin than on the previously mentioned position

## **3. Results**

### **3.1. Sensor Solution**

#### **3.1.1. Selection and calculation of the appropriate sensor element**

##### **3.1.1.1. Selection of the piezo element type**

As a result, that the sensor solution is contemplated to be flexible, and that only low power as well as low voltage (protective extra low voltage) is available two piezo materials are privileged as piezo sensor elements. On the one side the piezo material should be flexible and on the other side, the dielectric charge constant should be as high as possible, that the applied low voltage results in a movement as large as possible. Subsequently research lead to two potential materials, the PVDF Polymer film and the PZT ceramics. The PVDF polymer film is a flexible piezo electric material and the PZT ceramics is nowadays the material featuring the highest available dielectric charge constant. Comparison of both materials is done in Table 6.

Material	PVDF	PZT
Pro	<ul style="list-style-type: none"> <li>flexible</li> </ul>	<ul style="list-style-type: none"> <li>high dielectric charge constant</li> <li><math>d_{31} \approx -315 \frac{10^{-12}C}{N}</math></li> <li><math>d_{33} \approx 640 \frac{10^{-12}C}{N}</math> [76]</li> <li>mass production of piezo discs and rings</li> <li>mass production of round and plate bending membranes</li> </ul>
Contra	<ul style="list-style-type: none"> <li>low dielectric charge constant</li> <li><math>d_{31} \approx 21 \frac{10^{-12}C}{N}</math></li> <li><math>d_{33} \approx -32 \frac{10^{-12}C}{N}</math> [76]</li> </ul>	<ul style="list-style-type: none"> <li>fragile</li> <li>contains lead</li> </ul>
Other properties	<ul style="list-style-type: none"> <li>Young modulus</li> <li><math>E = \frac{1}{s_{11}^E} \approx 2.5GPa</math> [76]</li> <li>Density:</li> <li><math>\rho \approx 1780 \frac{kg}{m^3}</math> [111]</li> </ul>	<ul style="list-style-type: none"> <li>Young modulus</li> <li><math>E = \frac{1}{s_{11}^E} \approx 70.4GPa</math> [76]</li> <li>Density:</li> <li><math>\rho \approx 8100 \frac{kg}{m^3}</math> [76]t</li> </ul>

Table 6: Comparison of piezoelectric materials

Using the material constants of both materials the resonant frequency of tiny piezo elements was approximated using the above-mentioned formulas (the sizes of the elements were chosen):

Element type	Round disc	Round ring	Bending plate	Bending disc
Dimensions	d=6.5mm t=0.2mm	d <sub>in</sub> =3mm d <sub>out</sub> =6.5mm t=0.2mm	d=6.5mm t=0.2mm	d=6.5mm t=0.2mm
Resonant frequency	f <sub>R_thk</sub> ≈3-7MHz f <sub>R_rad</sub> ≈50-200kHz	f <sub>R_thk</sub> ≈3-7MHz f <sub>R_rad</sub> ≈80-200kHz f <sub>R_wall</sub> ≈0.3-1MHz	f <sub>R</sub> ≈1.5-5kHz	f <sub>R</sub> ≈13.5kHz [112]

Table 7: Comparison of resonant frequencies of piezo elements featuring various shapes

As shown above, only the resonant frequencies of the bending plates as well as the bending discs are in range of the measurement frequencies determined, for stimulation of elastic waves using shear waves.



For round discs or rings, the diameter as well as the thickness of the elements would exceed the previously specified limitations, if elements should be built in the desired frequency range below 30kHz.

As a result, that the piezo bending elements made of PZT material are available in stock, cheap and offered in various sizes they were preferred for development of an initial prototype. For a primary sensor solution, it was decided to use the bending piezo discs, thus they can be laid directly onto the surface of the skin for exciting elastic waves in it. Additionally, the round membranes emit circle elastic waves, which subsequently can be received in all surface directions on the skin. Piezo bending plates must be placed in upright position to inject an elastic wave in the tissue. It was assumed, that the construction of a sensor solution using piezo bending plates lead to a sensor solution thicker than specified in the predefined guidelines. Thus, the round piezo bending membranes were chosen for development.

### 3.1.1.2. Calculation of round piezo bending membranes

A market research showed, that there are various dimensions made of different materials of round piezo bending membranes available. But for evaluation of the anisotropy of the skin the transmission and reception area of the sensor must be as small as possible. Best would be a dot-like send respectively receiving area to get highest accuracy in direction, thus the smaller the diameter of the piezo membrane the more accurate the evaluation of the anisotropy and the phase velocity.

In general, the resonant frequency of the piezo bending membranes is suggested being lower than 30kHz like described in 1.5.1.5..

The smallest round piezo membrane found on market featured a diameter of 6.5mm, a thickness of 0.2mm and resonant frequency of 13.5kHz [112], [113]. As described in 1.5.1.5 the maximal measurement frequency mentioned in literature is approximately 30kHz, and the smaller the diameter of the membrane the more accurate the measurement values. Therefore, it was tried to develop the smallest possible membrane within this frequency range.

PI Ceramic GmbH & Co. KG offered the production of a tiny batch of 10 piece of round piezo membranes for an acceptable price. Hence, the piezo disc with the lowest diameter featuring a low thickness from this company was chosen. To achieve high deformation with low voltage application of the three-component structure the material with the highest available piezoelectric charge constant  $d_{31}$  was selected [114]. The properties of the offered piezo disc was:

diameter [mm]	3.0
thickness [mm]	0.15
material	c255
density [kg/m <sup>3</sup> ]	7800
Poisson ratio	0.34
charge coefficient $d_{31}[\frac{10^{-12}C}{N}]$	-180
Young modulus [N/m <sup>2</sup> ]	$4.83 \cdot 10^{10}$

Table 8:Parameter of the selected round piezo disc from PI Ceramic GmbH & Co. KG

Primarily various materials were considered as membrane material, like brass-alloys, CuBe2, stainless steel and nickel-alloys. Initially, CuBe2 and nickel-alloys were rejected because of the harmful material beryllium and possible allergies to nickel. As a fact, that the lower the Young modulus of the membrane material, the lower the resonant frequency of the three-layer structure, brass a metal with a very low Young modulus in comparison to other metals was chosen as membrane material. Additionally, the material of the membrane should be manufactured in condition of spring-hardness to ensure the necessary oscillation properties which is important for the application.

material	CuZn30
density [kg/m <sup>3</sup> ]	8550
Poisson ratio	0.35
Young modulus [N/m <sup>2</sup> ]	$11.5 \cdot 10^{10}$

Table 9:Parameter of the selected brass alloy [115],[116]

Usually the bonding layer between the two materials consists of epoxy resin [86]. The thickness of this layer was assumed to 20μm.

material	Epoxy Resin
density [kg/m <sup>3</sup> ]	1250
Poisson ratio	0.30
Young modulus [N/m <sup>2</sup> ]	$0.35 \cdot 10^{10}$

Table 10: Parameter of the epoxy resin layer [86], [117]

The minimal diameter of the necessary metal membrane then can be calculated according to the formulas mentioned in 2.2.1. The vibration constant in the lowest oscillation mode is given as  $\alpha_1=3.196$ , and as

resonance frequency of 20kHz was chosen to have adequate space to the limit of 30kHz, mentioned in 1.5.1.5 [84].

For a membrane thickness of 0.05 – 0.1mm a minimal diameter of 4.5 – 5mm resulted. As the manufacturer told, that the thicker membranes are easier to handle, because they don't get harmed as easy than the thinner ones, membranes featuring a thickness of 0.1mm and a diameter of 5mm were chosen. Additionally, the slightly bigger membrane is simpler to connect via soldering, than the smaller one.

The finally resulting piezo membranes were characterized by the manufacturer using the Impedance Analyzer 4294A from Agilent leading to the following characteristic mean values of the 10 ordered piezo bending membranes:

	C [pf]	tan( $\delta$ ) [ $10^{-3}$ ]	$R_s$ [ $\Omega$ ]	$f_s$ [kHz]	$f_p$ [kHz]	$k_{eff}$
Minimum	843.6	20.9	1154.6	19.6	20.4	0.23
Mean	865.8	21.4	1615.36	20.17	20.9	0.257
Maximum	883.5	22.0	2076.6	21.2	21.8	0.28
STDDEV	12.43	0.36	373.15	0.49	0.43	0.02

*Table 11: characteristic values of the piezo bending membranes ordered from PI Ceramics*

The finally delivered membranes were handmade, because we only ordered a small batch of 10 pieces by the manufacturer. During hardening in the furnace of the agglutinated three-layer structure, the piezo disc aquaplaned on the brass membrane and the glue, hence the piezo disc was finally not placed in the center of the brass membrane, which could have been led to a quality loss of the signal received with them.

### 3.1.2. Selection of the backing material

Combinations of various materials mentioned above were tried as backing and vibration isolation. With usage of bitumen and epoxy resin as backing the membranes were damped too intense, that no signal could be registered anymore. Using combinations of other materials, showed high leakage of vibration through the material and the structure of the sensor solution. Finally, the best solution was made of one layer of the light weight closed cell foam chosen as backing material agglomerated directly onto the connection side of the round piezo membrane and beneath one layer of felt connecting the damped sensor to the structure for vibration isolation. Additionally, the enameled copper wires connecting the piezo membranes were 0.1mm in diameter, that vibrations from the piezo membranes can hardly propagate through the wire to the circuit board.

### 3.1.3. Amplification and filtering circuit

Like shown above, the resonant frequency of the piezo bending membranes is around 20kHz, subsequently the passband of the whole amplification and filter circuit was chosen to be in range between 1-20kHz, leading to a critical frequency of the high pass filter of 1kHz. During investigation it has been shown, that an amplification factor of 60dB is adequate for robust evaluation of the receiving signals and that a filter slope of 40dB/decade is effectual for filtration of the low frequent signals. Hence, two non-inverting active high-pass filters in serial to each other has been chosen as amplification and filtration circuit, shown in Fig. 32.

Since the amplification factors were split to both amplifiers of the circuit and the E12 series for resistor selection has been used, the pre-amplifier features a slightly lower gain than the subsequent one. To obtain a high input resistance despite the preconnected passive high pass circuit, the resistor R1 was chosen to 1M $\Omega$ , leading to a capacitor C1 of 180pF and finally to an input impedance of 1.88M $\Omega$  at the critical frequency. To obtain a critical frequency of 1kHz at a 3dB drop-off with two filter stages, the critical frequency of the first stage has yield to 884Hz and of the second stage to 219Hz under usage of the E12 series of resistors and capacitors. Thus, the critical frequency of the entire circuit is 936Hz.

Since the input of the amplification circuit must feature a high input impedance as well as a high unity gain bandwidth an OPA604 has been chosen as pre-amplifier. This amplifier features an FET as input, thus exhibiting an input resistance of  $r_i = 10^{12}\Omega$ . For selection of the second amplifier only a wide unity gain as well as a low current consumption was important, leading to selection of the NE5532A. The circuit has been established on a circuit board using the 0603 SMD package size for resistors and capacitors. The amplifiers featured a package size of SOIC-8. The frequency and phase response of the amplification circuit, shown in Fig. 33, has performed using the devices mentioned in Table 1.

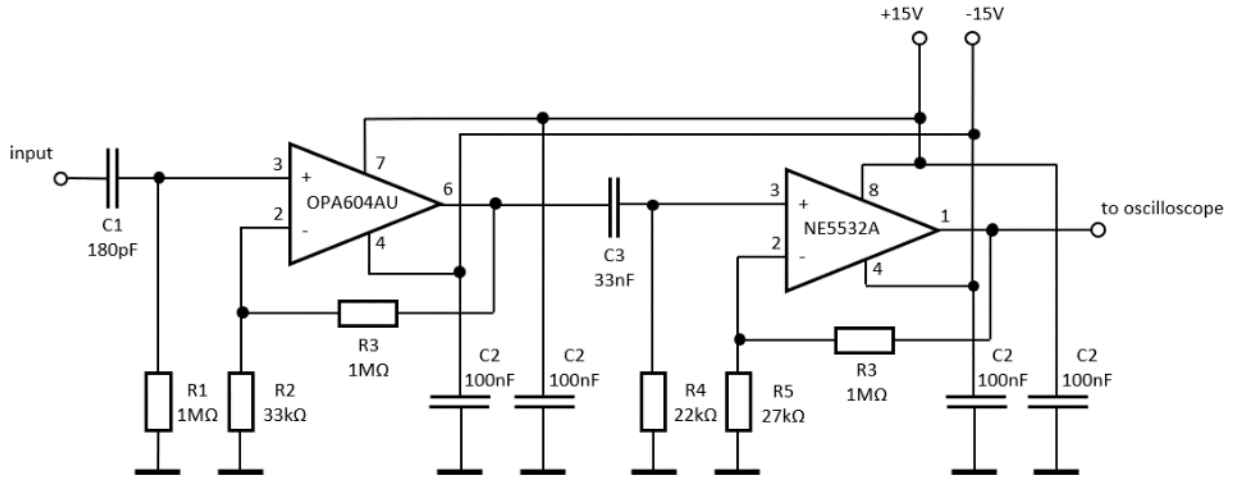


Fig. 32: circuit diagram for amplification of the individual receiver signal

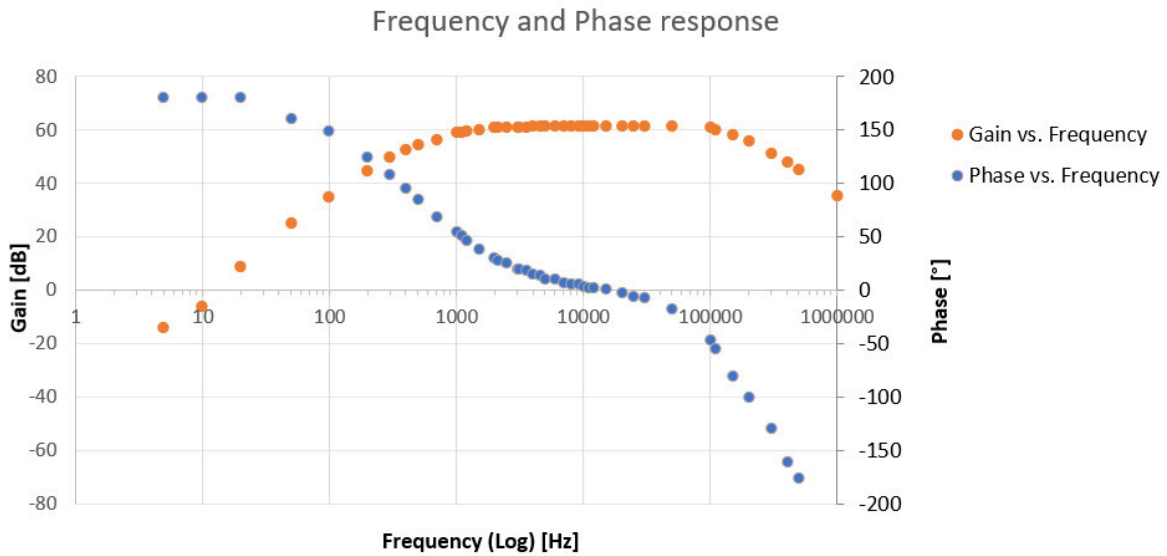


Fig. 33: frequency and phase response of the filtering an amplification circuit

The filtering and amplification circuits for both receivers had been established identical.

### 3.1.4. Contact pressure measurement

The contact pressure measurement was executed with force sensing resistors placed directly under the damping of the individual receiver, to evaluate all the stylus force. The resistor value of the load cell is transformed to a voltage signal using the impedance converter circuit shown in Fig. 34

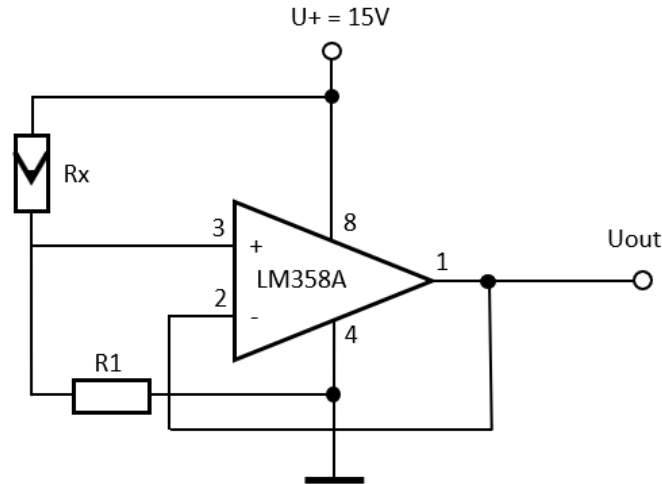


Fig. 34: impedance conversion circuit for evaluation of the force sensing resistor; Rx...force sensing resistor, R1 =200kΩ

The resistor R1 has been chosen to 200kΩ to obtain a good voltage to force ratio in the area around 500mN. To convert the individual measurement value of the load cells into physical force values the characteristic curve of the load cells was determined by application of various predefined weights onto the load cell while the output voltage of the amplification circuit was measured. The resulting characteristic curve shown in Fig. 35, was averaged and subsequently fitted using a homemade MATLAB script is.

The equation of the curve fit is given as:

$$F = \frac{e^{\frac{U_L - 3.626}{1.605}} + 43.28}{233.5} \text{ [N]} \quad (43)$$

Here  $U_L$  is the voltage obtained after the impedance converter of the force sensing resistor.

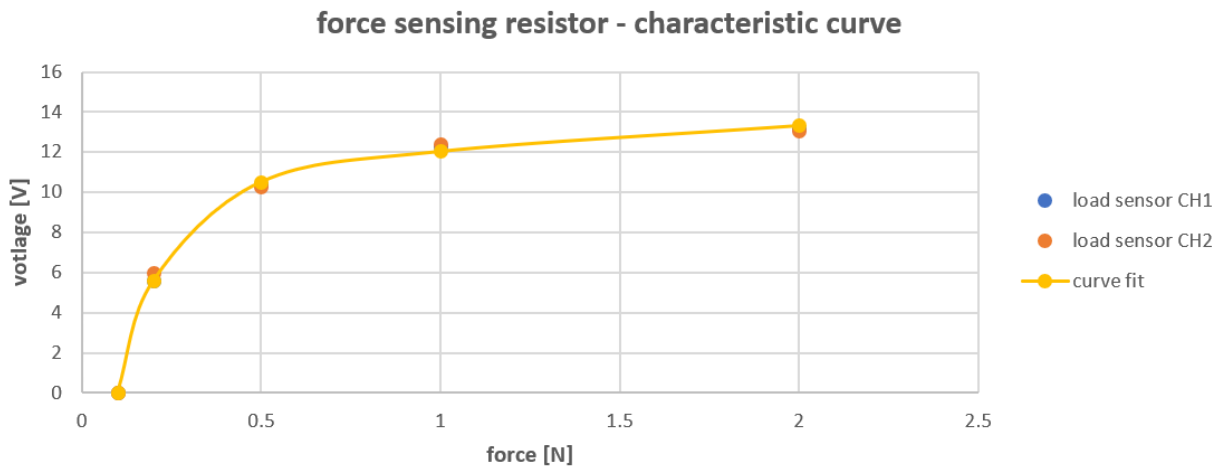


Fig. 35: characteristic curve of the force sensing resistor connected to the impedance conversion circuit, obtained using various known weights applied onto it; the resulting values were fitted subsequently in MATLAB

### 3.1.5. Composition of the sensor solution

The sensor solution is established on a circuit board featuring a thickness of 1mm, since the sensors can be placed on the one side of the pattern while the amplification circuits and connections are soldered on the other side of it.

The distance between the sender and the receivers were chosen to 3mm for receiver 1 and 10mm for receiver 2 respectively. These distances were chosen to satisfy a compromise. If the distance between the sender and one receiver is too narrow, the two piezo membranes could touch each other, due to the soft and shaky structure of the backing material. If the distance between the sender and receiver is too wide, the received signal is too weak for the achievement of robust results.

Since the distance between the sender and the receiver 2 is 10mm an adequate gap between the skin wrinkle shaped by the press on force and the case of the sensor solution was required. Therefore, stabilizers featuring a small recess for inclusion of the soft damping material bonded to the piezo bending membrane were modelled and printed in a 3d printer. Between the circuit board and the stabilizers, the force sensing resistors were applied to absorb the total contact pressure of the individual receiver. Since the sender is in between of the two receivers no force measurement was required.

The total size of the final sensor solution without the cables is (l x b x h) 56mm x 48mm x 14mm.

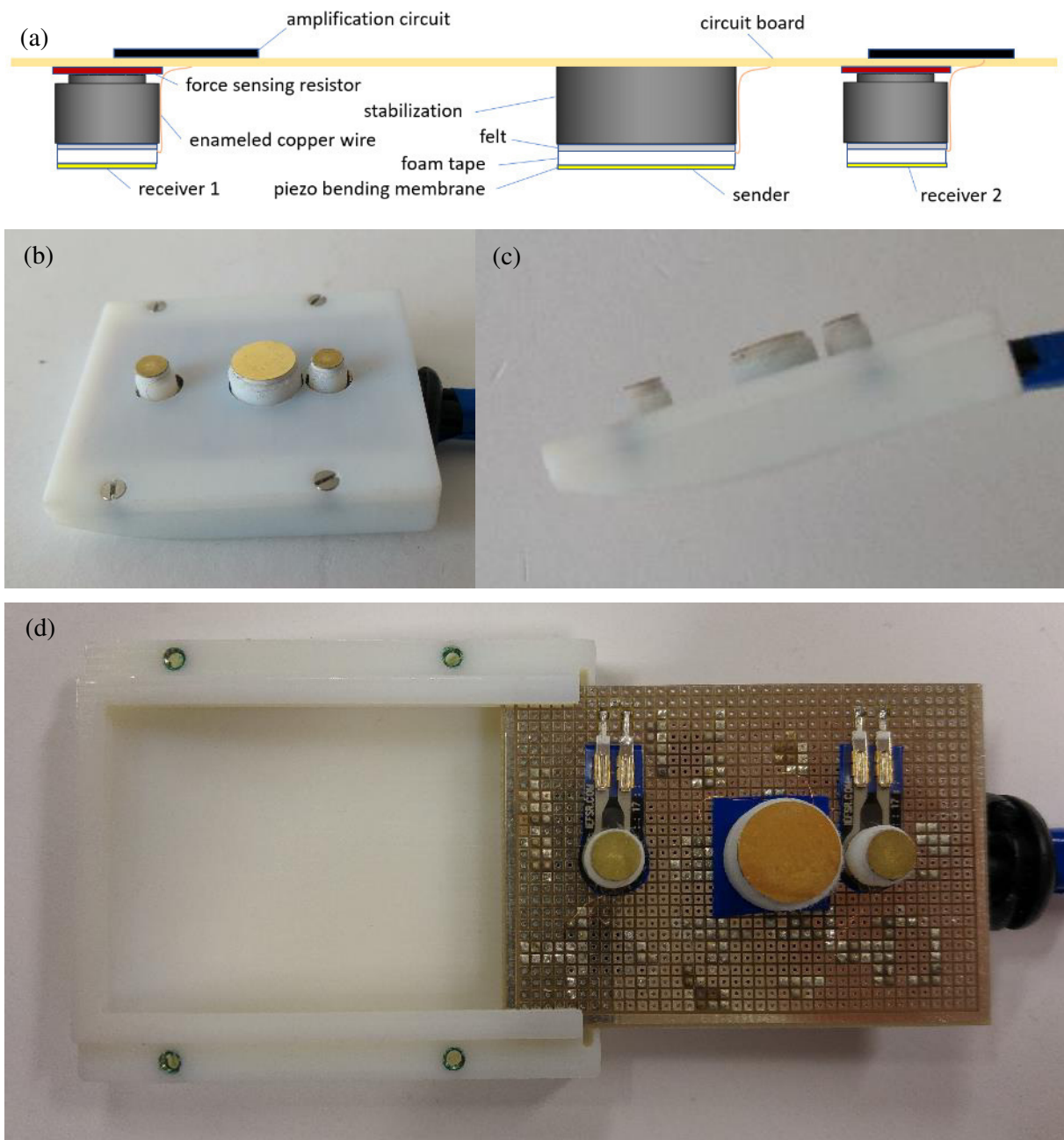


Fig. 36: Composition of the final sensor solution; a) schematic representation of the final sensor solution; b) oblique view of the sensor solution inside the case; c) side view; d) top view of the sensor solution, when the bottom of the case is removed;

## 3.2. Phantoms

To establish a validity of the developed sensor solution initial tests had performed on rubber plates featuring a dimension of 10x10cm and 5mm thickness. The rubber plates were made of EPDM material exhibiting a shore A hardness between 25 to 80. For further investigation measurements on self-made skin phantoms of



gelatin and agar powder were performed, thus these phantoms were isotropic and homogenous in comparison to human skin in vivo. For evaluation of the measurement values only the method based on observation of the center oscillation using a threshold value, described in 2.4 was applied.

### 3.2.1. Rubber material

Measurements were performed on the center of the rubber plate to ensure, that influence of boundary effects caused by reflections or other side effects are minimized.

In general, five measurements per rubber plate were performed to receive a statistic over the measurement values. After each single measurement the sensor solution was totally lifted from the specimen and placed again on the center of the rubber plate to ensure, that there are no systematically faults generated by placing the sensor solution on the plate. During investigation measurements on the rubber plates had been performed featuring various center frequencies of the gaussian wave package. Most robust results had been established under preset of 8.1kHz as center frequency. With lower frequencies the amplitude of the signals on hard rubber materials like shore 80 was too low, and with higher frequencies highly fluctuating measurement values were observed.

The Young modulus was obtained out of the amplitudes  $A_1, A_2$  measured, the wave velocity  $c_s$  calculated by formula (45) and the equations (8)(10)(11)(12)(13)(14), leading to:

$$E = 2(1 + \nu) \sqrt{\left( \frac{\left( \frac{\omega}{c_s} \right)^2 - \left( \frac{\ln \left( \frac{A_1}{A_2} \right)}{d_2 - d_1} \right)^2}{\left( \frac{\omega}{c_s} \right)^2 + \left( \frac{\ln \left( \frac{A_1}{A_2} \right)}{d_2 - d_1} \right)^2} \right)^2 + \left( \frac{\left( \frac{\omega}{c_s} \right) \cdot \left( \frac{\ln \left( \frac{A_1}{A_2} \right)}{d_2 - d_1} \right)}{\left( \frac{\omega}{c_s} \right)^2 + \left( \frac{\ln \left( \frac{A_1}{A_2} \right)}{d_2 - d_1} \right)^2} \right)^2} \quad (44)$$

Here  $\nu$  is the Poisson ratio and  $\rho$  the density of the investigated material, and  $\omega = 2\pi f$  is the angular frequency. The values for  $\nu, \rho$  were taken from Table 3.

The wave velocity is given by:

$$c_s = \frac{d_2 - d_1}{t_2 - t_1} \quad (45)$$

Here  $d_1 = 3mm$  and  $d_2 = 10mm$  are the distances from the sender to the individual receiver, and  $t_1, t_2$  are the running times measured to them.

The resulting measurement data for the Young modulus were compared to theoretical values mentioned in literature using equation (42).

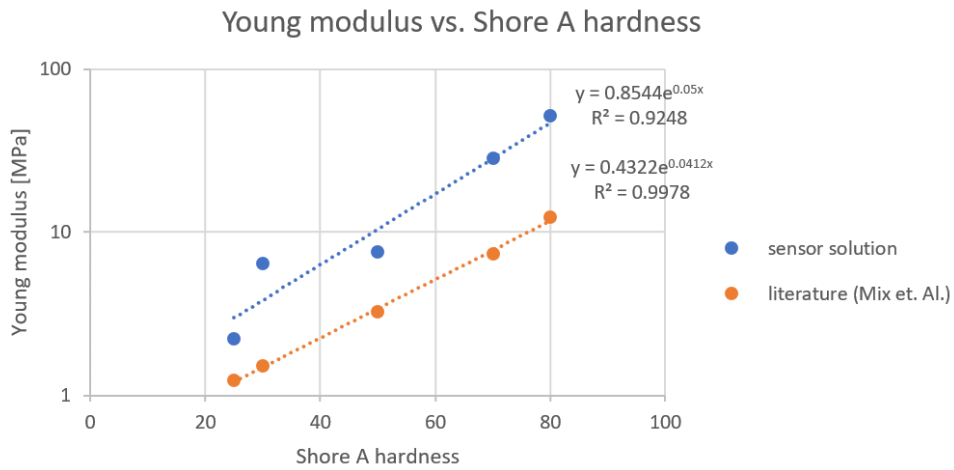


Fig. 37: result of the measurement data observed on the rubber phantoms compared to values calculated out of an equation mentioned in literature

The measurement values are in good agreement with the theoretical values from literature [118]. Especially the exponential coefficient shows a similar value [97].

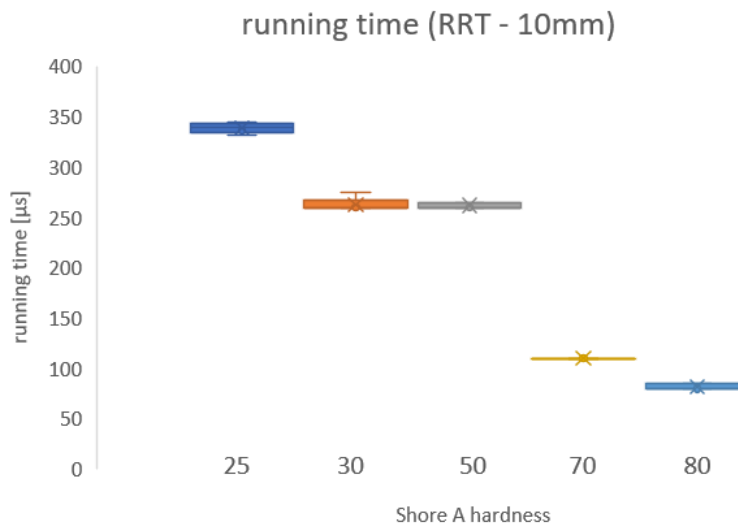


Fig. 38: running time data of the receiver in 10mm distance to the sender observed on the rubber phantoms

In literature various sites on healthy human skin in vivo were investigated using a shore O durometer leading to measurement values 25-58 in shore O readings [119], yielding to shore A hardness of 20-45 [120].

### 3.2.2. Self-made phantoms

Measurements were performed as far as possible on the center of the skin phantom to ensure, that influence of boundary effects caused by reflections or other side effects are minimized.

Five measurements were performed on each measurement day to obtain a statistic over the measurement values. After each measurement the sensor solution was totally lifted from the specimen and again placed on the center to ensure, that there are no systematically faults generated by placing the sensor solution. Measurements of the skin phantom were performed with 2.7kHz center frequency of the gaussian wave package.

For comparison of the measurement values obtained from the skin phantom the same position was observed by the Cutometer. Cutometer measurements were executed using the test probe featuring a diameter of 2mm. The time/strain mode was applied with three consecutive cycles of a 2 sec suction, followed by a 2 sec relaxation period. A suction pressure of 500mbar was preset.

Measurement results of the sensor solution are compared to the results from the Cutometer shown in Fig. 39.

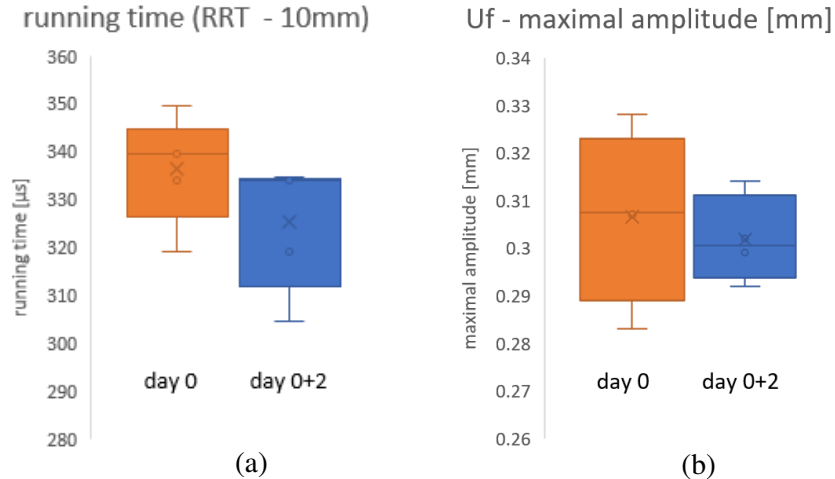


Fig. 39: comparison of the measurement data observed using the sensor solution to the data recorded with the Cutometer on the skin phantom at a specific day and two days later; a) running time obtained with the receiver in 10mm distance to the sender; b) distensibility  $U_f$  measured with the Cutometer

Like seen in Fig. 39 the running time in distance of 10mm measured by the sensor solution as well as the distensibility -  $U_f$  measured by the Cutometer slightly reduces after two days from the first measurement. In comparison to the rubber phantoms, the skin phantom has similar running time values like the rubber material featuring a Shore A hardness between 25-30.

	day 0	day 0+2
shear modulus [MPa]	10.4	4.98
Young modulus [MPa]	27.46	13.15
attenuation coefficient [1/m]	31.8	82.5
time difference [ $\mu$ s]	67.3	93.2
wave velocity [m/s]	103.9	75.1
amplitude 10mm [V]	0.91	0.63

Table 12: Results obtained on the skin phantom using the sensor solution [121]

The wave velocity as well as the shear modulus of the skin phantom shows lower values two days after the primary observed data. These values stay in contrast to the one obtained for the running time in 10mm distance, thus interpretation of these values is vaguely possible.

### 3.3. In vivo measurements

As stated earlier, all skin sites investigated had been tested primarily using the sensor solution and afterwards by the Cutometer for comparison. Measurements with the Cutometer were taken with the sensing probe featuring an aperture of 2mm. The time/strain mode was applied with three consecutive cycles of a 2 sec suction followed by a 2 sec relaxation period. A suction pressure of 500mbar was preset. All measurements were performed under constant ambient conditions of 20°C  $\pm$ 3°C and 40-60% relative humidity.

During investigation it has been shown, that the wave velocity in skin rise with higher frequencies and that the lower the frequency, the more robust the results. Since the resonant frequency of the receiving piezo membranes is around 20kHz, signals with frequencies below approximately 2kHz are not sensed well by the piezo bending membranes. Best results had been observed at 2.7kHz on various skin positions.

### 3.3.1. Measurements without moisture

Measurement protocol:

- Each test person primarily had to find a relaxed position for his arms
- The test sites on the arm were cleaned using alcohol pads and subsequently a drying phase of approximately 2 minutes was awaited
- All four sites were investigated by the sensor solution. On each position ten measurements were taken for statistics while in between each measurement the sensor solution was slightly lifted from the testing site and subsequently placed again for prevention of systematical faults.
- Subsequently all four sites were investigated by the Cutometer, one measurement on each testing site
- Then same steps were repeated for the right arm

Measurement values investigated on the side of the hand under the small finger had been removed from the evaluation, thus the skin in this site consists of combination skin. Further explanation is given in 4.5.

In literature the two gold standard appliances the Cutometer and the Reviscometer had been compared to each other under investigation of human skin in vivo mentioned in 1.5.3. Like shown in Fig. 15 a positive correlation had been found in literature, between the distensibility -  $U_f$  obtained by the Cutometer versus the running time (RRT – in a distance of 2mm under usage of an elastic wave featuring a frequency of 4.5kHz) received using the Reviscometer on the same skin site. A similar correlation was found with the sensor solution shown in Fig. 40.

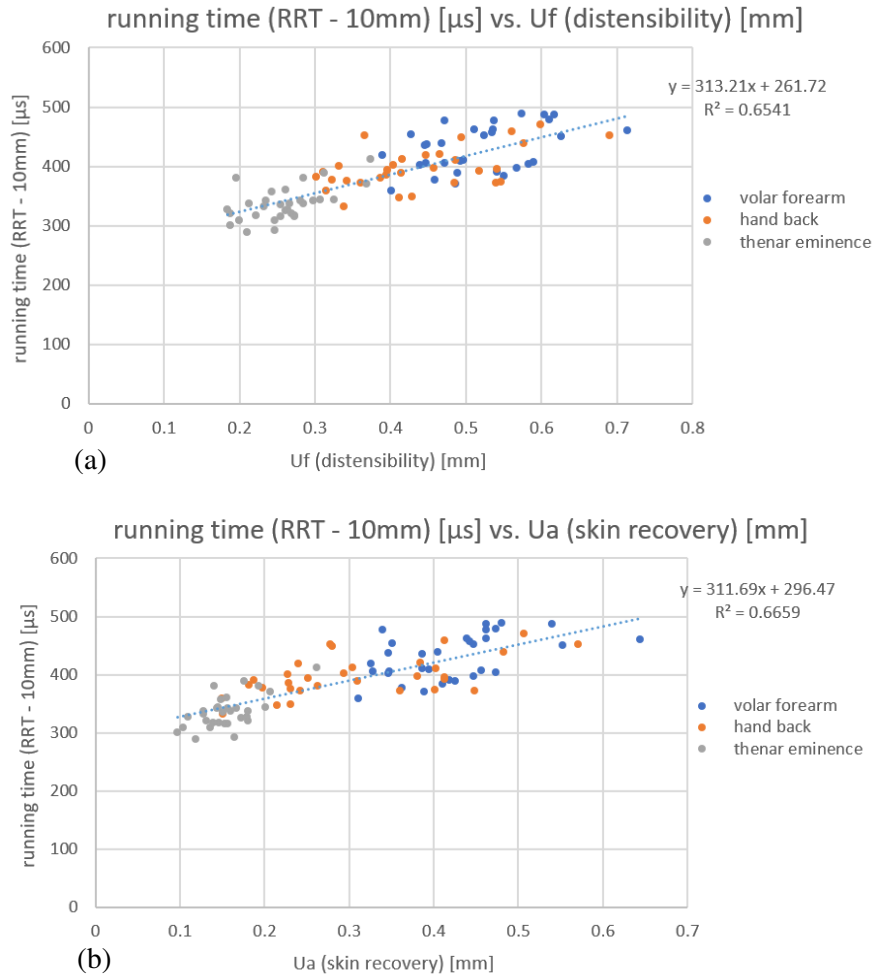


Fig. 40: Correlations between measurement values of the Cutometer and the sensor solution; Similar correlations were found in literature shown in Fig. 15 a) distensibility  $U_f$  of the Cutometer vs. the running time to the receiver in 10mm distance to the sender of the sensor solution; b) skin recovery  $U_a$  measured by the Cutometer vs. the running time to the receiver in 10mm distance to the sender of the sensor solution;

Additionally, it is well seen in the image above, that “hard” skin like on the thenar eminence is classified in the low running time, low distensibility area, and the values obtained on the volar forearm is assorted in the higher values of both measurement techniques. As mentioned in literature, human skin is comparable to shore hardness values between 20-45, mentioned in 2.5.1, the running time on human skin shows values between 300-500 $\mu$ s while on rubber with shore A hardness between 25 to 50 yield to running time values from 250 - 350 $\mu$ s shown in Fig. 38.

Calculation of the wave velocity is done according to equation (45). As a result, that the distances are fixed on the sensor solution it is evident, that the resulting values lead to a hyperbolic-function, if they are compared to the distensibility of the Cutometer, shown in Fig. 41.

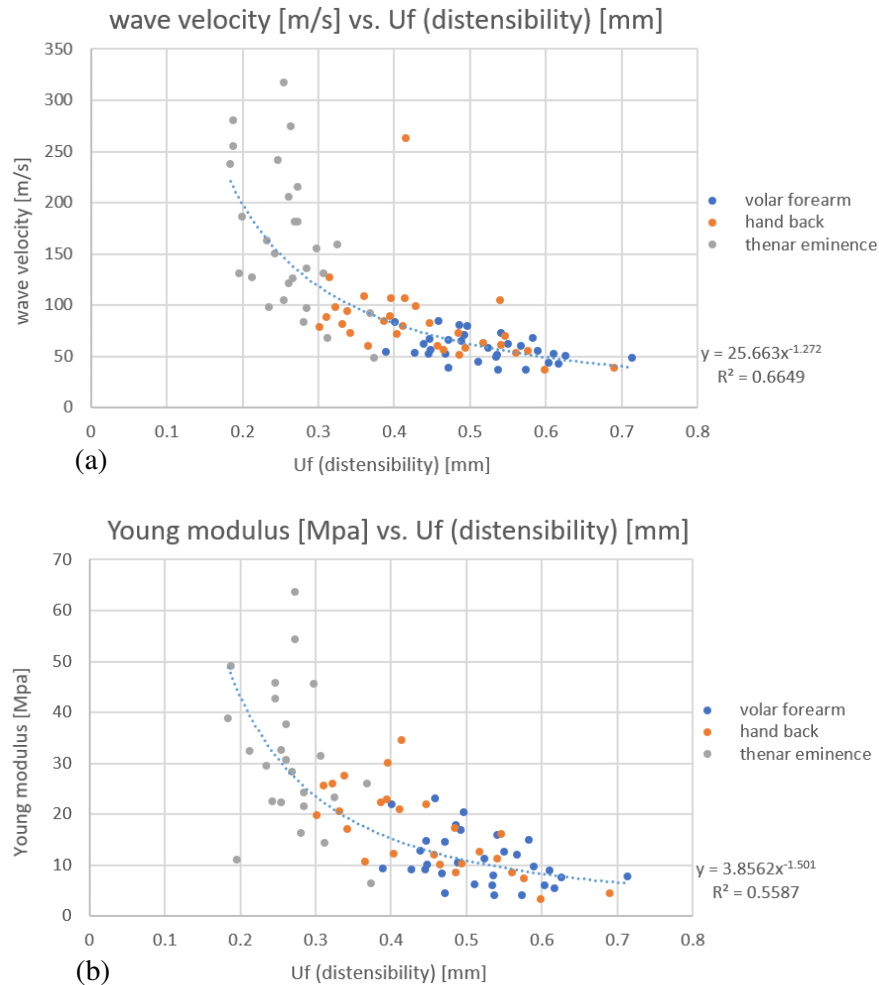


Fig. 41: Correlations between measurement values of the Cutometer and the sensor solution; a) distensibility  $U_f$  of the Cutometer vs. wave velocity calculated of values measured by the sensor solution; b) distensibility  $U_f$  of the Cutometer vs. the Young modulus obtained of values measured by the sensor solution

The values of the Young modulus obtained on human skin in vivo are significantly higher, than the data examined by measurements on the rubber material, matchable to skin hardness.

The maximal amplitude of the signal measured on the receiver in 3mm distance to the sender as well shows a correlation with the measurement data of the Cutometer. It can be well seen in Fig. 42, that hard skin like on the thenar eminence lead to high amplitude values, and soft skin in contrast to lower ones.

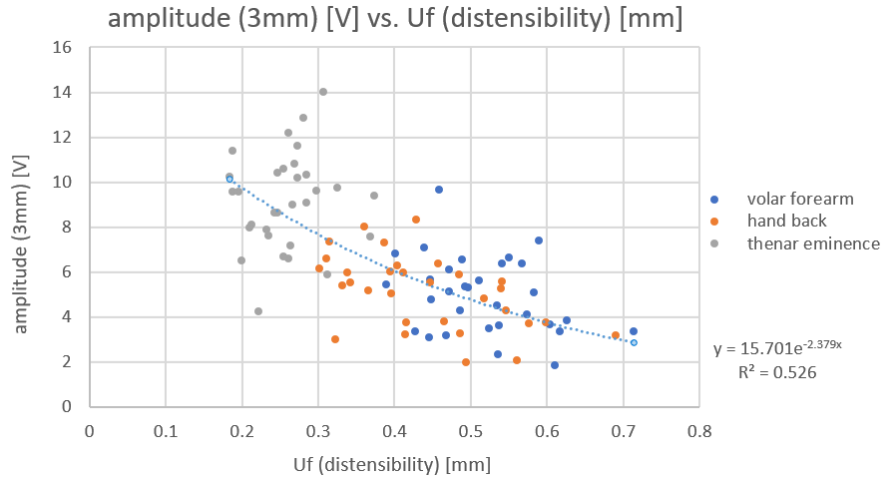


Fig. 42: correlation between the distensibility - Uf of the Cutometer vs. the Young modulus obtained of values measured by the sensor solution

The wave velocity on the volar forearm shows a correlation between the values measured on the left vs. the values measured on the right side of each proband. These values are in good agreement with measurement data obtained using a comparable device mentioned in literature, shown in Fig. 14.

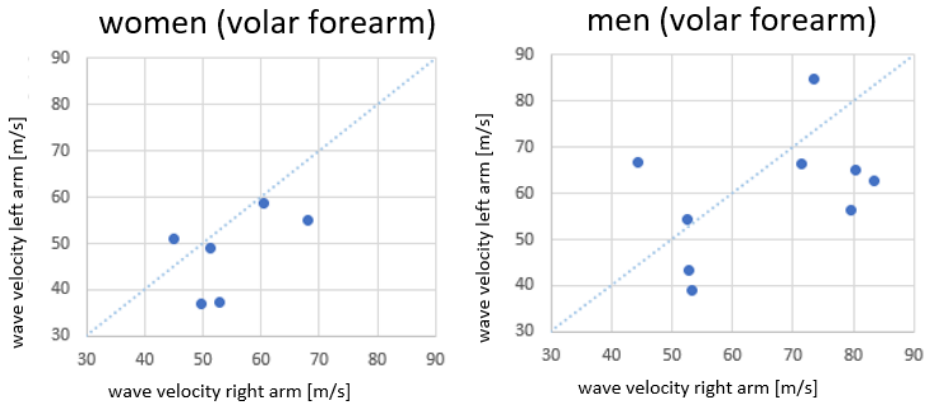


Fig. 43: wave velocity obtained on human skin in vivo; comparison between left and right forearm in healthy females and males; Similar values for the wave velocity were found in literature shown in Fig. 14

For a better comparison between the Cutometer and the novel sensor solution a Bland-Altman analysis was applied. The most significant values of the sensor solution in comparison with the Cutometer were the running time, measured in 10mm distance to the sender, shown in Fig. 40, and the wave velocity, shown in Fig. 41. For identification of the more reliable variable, a Bland-Altman-Analysis for both measurement methods were performed.



The correlation equation for conversion of running time respectively the wave velocity data to Cutometer values, obtained from measurement data of eight randomly chosen probands is given by:

$$U_{f_{t_{10}}} = \frac{t_{10} - 263.84\mu s}{330.71 \frac{\mu s}{mm}} [mm] \quad (46)$$

$$U_{f_{c_s}} = 3.5915 \cdot c_s^{-0.506} [mm] \quad (47)$$

Here  $U_{f_{t_{10}}}$ ,  $U_{f_{c_s}}$  represents the Cutometer value  $U_f$  – distensibility, calculated out of data from the sensor solution,  $t_{10}$  is the running time [ $\mu s$ ] to the receiver in 10mm distance to the sender and  $c_s$  is the wave velocity.

After application of the Kolmogorov-Smirnov-Test onto the data calculated from  $U_f[i] - U_{f_{t_{10}}}[i]$  and  $U_f[i] - U_{f_{c_s}}[i]$  respectively, it was evident, that the values are normally distributed with a significance level of  $P < 0.05$ . Thus, the Bland-Altman-Analysis was applied, leading to the graphics shown in Fig. 44 and Fig. 45.

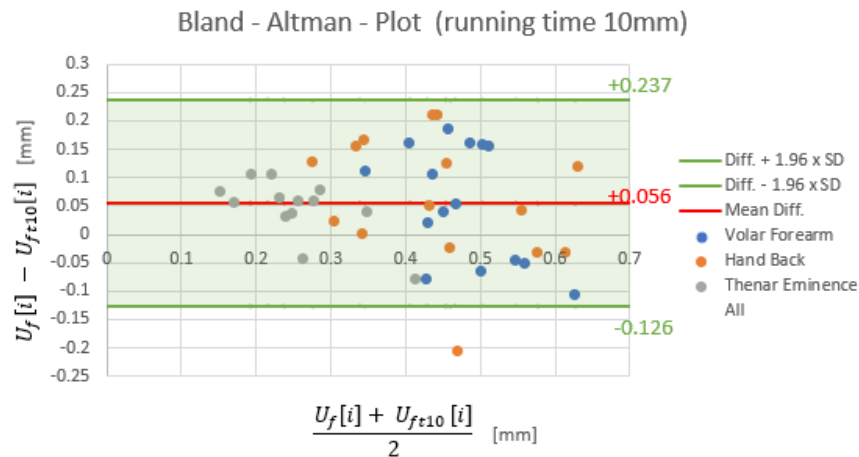
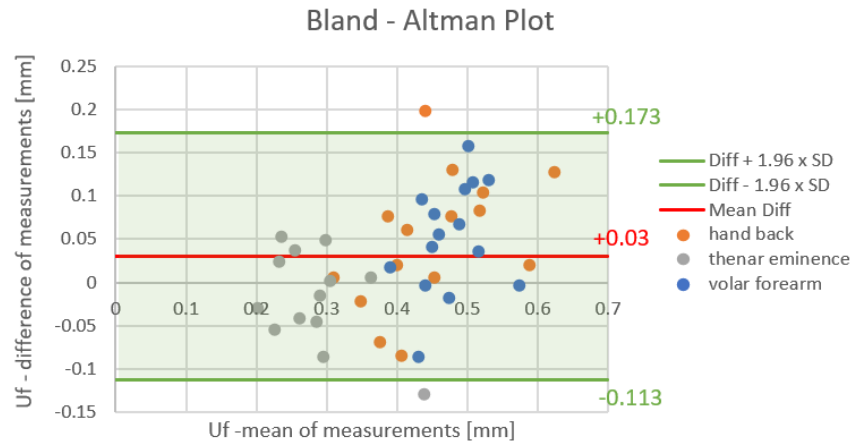


Fig. 44: Bland-Altman Plot: values of the running time to the receiver in distance of 10mm from the sensor solution were converted to Cutometer distensibility -  $U_f$  data and finally compared to obtained distensibility -  $U_f$  data of the Cutometer;

The mean difference of the plot shown in Fig. 44 is close to zero and the values are almost within both lines of agreement, additionally the limits of agreement are smaller than the range of the average value, and the scatterplot doesn't show a significant slope. In total, this led to the fact, that there is no systematic difference between the two methods. But the plot shows an increased variability of the differences at high values of the measurement data, which means that the reference measurement is less reliable at high values respectively at probing on soft tissue.



*Fig. 45: Bland-Altman Plot: values of the wave velocity observed by the sensor solution were converted to Cutometer distensibility - Uf data and finally compared to obtained distensibility - Uf data of the Cutometer;*

In the Bland-Altman plot shown in Fig. 45 the mean difference is close to zero and the values are almost within both lines of agreement, but the difference between the two measurement values increase with higher values, thus a slope is recognizable in the scatter plot.

### 3.3.2. Measurements with moisture

The measurement protocol was done in quite the same way than without moisture, mentioned in 3.3.1, except that after measurement of both arms with both appliances on all skin sites a moisturizer was applied on all testing sites and gently massaged in. Afterwards, 10 minutes were awaited till the moisturizer was fully absorbed by the skin, when subsequently the same measurement protocol was repeated by both appliances, the Cutometer and the sensor solution.

The results from measurements before and after moisturization are compared, shown in Fig. 46. The measured values are in good agreement to the values obtained on human skin without moisture shown in 3.3.1.

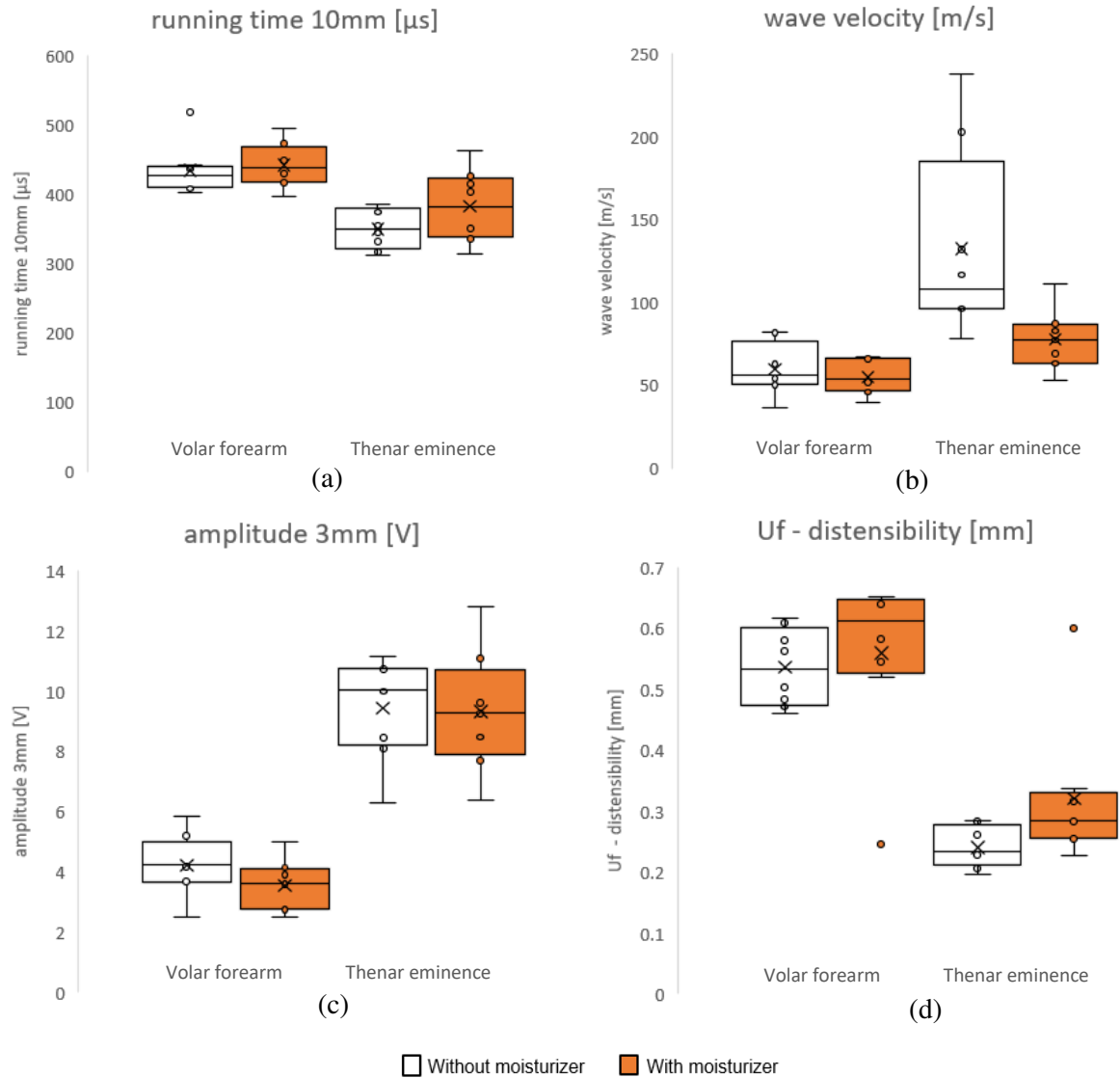


Fig. 46: measurement results with/without moisture on the volar forearm and the thenar eminence. a) running time in 10mm distance to the sender measured by the sensor solution; b) wave velocity measured by the sensor solution; c) maximal amplitude of the received signal measured in 3mm distance to the sender by the sensor solution; d) distensibility - Uf measured by the Cutometer

In most values measured the effect of moisturizer to skin can be observed. As mentioned in literature stated in 1.2.3 the resonant running time of the Reviscometer slightly increased after a daily treatment with moisturizer, and as well the distensibility - Uf measured by the Cutometer increased with application of moisturizer. Same results can be observed in Fig. 46.

## 4. Discussion

In this thesis the composition of a sensor solution for non-invasive in-vivo determination of human skin viscoelasticity based on elastic wave propagation is presented. The final version developed shows good correlations to the gold standard appliance, the Cutometer, shown in 3.3.1. Further development for uncoupling of the sensor solution from power supply and the oscilloscope to a smart sensor solution is pending but feasible under usage of a microcontroller integrated onboard.

In advance several soft boundary conditions for development of a smart sensor solution had been specified in 1.3, which not all of them could be realized so far.

The size of the sensor solution was predefined to 4x4cm and 5mm in thickness, since a flexible device was contemplated, that measurements on various even curved skin sites can be observed. The current version of the sensor solution exhibits a size of approximately 5x6cm and a thickness of 15mm and is not flexible. But for future developments, if the circuit is manufactured industrially its size can be reduced. If the stabilizers of the individual sensor element are replaced by a guided-spring construction like described in 4.3, the sensing area may remain flexible in future versions.

As a fact, that the current consumption of the present sensor solution is in range of 30mA, and that signal evaluation can be performed by a microcontroller the conversion to a self-sufficient appliance featuring an NFC or BLE interface for communication with smart hosts like a smartphone, tablet or laptop is feasible with any big changes in size of the sensor solution. Additionally, if for future developments the utilized amplifiers are replaced by ultra-low power ones, the current consumption may drop below the predefined specification of 3mA, otherwise maybe a battery is necessary.

The probing time for a single measurement is in range of several tenth of milliseconds, the time for evaluation not included. Therefore, within the specified time of 10 seconds multiple measurements featuring various signals can be obtained, discussed in 5.1.

The cost of production can hardly be evaluated. Nevertheless, the price of the individual parts used in the final sensor solution are listed in Table 13, leading to a final price of approximately 14€, if it would be produced in large-scales. Since the sensor solution is reusable, the predefined guideline specified to 1€/measurement is adhered.

Part	Single price	Single price in mass production	Total in mass production
high precision piezo bending membrane	~30€	~3€	~9€
backing material			~0.1€
circuit board[122]	~35	0.37	~0.37
OPA604AP[123]	~3€	~1.5	~3
NE5532AD[123]	~1€	~0.5	~0.5€
LM358AD[123]	~0.4€	~0.1€	~0.1€
resistors/capacitors			~0.1€
Housing			~1€
			<b>Total: ~14€</b>

Table 13: price of all parts used in the final version of the sensor solution, except the cables for connection to the oscilloscope, DC power supply and arbitrary wave generator.

## 4.1. Sensor Solution

### 4.1.1. Calculation of the round bending element

As mentioned in 2.2.1. the manufacturer of the piezo bending membrane recommended to use a membrane featuring a thickness of 0.1mm, thus thinner membranes would be deformed and destroyed easier and the thicker membranes are simpler to handle. But as it is evident, if a thinner piezo bending membrane is applied the resonance frequency of the resulting piezo bending membrane is lower. As an example, if a brass membrane featuring a thickness of 0.05mm is used the resonance frequency reduces from 20kHz down to 15kHz. The lower resonant frequency of the receiver would allow to take measurements with lower frequencies leading to more robust and less fluctuating measurement results. Therefore, in future versions the cutoff frequency of the amplification circuit maybe needs to be reduced and the filter-slope increased to 60db/decade.

The advantage of the most commonly used piezo electric materials, the PZT ceramics is that they exhibit the highest available dielectric charge constant, but on the opposite this material consists of lead which is harmful for health and environment. Thus, in future sensor solutions or if mass production is considered, a harmless material like the lead-free piezo ceramics is recommended to be used.

For further development of the sensor solution it can be considered, that for size reduction only one movable receiver could be applied, instead of two receivers fixed on two different positions. Subsequently, the measurement time will increase, since two measurements with different distance to the sender are necessary for evaluation of the wave velocity and elastic modulus.

#### 4.1.2. Probing signals

Additionally, to the probing signal featuring a narrow frequency bandwidth like described in 2.2.3 other signals providing a high bandwidth made of a signal sweep were tried. Via application of high bandwidth signals it was assumed that the transmission spectrum of the investigated material can be evaluated. This was tried on the rubber phantoms, shown in Fig. 47.

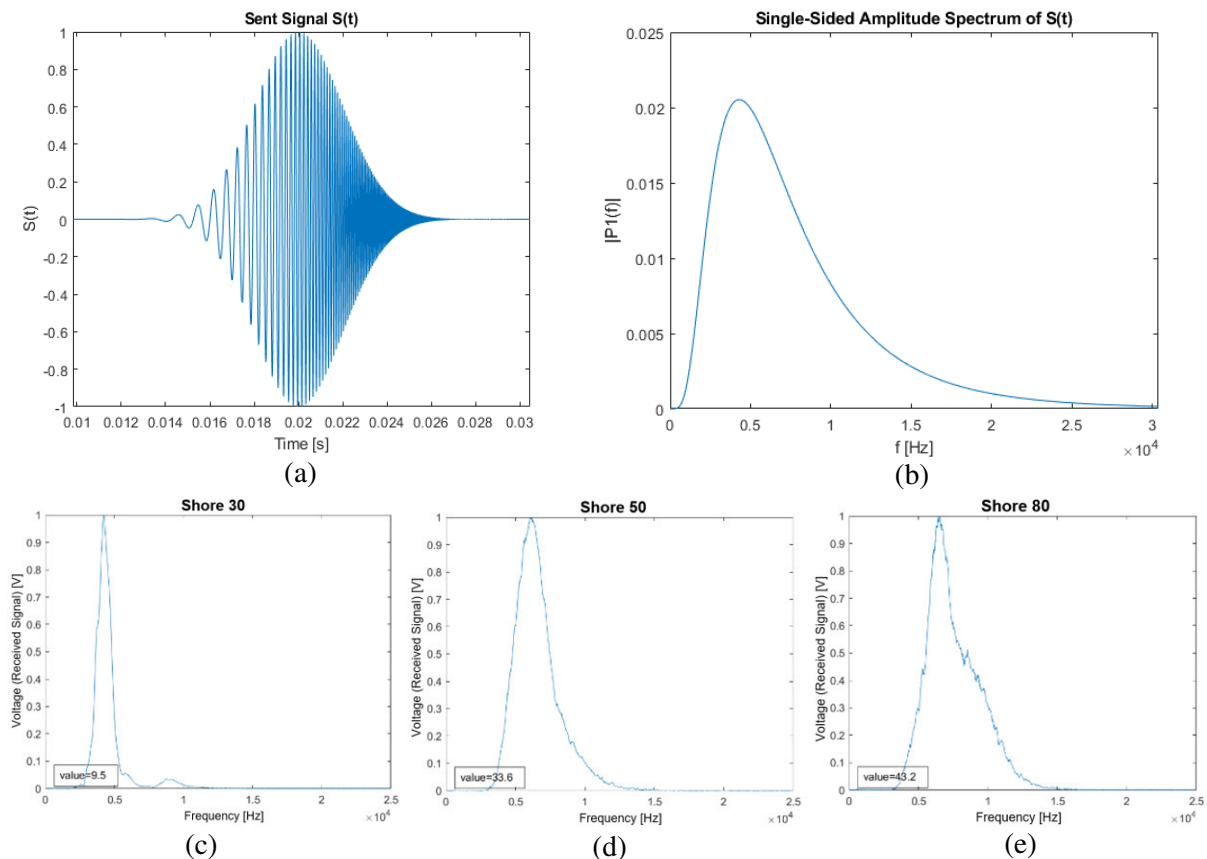


*Fig. 47: High bandwidth probing signal for evaluation of the transmission spectrum of the investigated material; In the measurement results C-E a rising peak frequency with rising shore hardness is apparent a) Probing signal; b) frequency spectrum of the probing signal; c) transmission spectrum of the shore 30 rubber material; d) transmission spectrum of the shore 50 rubber material; e) transmission spectrum of the shore 80 rubber material; the calculated “value” is an arbitrary value estimated out of the surface under the graph*

By the reason, that the piezo bending membranes featuring a specific resonance frequency and an intrinsic vibration response the transmission spectra of the measured rubber plates are not accurate, but it can be recognized, that the peak value of the transmission spectrum features a higher frequency, the harder the material. Only few measurements had been taken using wide-band signals, thus this field of testing seems to be very interesting for future investigations.

### 4.1.3. Conduction force measurement

The transformation of the resistor value given by the force sensing resistor to a voltage signal is done by an impedance converter circuit. Using this circuit, the resulting characteristic curve of the whole set-up yield to a logarithmic function. Hence, the measurement signal is very imprecisely in the higher conduction force level, above approximately 1N.

To receive an almost linear function out of the logarithmic characteristic curve of the force sensing resistor, the circuit shown in Fig. 48 could be applied.

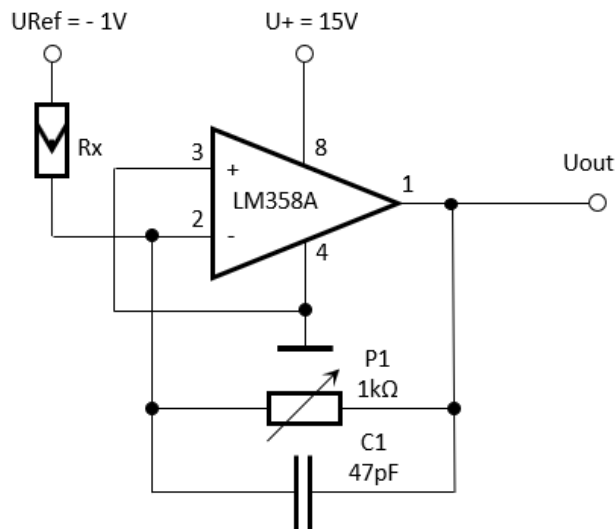
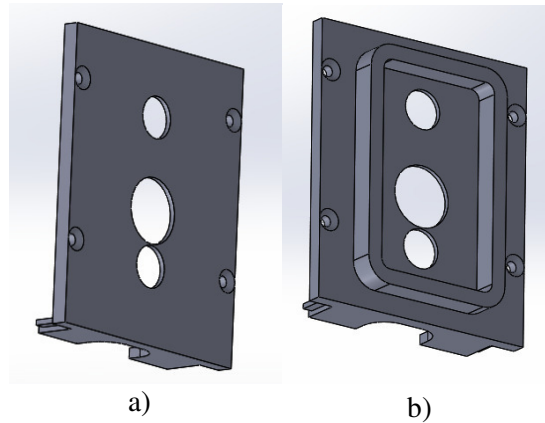


Fig. 48: circuit diagram for resistor to voltage conversion and linearization of the characteristic curve of the force sensing resistor [124]

Another method to ensure, that the conduction force onto the sender and receiver sensors stays constant and within a specified range during measurement, is to apply a spring mechanism under the sensing unit. Either one spring packed inside a guiding frame under the backing material of each individual receiver respectively sender or building a separate sensing unit featuring all three sensors which is connected via springs to the main unit held by the user, could be performed. To avoid too low or too high conduction forces the extreme



positions of the springs can be monitored during measurement, thus the springs are not fully expanded or compressed. Additionally, a force sensing resistor can be integrated for recording the stylus force applied to the individual sensor. To prevent tilting of the sensing unit the sensor case may be equipped with a stabilizing enclosure around the contact area shown in Fig. 49.



*Fig. 49: Bottom of the case of the sensor solution; A) without stabilizing enclosure B) with stabilizing enclosure*

## 4.2. Evaluation of the measurement signal

Primarily both evaluation methods mentioned in 2.4 had been used for analyzing the running time of the probing signal. But the calculation of the envelope of the received gaussian wave package implicated additional impreciseness leading to higher fluctuating values than the evaluation via determination of the center maxima of the individual oscillations. Therefore, only the later mentioned method was applied for evaluation of the measurement data.

Primarily the force sensing resistor was applied to be used for insurance, that the contact pressure onto both receivers is roughly equal and that the stylus force stays below a specific value, that no dents and skin hardening occurs. Since, the amplitude of the signal is increasing linearly with rising stylus force, shown in 2.2.5 the obtained values of the force sensing circuit can be used for future scaling of the signal amplitude.

Like mentioned in 2.4 the amplitudes of the received signals are calculated via evaluation of the maximal peak value of the obtained oscillations. Since the phase velocity slightly differ from the group velocity it can be considered to evaluate the maximal amplitude out of the wave group via calculation of an envelope of the oscillation. But as described above, the peak-values of the gaussian envelopes were highly fluctuating, which in future then my lead to an additional inaccuracy.

All measurements obtained with the same frequency were performed using a digital storage oscilloscope with an identical time base preset. For the measurements performed on human skin a time base of 500 $\mu$ s/division was applied. Since only 1000 points of the screen data of the oscilloscope can be written to a csv – file a systematic inaccuracy of  $\pm 3\mu$ s results. Via integration of a high sampling rate microcontroller within the sensor solution this source of inaccuracy can be reduced to a minimum.

## 4.3. Composition of the sensor solution

Like mentioned in 2.2.5 the measurements taken, using the sensor solution are not uniaxial, rather the individual receiver observes signals from a specific angular range. The receiver located closer to the sender receives signals from a bigger angular range than the other receiver, leading to more inaccurate values. If the sender is exchanged by the same piezo bending membranes as utilized for the receivers, the angular range of both receivers shrinks, which is assumed that this will lead to more accurate values. Additionally, each individual receiver can as well be used as a sending piezo, and the sender in the center could as well act as a receiver, thus measurements could be performed bidirectionally.

The backing material made of felt and double-sided adhesive foam tape is furthermore a shaky construction leading to inaccuracy of  $\pm 1$ mm in distance between the sender and each individual receiver. If stabilizers would feature a greater recess the backing material may be more stable.

In the current sensor solution, the sensing elements are connected using an unshielded enameled copper wire featuring a diameter of 0.1mm. Via usage of shielded wires to the piezo bending membranes, signal leakage and inductive coupling from external signals can be minimized.

The circuit of the sensor solution was manually wired and soldered, without any ground plane on the circuit board. For future developments an industrial manufactured circuit board featuring a big ground plane is recommended to prevent of interference by external signals.

## 4.4. Phantoms

### 4.4.1. Rubber material

The rubber plates used as phantoms for comparison with the literature were somewhat too thin. If measurements were performed on a rubber plate featuring a low shore hardness, like shore 30 and another rubber plate featuring a higher shore hardness, like shore 80 was placed beneath the one measured, a slightly

lower running time was observed, than if a rubber plate with shore 25 was placed below. It was assumed, that this variability was caused by the penetration depth of the probing signal. Subsequently for future measurements it would be recommended, that thicker rubber plates are used.

The shore hardness value of the rubber plates used was determined by the manufacturer and mentioned in the datasheet included. For future measurements it is recommended that the shore hardness of the rubber plates used as phantoms are measured under application of a certified shore A durometer, featuring the standardized properties mentioned in literature [97].

The Young modulus of the individual rubber plate obtained with the sensor solution is somewhat higher than the Young modulus calculated using the formula mentioned in literature, shown in Fig. 37. Nevertheless, the values measured with the sensor solution in comparison to measurement values obtained using a shore durometer appliance exhibit similar values shown in Fig. 50 [118].

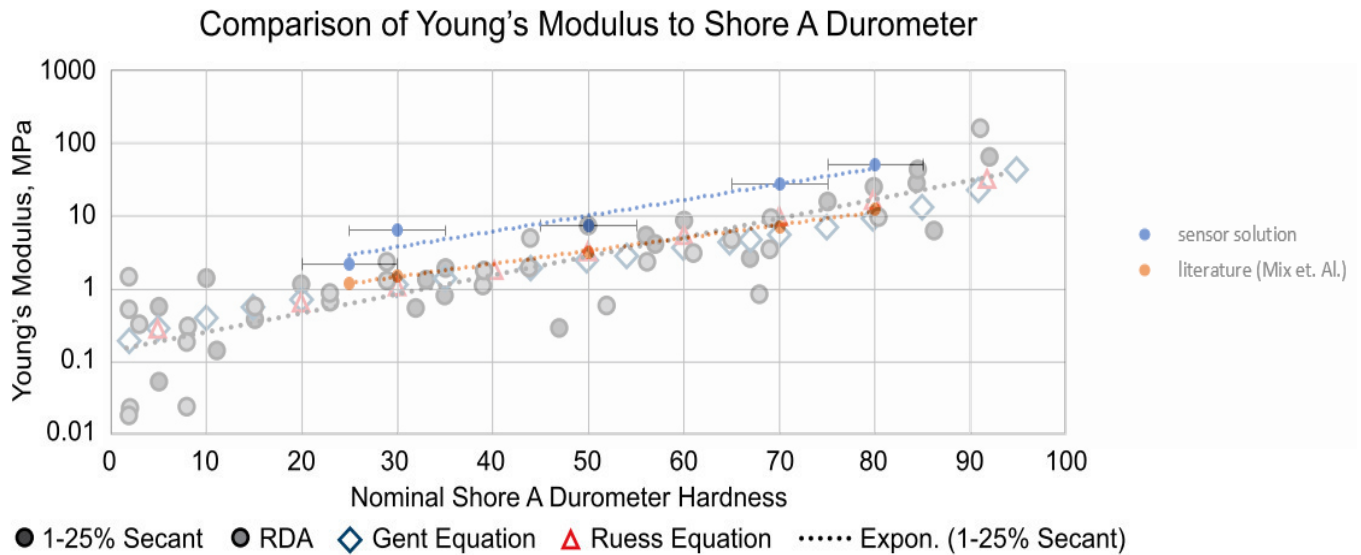


*Fig. 50: Comparison of the Young modulus measured on the rubber phantoms to values mentioned in literature; For easier comparison the picture from Fig. 37 is slightly made diaphanous and laid over the figure from literature. As seen the values obtained using the sensor solution are within the tolerances of measurement data obtained on similar rubber material published in literature [118]*

## 4.5. In-vivo measurements

As mentioned in 3.3.1 the measurement values investigated on the side of the hand were removed from further evaluations, because the skin on this side consists of combination skin, thus the soft skin from the back of the hand changes to the hard skin from the hand inside. Since the Cutometer probe only has a sensing surface of 2mm in diameter, and the sensor solution approximately a sensing area of 34 mm x 11mm the values measured on this site can hardly be compared.

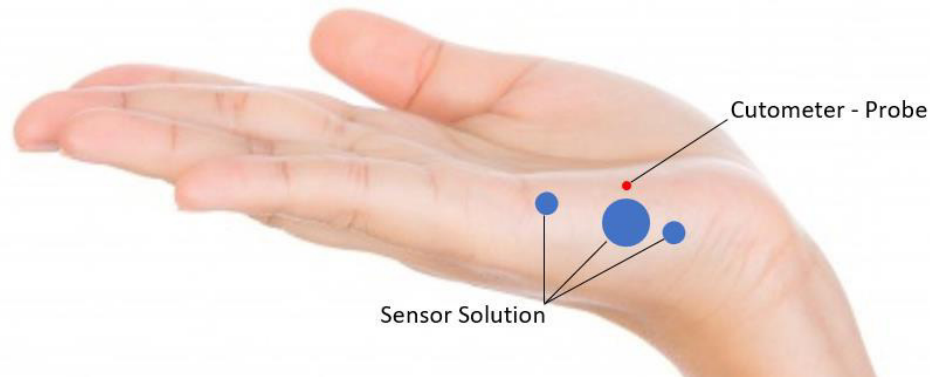


*Fig. 51: Comparison of the probe size between the Cutometer and the Sensor Solution; The sensing area of the Cutometer only exhibit a diameter of 2mm. Therefore, measurement data on sites where soft and hard skin is combined are hardly comparable;*

Nevertheless, the values measured on this side show some other interesting results:

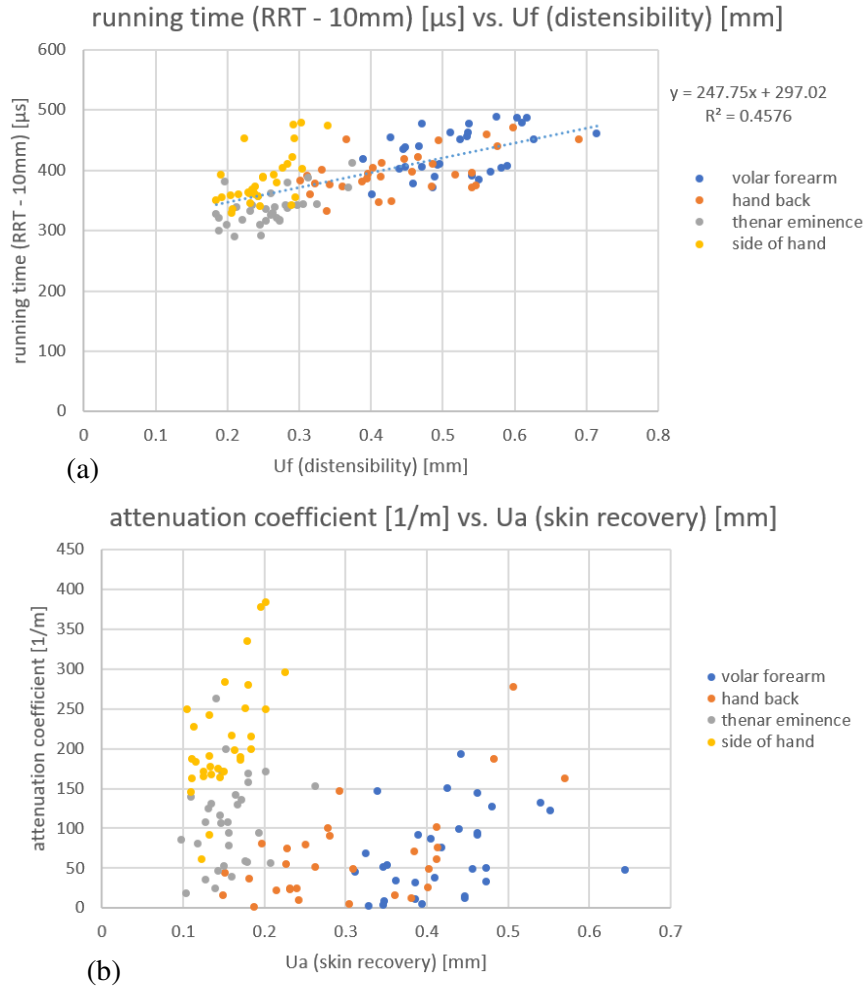


Fig. 52: Results of the measurement on 16 probands without moisture including the side of the hand; a) running time of the receiver in 10mm distance to the sender vs. the distensibility -  $U_f$  measured by the Cutometer. b) attenuation coefficient vs. the distensibility -  $U_f$  of the Cutometer

Like shown in Fig. 52 the data measured on the side of the hand using the sensor solution similar values like the data measured on the back of the hand in the running time plot are obtained, when the data measured with the Cutometer, related values to the thenar eminence were observed. Nevertheless, this measurement site exhibits the highest attenuation coefficient in comparison to all other sites. The attenuation coefficient doesn't really show correlations to any of the values measured by the Cutometer. Thus, this value represents an interesting parameter for future investigations, shown in Fig. 52.

There are only four measurement values obtained with the novel sensor solution, the running time and the amplitude of each receiver. But in total, various interesting data can be calculated out of them. Some of

them are: wave velocity, shear elasticity, shear viscosity, shear modulus, Young modulus, intercept of the linear function built between the two running time values, attenuation coefficient;

All of them were evaluated for each of the test materials and for the measurements on human skin in vivo. The correlation obtained for the wave velocity in comparison to the distensibility -Uf, measured by the Cutometer shown in Fig. 41, show highly fluctuating values in wave velocity below 0.3mm of the distensibility. The reason for this is, that the wave velocity is calculated out of the difference of the receiver distances, which provides a constant value, divided by the difference of the running times between the sender and the receivers, leading to a hyperbolic relation. As a reason, that the shear modulus and the Young modulus is roughly proportional to the wave velocity squared, these plots show equal relations to the Cutometer distensibility - Uf like the wave velocity.

In total it is assumed, that the most reliable and robust measurement value of the sensor solution is the running time to the receiver in 10mm distance to the sender. Because the Bland-Altman Analysis shows a good agreement between this value from the sensor solution in comparison to the distensibility - Uf value of the Cutometer. Additionally, the running time in 10mm distance is well comparable between the rubber material, the skin phantom, and the measurements on human skin in vivo.

## 5. Outlook

Like described in 4, several optimizations of the sensor solution can be done, that more accurate and robust results are obtained:

- Exchange of the stabilizers of the damping material by a spring mechanism to ensure, that the conduction force is equally distributed
- Supplement the bottom of the case by a stabilizing enclosure to prevent tilting of the sensor solution
- Improved stabilization of the damping material to prevent tilting of the individual piezo bending membrane, and consequently more accurate distance between the sender and the receiver piezo membrane
- Fabrication of high precession piezo bending membranes featuring a thinner target material for enabling lower probing frequencies
- Exchange of the sender with a piezo membrane equally to the receiver for bidirectional measurement of the running time and the amplitude
- Implementation of a Microcontroller for evaluation of the measurement signals to reduce transmission losses by cables and evaluation errors caused by the oscilloscope
- Usage of shielded wires to the piezo bending membranes to minimize signal leakage and inductive coupling from external signals
- Industrially manufactured circuit board
- Optimization of the measurement process and the measurement protocol

### 5.1. How the sensor solution is planned to operate

It is assumed, that if several improvements like described above are fulfilled, the accuracy of the measurement is enhanced in that way, that finally the anisotropy of the skin can be investigated.

When the sensor solution finally is working self-sufficient featuring a microcontroller, the testing time for one single measurement is reduced to approximately 100ms. Subsequently, within the whole test period of let's say 3 seconds on one test site, several measurements with probing signals featuring various center frequencies could be performed, leading to more accurate and more informative values. Additionally, the transmission spectra of the site investigated may be obtained, as described in 4.1.2.

A further idea is to clip the sensor solution directly onto the backside of a smartphone. Under usage of the gyroscope of the smartphone the rotation angle of the sensor solution can be evaluated. Via recording several measurements among various angles on one specific skin site the anisotropy can be investigated, resulting in the knowledge of the direction of the Langer-Lines.

## 5.2. Next steps

For further development of the sensor solution an investor needs to be found.

Nevertheless, the sensor solution should be optimized according to the improvements mentioned above. Then a full-scale study at a dermatologist or hospital should be fulfilled, to realize the whole capability of the sensor solution and all calculatable measurement results. As mentioned in 4.5 the attenuation coefficient for example delivers interesting measurement results which cannot be interpreted correctly now. Additionally, the transmission spectra of the material investigated may be obtained more accurate in future and its data may lead to interesting inestimable information's.



## 6. Conclusion

In this master thesis the development of a novel sensor solution for in vivo determination of human skin viscoelasticity based on elastic wave propagation is presented. As assumed in the hypothesis, elastic waves, generated and subsequently recorded via low energy consuming and cheap manufacturable round piezo bending transducers are utilized to determine the stimulation time, propagation speed and the damping coefficient of the investigated skin part. The sensor solution is built of three piezo bending transducers arranged in a line, with the middle one being the sender of the elastic waves. The other transducers feature different distances to the center one and operate as receivers. Via quantification of the running time as well as the amplitude of the elastic waves to the unequal distances from the sender, the stimulation time, propagation speed and damping coefficient is determinable. Out of these three main values several other interesting skin parameters like the elasticity, Young's modulus and viscoelasticity can be estimated. By using low energy consuming and small manufacturable piezo elements the final version of the sensor solution is small in size, measuring (l x b x h) 56mm x 48mm x 14mm and features a low current consumption of about 30mA. Due to the high measurement frequencies, several measurements may be performed within a second.

In the context of this work it is shown, that the Young's modulus estimated by fitting the measurement values, determined on rubber material featuring shore A hardness between 25-80, show similar values like described in literature.

Via in vivo measurements on the volar forearm, the backside of the hand and the thenar eminence of 16 healthy probands good correlations between measurement values of the sensor solution and the well-established gold standard appliance Cutometer could be found. A similar correlation between the commercially available Reviscometer, using the elastic wave propagation method as well, and the Cutometer is mentioned in literature and was used for comparison. Additionally, it could be shown, that the elasticity parameters of human skin are slightly different before and after usage of skin moisturizer.

Due to the low current consumption of the sensor solution the transition to an energy autonomous and microprocessor-controlled appliance is feasible and recommended as next step in development. Under usage of a microprocessor, the connection to a smartphone or tablet via NFC or BLE is possible. For an investigation of the whole capability of the sensor solution and all discoverable skin parameters, a full-scale study involving various probands and on different skin sites performed at a hospital or dermatologist is recommended.

In future this sensor solution may not replace the usage of the more accurate and more complex tabletop appliances like the Cutometer, but due to the handy size and easy usage it can be applied by the individual laymen at home.

# 7. References

## 7.1. Bibliography

- [1] “Home - PubMed - NCBI.” [Online]. Available: <https://www.ncbi.nlm.nih.gov/pubmed/>. [Accessed: 10-Feb-2018].
- [2] K. I. Bland and A. Csendes, *General Surgery: Principles and International Practice*, vol. 12. Springer, 2008.
- [3] C. Li, G. Guan, R. Reif, Z. Huang, and R. K. Wang, “Determining elastic properties of skin by measuring surface waves from an impulse mechanical stimulus using phase-sensitive optical coherence tomography,” *J. R. Soc. Interface*, vol. 9, no. 70, pp. 831–841, 2012.
- [4] R. P. J. B. Weller, J. A. A. Hunter, J. A. Savin, and M. V. Dahl, *Clinical Dermatology, fourth edition*. Oxford, UK, 2009.
- [5] H. Lenz *et al.*, “The creatine kinase system in human skin: Protective effects of creatine against oxidative and UV damage in vitro and in vivo,” *J. Invest. Dermatol.*, vol. 124, no. 2, pp. 443–452, 2005.
- [6] F. M. Hendriks, “Mechanical Behaviour of Human Skin in Vivo A Literature Review,” 2001.
- [7] J. A. A. Hunter *et al.*, *Clinical Dermatology*. Blackwell Science, 2013.
- [8] H. Kerl, C. Garbe, L. Cerroni, and H. H. Wolff, *Histopathologie der Haut*. 2003.
- [9] L. Baumann and L. Baumann, *Cosmetic dermatology : principles and practice*. McGraw-Hill Medical, 2009.
- [10] P. Humbert, F. Fanian, H. I. Maibach, and P. Agache, Eds., *Agache’s Measuring the Skin*. Cham: Springer International Publishing, 2017.
- [11] P. Fritsch, *Dermatologie und Venerologie für das Studium*. Berlin, Heidelberg: Springer Berlin Heidelberg, 2009.
- [12] M. Pawlaczyk, M. Lelonkiewicz, and M. Wieczorowski, “Age-dependent biomechanical properties of the skin,” *Postep. Dermatologii i Alergol.*, vol. 30, no. 5, pp. 302–306, 2013.
- [13] C. Pailler-Mattei, S. Bec, and H. Zahouani, “In vivo measurements of the elastic mechanical

- properties of human skin by indentation tests,” *Med. Eng. Phys.*, vol. 30, no. 5, pp. 599–606, 2008.
- [14] R. Marks and P. A. Payne, *Bioengineering and the Skin : Based on the Proceedings of the European Society for Dermatological Research Symposium, held at the Welsh National School of Medicine, Cardiff, 19-21 July 1979*. Springer Netherlands, 1982.
- [15] A. I. Malkin and A. I. Isayev, *Rheology : concepts, methods, and applications*. .
- [16] E. Berardesca, H. I. Maibach, and K.-P. Wilhelm, *Non invasive diagnostic techniques in clinical dermatology*. 2006.
- [17] A. P. Sarvazyan, M. W. Urban, and J. F. Greenleaf, “Acoustic Waves in Medical Imaging and Diagnostics,” *Ultrasound Med. Biol.*, vol. 39, no. 7, pp. 1133–1146, 2013.
- [18] H. L. Oestreicher, “Field and Impedance of an Oscillating Sphere in a Viscoelastic Medium with an Application to Biophysics,” *J. Acoust. Soc. Am.*, vol. 23, no. 6, pp. 707–714, Nov. 1951.
- [19] M. Steinbach and B. Abali, “Numerische Analyse der Wellenausbreitung in elastischen Medien und ihre analytische Verifikation,” *lkm.tu-berlin.de*.
- [20] W. H. 1959- Müller and F. Ferber, *Technische Mechanik für Ingenieure mit einer Multimedia-CD-ROM &quot;Technische Mechanik mit mechANIma&quot;*; Fachbuchverl. Leipzig im Carl-Hanser-Verl, 2012.
- [21] “Kelvin–Voigt material - Wikipedia.” [Online]. Available: [https://en.wikipedia.org/wiki/Kelvin-Voigt\\_material](https://en.wikipedia.org/wiki/Kelvin-Voigt_material). [Accessed: 12-Nov-2018].
- [22] Y. Zheng *et al.*, “Shear Wave Propagation in Soft Tissue and Ultrasound Vibrometry,” in *Wave Propagation Theories and Applications*, InTech, 2013.
- [23] R. O. O. Potts, D. A. Chrisman, E. M. Buras, D. A. Chrisman Jr., and E. M. Buras Jr., “The dynamic mechanical properties of human skin in vivo.,” *J. Biomech.*, vol. 16, no. 6, pp. 365–72, 1983.
- [24] E. C. Ruvolo, G. N. Stamatias, and N. Kollias, “Skin viscoelasticity displays site- and age-dependent angular anisotropy,” *Skin Pharmacol. Physiol.*, vol. 20, no. 6, pp. 313–321, 2007.
- [25] B. Qiang, X. Zhang, and J. Greenleaf, “Estimation of skin elasticity by measuring surface wave velocity under impulse stimulus using compact optical sensors,” *Proc. - IEEE Ultrason. Symp.*, pp. 185–188, 2009.

- [26] J. D. Achenbach, *Wave propagation in Elastic Solids*. North-Holland Pub. Co, 1973.
- [27] E. Soczkiewicz, “Penetration depth of the Rayleigh surface waves,” *Nondestruct. Test. Eval.*, vol. 13, no. 2, pp. 113–119, 1997.
- [28] A. P. Sarvazyan, O. V Rudenko, S. D. Swanson, J. B. Fowlkes, and S. Y. Emelianov, “Shear Wave Elasticity Imaging : A new ultrasonic technology of medical diagnostic,” *Ultrasound Med. Biol.*, vol. 24, no. 9, pp. 1419–1435, 1998.
- [29] C. Castelo-Branco, F. Pons, E. Gratacós, A. Fortuny, J. a Vanrell, and J. González-Merlo, “Relationship between skin collagen and bone changes during aging,” *Maturitas*, vol. 18, no. 3, pp. 199–206, 1994.
- [30] A. Firooz *et al.*, “Variation of biophysical parameters of the skin with age, gender, and body region,” *Sci. World J.*, vol. 2012, pp. 1–5, 2012.
- [31] T. Hermanns-Lê, F. Jonlet, A. Scheen, and G. E. Piérard, “Age- and body mass index-related changes in cutaneous shear wave velocity,” *Exp. Gerontol.*, vol. 36, no. 2, pp. 363–372, 2001.
- [32] M. Paye, S. Mac-Mary, A. Elkhyat, C. Tarrit, P. Mermet, and P. H. Humbert, “Use of the Reviscometer® for measuring cosmetics-induced skin surface effects,” *Ski. Res. Technol.*, vol. 13, no. 4, pp. 343–349, 2007.
- [33] P. D. H. M. Verhaegen, E. M. Res, A. Van Engelen, E. Middelkoop, and P. P. M. van Zuijlen, “A reliable, non-invasive measurement tool for anisotropy in normal skin and scar tissue,” *Ski. Res. Technol.*, vol. 16, no. 3, pp. 325–331, 2010.
- [34] M. J. Koehler *et al.*, “Intrinsic, solar and sunbed-induced skin aging measured in vivo by multiphoton laser tomography and biophysical methods,” *Ski. Res. Technol.*, vol. 15, no. 3, pp. 357–363, 2009.
- [35] P. Neto, M. Ferreira, F. Bahia, and P. Costa, “Improvement of the methods for skin mechanical properties evaluation through correlation between different techniques and factor analysis,” *Ski. Res. Technol.*, vol. 19, no. 4, pp. 405–416, 2013.
- [36] H. Ohshima *et al.*, “Relevance of the directionality of skin elasticity to aging and sagging of the face,” *Ski. Res. Technol.*, vol. 17, no. 1, pp. 101–107, 2011.
- [37] Y. Gabe, O. Osanai, and Y. Takema, “The relationship between skin aging and steady state ultraweak photon emission as an indicator of skin oxidative stress in vivo,” *Ski. Res. Technol.*, vol.

- 20, no. 3, pp. 315–321, 2014.
- [38] B. Nedelec *et al.*, “Skin characteristics: normative data for elasticity, erythema, melanin, and thickness at 16 different anatomical locations,” *Ski. Res. Technol.*, vol. 22, no. 3, pp. 263–275, 2016.
- [39] C. E. Coltman, J. R. Steele, and D. E. McGhee, “Effect of aging on breast skin thickness and elasticity: implications for breast support,” *Ski. Res. Technol.*, vol. 23, no. 3, pp. 303–311, 2017.
- [40] A. B. Cua, K.-P. P. Wilhelm, and H. I. Maibach, “Elastic properties of human skin: relation to age, sex, and anatomical region,” *Arch. Dermatol. Res.*, vol. 282, no. 5, pp. 283–288, 1990.
- [41] V. Couturaudl, “Influence of Age and Body Site By a Non-Invasive Method,” pp. 68–73, 1995.
- [42] A. O. Barel, R. Lambrecht, and P. Clarys, “Mechanical Function of the Skin: State of the Art,” *Ski. Bioeng.*, vol. 26, pp. 69–83, 1998.
- [43] P. A. Wendling and G. Dell’Acqua, “Skin biophysical properties of a population living in Valais, Switzerland,” *Ski. Res. Technol.*, vol. 9, no. 4, pp. 331–338, 2003.
- [44] H. S. Ryu, Y. H. Joo, S. O. Kim, K. C. Park, and S. W. Youn, “Influence of age and regional differences on skin elasticity as measured by the Cutometer®,” *Ski. Res. Technol.*, vol. 14, no. 3, pp. 354–358, 2008.
- [45] L. C. Gerhardt, A. Lenz, N. D. Spencer, T. Münzer, and S. Derler, “Skin-textile friction and skin elasticity in young and aged persons,” *Ski. Res. Technol.*, vol. 15, no. 3, pp. 288–298, 2009.
- [46] Y. Hara, Y. Masuda, T. Hirao, and N. Yoshikawa, “The relationship between the Young’s modulus of the stratum corneum and age: A pilot study,” *Ski. Res. Technol.*, vol. 19, no. 3, pp. 339–345, 2013.
- [47] S. Luebberding, N. Krueger, and M. Kerscher, “Mechanical properties of human skin in vivo: A comparative evaluation in 300 men and women,” *Ski. Res. Technol.*, vol. 20, no. 2, pp. 127–135, 2014.
- [48] B. R. Davis, E. Bahniuk, J. K. Young, C. M. Barnard, and J. M. Mansour, “Age-dependent changes in the shear wave propagation through human skin,” *Exp. Gerontol.*, vol. 24, no. 3, pp. 201–210, 1989.
- [49] R. O. Potts, E. M. Buras, and D. A. Chrisman, “Changes with Age in the Moisture Content of Human Skin,” *J. Invest. Dermatol.*, vol. 82, no. 1, pp. 97–100, 1984.

- [50] J. W. Jung, Y. W. Lee, Y. B. Choe, and K. J. Ahn, "An 8-week face-split study to evaluate the efficacy of cosmeceuticals using non-invasive bioengineering devices," *Ski. Res. Technol.*, vol. 19, no. 3, pp. 324–329, 2013.
- [51] H. Dobrev, "Use of Cutometer to assess epidermal hydration," *Ski. Res. Technol.*, vol. 6, no. 4, pp. 239–244, 2000.
- [52] F. Fanian *et al.*, "Efficacy of micronutrient supplementation on skin aging and seasonal variation: A randomized, placebo-controlled, double-blind study," *Clin. Interv. Aging*, vol. 8, pp. 1527–1537, 2013.
- [53] H. Seirafi *et al.*, "Biophysical characteristics of skin in diabetes: A controlled study," *J. Eur. Acad. Dermatology Venereol.*, vol. 23, no. 2, pp. 146–149, 2009.
- [54] A. Vexler, I. Polyansky, and R. Gorodetsky, "Evaluation of skin viscoelasticity and anisotropy by measurement of speed of shear wave propagation with viscoelasticity skin analyzer," *J. Invest. Dermatol.*, vol. 113, no. 5, pp. 732–739, 1999.
- [55] X. Liang and S. Boppart, "Biomechanical properties of in vivo human skin from dynamic optical coherence elastography," *Biomed. Eng. IEEE Trans.*, vol. 57, no. 4, pp. 953–959, 2010.
- [56] C. Dagdeviren *et al.*, "Conformal piezoelectric systems for clinical and experimental characterization of soft tissue biomechanics," *Nat. Mater.*, vol. 14, no. 7, pp. 728–736, 2015.
- [57] Y. Shi, C. Dagdeviren, J. A. Rogers, C. F. Gao, and Y. Huang, "An Analytic Model for Skin Modulus Measurement Via Conformal Piezoelectric Systems," *J. Appl. Mech.*, vol. 82, no. 9, p. 091007, 2015.
- [58] R. H. Guy, *Handbook of non-invasive methods and the skin*, vol. 42, no. 1. 1996.
- [59] P. G. Agache, C. Monneur, J. L. Leveque, and J. De Rigal, "Mechanical properties and Young's modulus of human skin in vivo," *Arch. Dermatol. Res.*, vol. 269, no. 3, pp. 221–232, Dec. 1980.
- [60] C. Rosado *et al.*, "About the in vivo quantitation of skin anisotropy," *Ski. Res. Technol.*, vol. 23, no. 3, pp. 429–436, 2017.
- [61] Courage&Khazaka, "CutisScan CS 100 - Brochure." [Online]. Available: [http://www.courage-khazaka.de/images/phocadownload/Brochures/Brochure\\_CS100.pdf](http://www.courage-khazaka.de/images/phocadownload/Brochures/Brochure_CS100.pdf). [Accessed: 25-Apr-2018].
- [62] R. Sanders, "Torsional elasticity of human skin in vivo," *Pflügers Arch. Eur. J. Physiol.*, vol. 342, no. 3, pp. 255–260, 1973.

- [63] J. F. Manschot and a J. Brakkee, “The measurement and modelling of the mechanical properties of human skin in vivo--I. The measurement,” *J Biomech*, vol. 19, no. 7, pp. 511–515, 1986.
- [64] G. E. Piérard, “Evaluation de propriétés mécaniques de la peau par les méthodes d’indentation et de compression,” *Dermatology*, vol. 168, no. 2, pp. 61–66, 1984.
- [65] Y. Lanir, V. Manny, A. Zlotogorski, A. Shafran, and S. Dikstein, “Influence of ageing on the in vivo mechanics of the skin.,” *Skin Pharmacol.*, vol. 6, no. 3, pp. 223–230, 1993.
- [66] H. Zahouani, C. Pailler-Mattei, B. Sohm, R. Vargiolu, V. Cenizo, and R. Debret, “Characterization of the mechanical properties of a dermal equivalent compared with human skin in vivo by indentation and static friction tests,” *Ski. Res. Technol.*, vol. 15, no. 1, pp. 68–76, 2009.
- [67] M. Mridha, S. Ödman, and P. Å. Öberg, “Mechanical pulse wave propagation in gel, normal and oedematous tissues,” *J. Biomech.*, vol. 25, no. 10, 1992.
- [68] T. J. Moore, “A Survey of the Mechanical Characteristics of Skin and Tissue in Response to Vibratory Stimulation,” *IEEE Trans. Man-Machine Syst.*, vol. 11, no. 1, pp. 79–84, 1970.
- [69] J. M. M. Pereira, J. M. M. Mansour, and B. R. R. Davis, “Analysis of shear wave propagation in skin; application to an experimental procedure,” *J. Biomech.*, vol. 23, no. 8, pp. 745–751, 1990.
- [70] Sarvazyan et al., “Method and device for acoustic testing of elasticity of biological tissues,” Aug. 1988.
- [71] P. Dorogi, G. Dewitt, B. Stone, and E. Buras, “Viscoelastometry of skin in vivo using shear wave propagation,” *Bioeng.*, vol. 23, no. 8, pp. 59–70, Feb. 1986.
- [72] J.-L. L. J.-L. Gennisson *et al.*, “Assessment of elastic parameters of human skin using dynamic elastography.,” *IEEE Trans. Ultrason. Ferroelectr. Freq. Control*, vol. 51, no. 8, pp. 980–9, 2004.
- [73] Ł. Sienkiewicz, M. Ronkowski, G. Kostro, and R. Ryndzionek, “Identification of the mechanical properties of the skin by electromechanical impedance analysis of resonant piezoelectric actuator,” pp. 3938–3943, 2013.
- [74] F. Hashmi, C. Nester, C. Wright, V. Newton, and S. Lam, “Characterising the biophysical properties of normal and hyperkeratotic foot skin,” *J. Foot Ankle Res.*, vol. 8, no. 1, pp. 1–10, 2015.
- [75] S. Vijaya, *Piezoelectric Materials and Devices: Applications in Engineering and Medical Sciences*. CRC Press, 2013.



- [76] J. Tichý, J. Erhart, E. Kittinger, and J. Přívratská, *Fundamentals of piezoelectric sensorics: Mechanical, dielectric, and thermodynamical properties of piezoelectric materials*. Berlin, Heidelberg: Springer Berlin Heidelberg, 2010.
- [77] “Piezokeramische Scheiben, Stäbe und Zylinder.” [Online]. Available: <https://www.piceramic.de/de/produkte/piezokeramische-bauelemente/scheiben-staebe-und-zylinder/>. [Accessed: 10-Feb-2019].
- [78] K. C. Cheng, H. Lai, and W. Chan, “Characterization of Piezoelectric Ring Used for Wire Bonding Transducer Application,” pp. 2–5.
- [79] “Piezo ring component - Noliac - Your Piezo Partner.” [Online]. Available: <http://www.noliac.com/products/components/ring/>. [Accessed: 10-Feb-2019].
- [80] “MAS.865 2018 How to Make Something that Makes (almost) Anything.” [Online]. Available: <http://fab.cba.mit.edu/classes/MAS.865/motion/piezoelectric/index.html>. [Accessed: 12-Jan-2019].
- [81] <http://www.fujicera.co.jp>, “Bimorph bending plates.” [Online]. Available: <http://www.fujicera.co.jp/en/product/bimorph/>.
- [82] X. He, W. Xu, N. Lin, B. B. Uzoejinwa, and Z. Deng, “Dynamics modeling and vibration analysis of a piezoelectric diaphragm applied in valveless micropump,” *J. Sound Vib.*, vol. 405, pp. 133–143, Sep. 2017.
- [83] “File:Piezo bending principle.jpg - Wikimedia Commons.” [Online]. Available: [https://commons.wikimedia.org/wiki/File:Piezo\\_bending\\_principle.jpg](https://commons.wikimedia.org/wiki/File:Piezo_bending_principle.jpg). [Accessed: 10-Mar-2019].
- [84] A. W. Leissa, “Vibration of plates,” *Sci. Tech. Inf. Div. NASA*, p. 362, Jan. 1969.
- [85] T.-H. Nguyen and B.-T. Lee, “Fabrication and characterization of cross-linked gelatin electro-spun nano-fibers,” *J. Biomed. Sci. Eng.*, vol. 03, no. 12, pp. 1117–1124, 2010.
- [86] S. Li and S. Chen, “Analytical analysis of a circular PZT actuator for valveless micropumps,” *Sensors Actuators, A Phys.*, vol. 104, no. 2, pp. 151–161, 2003.
- [87] H. Li, Z. D. Deng, Y. Yuan, and T. J. Carlson, “Design parameters of a miniaturized piezoelectric underwater acoustic transmitter,” *Sensors (Switzerland)*, vol. 12, no. 7, pp. 9098–9109, 2012.
- [88] L. F. F. Brown, “The effects of material selection for backing and wear protection/quarter-wave matching of piezoelectric polymer ultrasound transducers,” *2000 IEEE Ultrason. Symp. Proceedings. An Int. Symp. (Cat. No.00CH37121)*, vol. 2, pp. 1029–1032, 2000.

- [89] A. A. Abas, D. M. P. Ismail, S. Sani, M. Noorul, and I. Ahmed, “Effect of Backing layer Composition on Ultrasonic Probe Bandwidth,” *Unpublished*. pp. 1–5, 2010.
- [90] D. A. Harris, *Noise Control Manual*. 1991.
- [91] A. Haug and F. Haug, *Angewandte elektrische Messtechnik : Grundlagen, Sensorik, Messwertverarbeitung*. Vieweg, 1993.
- [92] H.-J. Gevatter, *Handbuch der Meß- und Automatisierungstechnik*. Berlin, Heidelberg: Springer Berlin Heidelberg, 1999.
- [93] G. Clayton and S. Winder, “Operational Amplifiers,” *Oper. Amplifiers*, vol. 53, no. 9, pp. 11–62, 2003.
- [94] A. Waters, *Active Filter Design*. .
- [95] “RESOSEAL, Flachdichtungen, Technische Dichtungen.” [Online]. Available: <https://www.resogoo.com/de/index.php#>. [Accessed: 20-Feb-2019].
- [96] D. Doran and B. Cather, *Construction materials reference book*. Routledge.
- [97] A. W. Mix and A. J. Giacomini, “Standardized Polymer Durometry,” *J. Test. Eval.*, vol. 39, no. 4, 2011.
- [98] C. L. De Korte, E. I. Céspedes, A. F. W. Van Der Steen, B. Norder, and K. Te Nijenhuis, “Elastic and acoustic properties of vessel mimicking material for elasticity imaging,” *Ultrason. Imaging*, vol. 19, no. 2, pp. 112–126, 1997.
- [99] M. Earle, G. De Portu, and E. Devos, “Agar ultrasound phantoms for low-cost training without refrigeration,” *African J. Emerg. Med.*, vol. 6, no. 1, pp. 18–23, 2016.
- [100] A. I. Chen *et al.*, “Multilayered tissue mimicking skin and vessel phantoms with tunable mechanical, optical, and acoustic properties,” *Med. Phys.*, vol. 43, no. 6, pp. 3117–3131, 2016.
- [101] C. Li, G. Guan, R. Reif, Z. Huang, and R. K. Wang, “Determining elastic properties of skin by measuring surface waves from an impulse mechanical stimulus using phase-sensitive optical coherence tomography,” *J. R. Soc. Interface*, vol. 9, no. 70, pp. 831–841, 2012.
- [102] A. Hellerbach, V. Schuster, A. Jansen, and J. Sommer, “MRI Phantoms - Are There Alternatives to Agar?,” *PLoS One*, vol. 8, no. 8, 2013.
- [103] W. D. D’Souza, E. L. Madsen, O. Unal, K. K. Vigen, G. R. Frank, and B. R. Thomadsen, “Tissue

- mimicking materials for a multi-imaging modality prostate phantom,” *Med. Phys.*, vol. 28, no. 4, pp. 688–700, 2001.
- [104] V. T. Nayar, J. D. Weiland, C. S. Nelson, and A. M. Hodge, “Elastic and viscoelastic characterization of agar,” *J. Mech. Behav. Biomed. Mater.*, vol. 7, pp. 60–68, 2012.
- [105] X. Zhang, B. Qiang, and J. Greenleaf, “Comparison of the surface wave method and the indentation method for measuring the elasticity of gelatin phantoms of different concentrations,” *Ultrasonics*, vol. 51, no. 2, pp. 157–164, Feb. 2011.
- [106] L. Gao, K. J. Parker, S. K. Alam, and R. M. Lernel, “Sonoelasticity imaging: theory and experimental verification.,” *J. Acoust. Soc. Am.*, vol. 97, no. 6, pp. 3875–3886, 1995.
- [107] F. Kallel, C. D. Prihoda, and J. Ophir, “Contrast-transfer efficiency for continuously varying tissue moduli: simulation and phantom validation,” *Ultrasound Med. Biol.*, vol. 27, no. 8, pp. 1115–1125, 2001.
- [108] S. Tupin, J. Molimard, V. Cenizo, T. Hoc, B. Sohm, and H. Zahouani, “Multiscale Approach to Characterize Mechanical Properties of Tissue Engineered Skin,” *Ann. Biomed. Eng.*, vol. 44, no. 9, pp. 2851–2862, 2016.
- [109] D. Giavarina, “Understanding Bland Altman analysis,” *Biochem. Medica*, vol. 25, no. 2, pp. 141–151, 2015.
- [110] J. Hedderich and L. Sachs, *Angewandte Statistik*. Berlin, Heidelberg: Springer Berlin Heidelberg, 2018.
- [111] B. Gusarov, “PVDF piezoelectric polymers : characterization and application to thermal energy harvesting PVDF polymères piézoélectriques : caractérisation et application pour la récupération d ’ énergie thermique,” 2015.
- [112] “Akustische Bauteile - Summer, Schallwandler von N&H.” [Online]. Available: <https://www.nh-technology.de/akustik-bauteile/akustische-bauteile>. [Accessed: 12-Jan-2019].
- [113] “PIEZO 6,5 | GES-ELECTRONICS.” [Online]. Available: <https://www.ges.cz/de/piezo-6-5-GES07004447.html>. [Accessed: 12-Jan-2019].
- [114] “Piezoceramic Materials.” [Online]. Available: <https://www.piceramic.com/en/products/piezoceramic-materials/#c15065>. [Accessed: 11-Jan-2019].

- [115] W. D. Callister and D. G. Rethwisch, *Materialwissenschaften und Werkstofftechnik : eine Einführung*. Wiley-VCH, 2013.
- [116] “Deutsches Kupferinstitut: Werkstoff Datenblätter.” [Online]. Available: <https://www.kupferinstitut.de/de/beratung-und-service/downloads/downloads/werkstoffe/werkstoff-datenblaetter.html>. [Accessed: 11-Jan-2019].
- [117] “Engineering Materials.” [Online]. Available: [https://www.engineeringtoolbox.com/engineering-materials-properties-d\\_1225.html](https://www.engineeringtoolbox.com/engineering-materials-properties-d_1225.html). [Accessed: 13-Jan-2019].
- [118] K. Larson, “Can You Estimate Modulus From Durometer Hardness for Silicones?,” pp. 1–6, 2016.
- [119] V. Falanga and B. Bucalo, “Use of a durometer to assess skin hardness.,” *J. Am. Acad. Dermatol.*, vol. 29, no. 1, pp. 47–51, Jul. 1993.
- [120] “Shore Durometer Conversion Chart.” [Online]. Available: <http://polymerdatabase.com/polymer-physics/Shore-Table.html>. [Accessed: 26-Feb-2019].
- [121] K. a Ross, “Agar Gel By Indentation,” *J. Texture Stud.*, vol. 1, no. Finney 1969, pp. 17–27, 1999.
- [122] “Leiterplatten-Kalkulator Online.” [Online]. Available: <https://portal.multi-circuit-boards.eu/>. [Accessed: 13-Mar-2019].
- [123] “Mouser Electronics Österreich - Elektronikkomponenten-Vertriebspartner.” [Online]. Available: <https://www.mouser.at/>. [Accessed: 13-Mar-2019].
- [124] “Small Force Sensing Resistor | FlexiForce ESS301 Sensor | Tekscan.” [Online]. Available: <https://www.tekscan.com/products-solutions/force-sensors/ess301>. [Accessed: 09-Mar-2019].

## 7.2. Table of figures

- Fig. 4 R. P. J. B. Weller, J. A. A. Hunter, J. A. Savin, and M. V. Dahl, *Clinical Dermatology, fourth edition*. Oxford, UK, 2009, page 11
- Fig. 5 F. M. Hendriks, “Mechanical Behaviour of Human Skin in Vivo A Literature Review,” 2001, page 24
- Fig. 6 R. Marks and P. A. Payne, *Bioengineering and the Skin : Based on the Proceedings of the European Society for Dermatological Research Symposium, held at the Welsh National School of Medicine, Cardiff, 19-21 July 1979*. Springer Netherlands, 1982, page 138

- Fig. 7a R. Marks and P. A. Payne, *Bioengineering and the Skin : Based on the Proceedings of the European Society for Dermatological Research Symposium, held at the Welsh National School of Medicine, Cardiff, 19-21 July 1979*. Springer Netherlands, 1982, page 139
- Fig. 7b E. Berardesca, H. I. Maibach, and K.-P. Wilhelm, *Non invasive diagnostic techniques in clinical dermatology*. 2006, page 236
- Fig. 8 [https://en.wikipedia.org/wiki/Kelvin%E2%80%93Voigt\\_material](https://en.wikipedia.org/wiki/Kelvin%E2%80%93Voigt_material); [Accessed: 13-Mar-2019].
- Fig. 9 A. P. Sarvazyan, O. V Rudenko, S. D. Swanson, J. B. Fowlkes, and S. Y. Emelianov, “Shear Wave Elasticity Imaging : A new ultrasonic technology of medical diagnostic,” *Ultrasound Med. Biol.*, vol. 24, no. 9, pp. 1419–1435, 1998.
- Fig. 10 P. Humbert, F. Fanian, H. I. Maibach, and P. Agache, Eds., *Agache’s Measuring the Skin*. Cham: Springer International Publishing, 2017, page 965
- Fig. 11 Courage&Khazaka, “CutiScan CS 100 - Brochure.” [Online]. Available: [http://www.courage-khazaka.de/images/phocadownload/Brochures/Brochure\\_CS100.pdf](http://www.courage-khazaka.de/images/phocadownload/Brochures/Brochure_CS100.pdf). [Accessed: 25-Apr-2018].
- Fig. 12 P. Humbert, F. Fanian, H. I. Maibach, and P. Agache, Eds., *Agache’s Measuring the Skin*. Cham: Springer International Publishing, 2017, page 971
- Fig. 13 H. Zahouani, C. Pailler-Mattei, B. Sohm, R. Vargiolu, V. Cenizo, and R. Debret, *Characterization of the mechanical properties of a dermal equivalent compared with human skin in vivo by indentation and static friction tests*, *Ski. Res. Technol.*, vol. 15, no. 1, pp. 68–76, 2009, page 70
- Fig. 14 A. Vexler, I. Polyansky, and R. Gorodetsky, “Evaluation of skin viscoelasticity and anisotropy by measurement of speed of shear wave propagation with viscoelasticity skin analyzer,” *J. Invest. Dermatol.*, vol. 113, no. 5, pp. 732–739, 1999.
- Fig. 15 C. Rosado *et al.*, “About the in vivo quantitation of skin anisotropy,” *Ski. Res. Technol.*, vol. 23, no. 3, pp. 429–436, 2017.
- Fig. 16 S. Vijaya, *Piezoelectric Materials and Devices: Applications in Engineering and Medical Sciences*. CRC Press, 2013, page 11
- Fig. 17 J. Tichý, J. Erhart, E. Kittinger, and J. Přívratská, *Fundamentals of piezoelectric sensorics: Mechanical, dielectric, and thermodynamical properties of piezoelectric materials*. Berlin, Heidelberg: Springer Berlin Heidelberg, 2010, page 83

- Fig. 20 <https://www.piceramic.de/de/produkte/piezokeramische-baelemente/scheiben-staebe-und-zyylinder/> ; [Accessed: 25-Nov-2018].
- Fig. 21 <http://www.noliac.com/products/components/ring/>; [Accessed: 12-Jan-2019].
- Fig. 22 <http://fab.cba.mit.edu/classes/MAS.865/motion/piezoelectric/index.html>; [Accessed: 12-Jan-2019].
- Fig. 23a X. He, W. Xu, N. Lin, B. B. Uzoejinwa, and Z. Deng, “Dynamics modeling and vibration analysis of a piezoelectric diaphragm applied in valveless micropump,” *J. Sound Vib.*, vol. 405, pp. 133–143, Sep. 2017.
- Fig. 23b [https://commons.wikimedia.org/wiki/File:Piezo\\_bending\\_principle.jpg](https://commons.wikimedia.org/wiki/File:Piezo_bending_principle.jpg) ; [Accessed: 15-Jan-2019].
- Fig. 50 K. Larson, “Can You Estimate Modulus From Durometer Hardness for Silicones ?,” pp. 1–6, 2016.

## **8. Supplementary**

Project: **Skin elasticity measurement**  
Project Number: 1.G5.00181.0.0

Date: 04.12.2018  
Security: **confidential**

Author: Konrad Leskovar

Document-  
Version: 1.0

## Test certificate Isolation transformer

### content

1. Introduction .....	2
2. Test Setup.....	2
2.1. Equipment under test (EUT).....	2
2.2. Testing and measuring instruments .....	2
3. Measurement .....	2
3.1. Visual check.....	2
3.2. Safety measurements .....	3
3.2.1. Measurement of the ground connection impedance according to ÖVE/ÖNORM EN 60601-1	3
3.2.2. Measurement of the earth leakage according to ÖVE/ÖNORM EN 60601-1.....	3
3.2.3. Measurement of the enclosure leakage according to ÖVE/ÖNORM EN 60601-1 .....	4
4. Release .....	4



## 1. Introduction

The isolation transformer must undergo a safety check featuring the subsequent tests. The transformer must be switched on during the whole safety check.

## 2. Test Setup

### 2.1. Equipment under test (EUT)

Name	Serial number	Description
Insulated Power supply	56119213	Isolation transformer Type: IPs-1400R3-2S Nominal voltage.: 230V 50/60Hz Max. Power supply: 1450VA

Version 3.2:

### 2.2. Testing and measuring instruments

Name	Type	Manufacturer	Serial number	Calibration Expiry
RIGEL 288	288	RIGEL	002062-28A-0930	04/2019
	<b>Function</b>		<b>Application</b>	
	Handheld electrical medical safety analyzer		Electrical medical safety measurements	

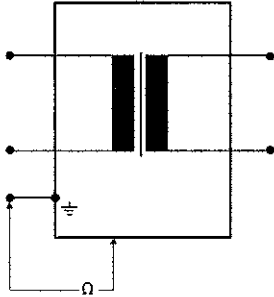
## 3. Measurement

### 3.1. Visual check

- Is the appliance and power line free from damage? ✓
- Are all labels on the appliances readable? ✓
- Are all fuses inserted according to the description labeled on the appliance? ✓
- Are all fuses functional? ✓

### 3.2. Safety measurements

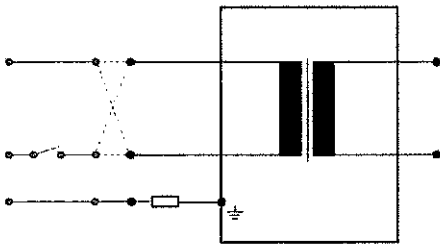
#### 3.2.1. Measurement of the ground connection impedance according to ÖVE/ÖNORM EN 60601-1



The isolation transformer is connected on the supply side to the "Equipment under Test" (EUT) socked on the measurement device and a test clip probe (connected to the earth bond probe socket (green)) is linked to an uncoated chassis part.

impedance [Ohm]	Measurement	Pass limit
	0,1265Ω	<0,2Ω (including power line)

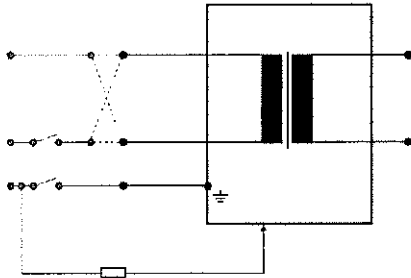
#### 3.2.2. Measurement of the earth leakage according to ÖVE/ÖNORM EN 60601-1



The isolation transformer is connected on the supply side to the "Equipment under Test" (EUT) socked on the measurement device.

condition	Measurement	Pass limit
L → ..... N → ..... PE → .....	16 μA	<500 μA
L → ..... N → ..... PE → .....	26 μA	<1000 μA
L → ..... N → ..... PE → .....	26 μA	<1000 μA
L → ..... N → ..... PE → .....	8 μA	<500 μA

### 3.2.3. Measurement of the enclosure leakage according to ÖVE/ÖNORM EN 60601-1



The isolation transformer is connected on the supply side to the "Equipment under Test" (EUT) socked on the measurement device and a test clip probe (connected to the earth bond probe socket (green)) is linked to an uncoated chassis part.

Fault condition	Measurement	Pass limit
L → → → → →	<i>&lt; 4 μA</i>	<100μA
N → → → → →		
PE → → → → →		
L → → → → →	<i>17 μA</i>	<500μA
N → → → → →		
PE → → → → →		
L → → → → →	<i>&lt; 4 μA</i>	<500μA
N → → → → →		
PE → → → → →		
L → → → → →	<i>&lt; 4 μA</i>	<500μA
N → → → → →		
PE → → → → →		
L → → → → →	<i>&lt; 4 μA</i>	<100μA
N → → → → →		
PE → → → → →		
L → → → → →	<i>8 μA</i>	<500μA
N → → → → →		
PE → → → → →		

## 4. Release

Created by:  
Konrad Leskovar

Measured by:

*09.12.2018 Leskovar Konrad*

Project: **Skin elasticity measurement**  
Project Number: 1.G5.00181.0.0

Date: 04.12.2018  
Security: **confidential**

Autor: Konrad Leskovar

Document- 1.0  
Version:

## Test certificate according to ÖVE/ÖNORM EN 60601-1 /62363

### Content

1. Introduction .....	2
2. Test Setup.....	2
2.1. Equipment under test (EUT).....	2
2.2. Testing and measuring instruments .....	2
3. Measurement .....	2
3.1. Visuelle check.....	2
3.2. Safety measurements .....	3
3.2.1. Measurement of the ground connection impedance according to ÖVE/ÖNORM EN 60601-1	3
3.2.2. Measurement of the insulation impedance according to ÖVE/ÖNORM EN 62353 .....	3
3.2.3. Measurement of the equipment leakage (direct) according to ÖVE/ÖNORM EN 62353 .....	4
3.2.4. Measurement of the patient leakage (direct) according to ÖVE/ÖNORM EN 62353 .....	5
3.2.5. Measurement of the earth leakage according to ÖVE/ÖNORM EN 60601-1.....	5
3.2.6. Measurement of the enclosure leakage according to ÖVE/ÖNORM EN 60601-1 .....	5
3.2.7. Measurement of the patient leakage (direct) according to ÖVE/ÖNORM EN 60601-1.....	6
3.2.8. Measurement of the patient leakage F-Type according to ÖVE/ÖNORM EN 60601-1.....	7
3.2.9. Measurement of the patient auxiliary current according to ÖVE/ÖNORM EN 60601-1.....	7
4. Release .....	7

## 1. Introduction

Check of a test setup for skin elasticity measurement under usage of an isolation transformer (ÖVE/ÖNORM EN 60601-1). The test setup is utilized for measurement of test persons. The transformer must be switched on during the whole safety check.

## 2. Test Setup

### 2.1. Equipment under test (EUT)

Name	Serial number	Description
Test setup for measurement of skin elasticity		Test setup using an oscilloscope, power supply and a waveform generator connected to an insulated power supply

Version: 0.1

### 2.2. Testing and measuring instruments

Name	Type	Manufacturer	Serial number	Calibration Expiry
RIGEL 288	288	RIGEL	002062-28A-0930	04/2019
	<b>Function</b>	<b>Application</b>		
	Handheld electrical medical safety analyzer	Electrical medical safety measurements		

## 3. Measurement

As a fact that the test setup does not represent an independent appliance within a separate chassis the power line to the supply side of the isolation transformer acts as supply cable for the electrical safety measurement. Therefore, the whole setup represents a Class 1 equipment featuring applied parts type BF (body floating), because the applied parts are not connected to the earth lead of the insulation transformer.

### 3.1. Visually check

- Are the appliances and power lines free from damage? ✓
- Are all labels on the appliances readable? ✓
- Are all fuses inserted according to the description labeled on the appliance? ✓
- Are all fuses functional? ✓

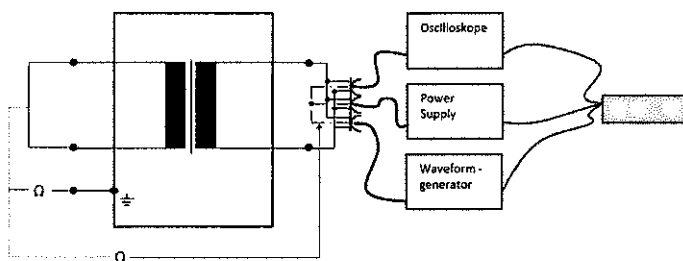
### 3.2. Safety measurements

#### 3.2.1. Measurement of the ground connection impedance according to ÖVE/ÖNORM EN 60601-1

Already measured, see test certificate isolation transformer.

#### 3.2.2. Measurement of the insulation impedance according to ÖVE/ÖNORM EN 62353

##### 3.2.2.1. Insulation resistance EUT



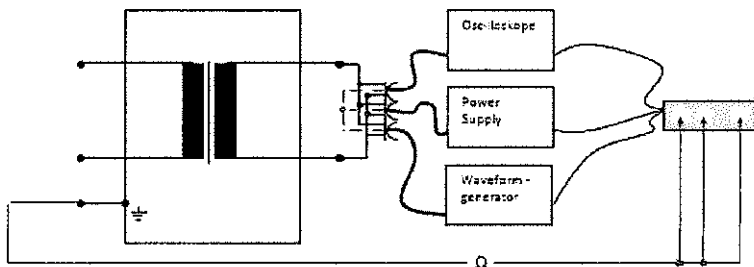
The isolation transformer is connected on the supply side to the "Equipment under Test" (EUT) socked on the measurement device and the first measurement is done directly onto the earth lead in the power supply cable, respectively the second test was to a test clip probe (connected to the earth bond probe socket (green)) is linked to the ground connection of a socked on

the secondary side of the isolation transformer.

Applied Voltage: *564 V*

	Measurement	Pass limit
Direct measurement	<i>&gt; 100 MΩ</i>	>2MΩ
Including test clip probe onto the ground connection of a socket on the secondary side of the insulation transformer	<i>&gt; 100 MΩ</i>	>2MΩ

##### 3.2.2.2. Insulation resistance applied parts

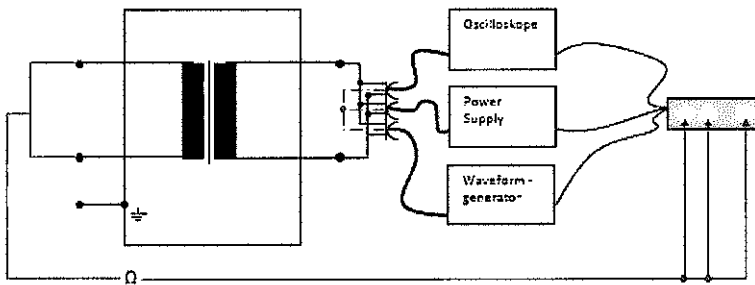


The isolation transformer is connected on the supply side to the "Equipment under Test" (EUT) socked on the measurement device. Measurement was done using the probe (connected to the applied part connector of the measurement device) linked to all three piezo-bending elements at the same time.

Applied Voltage: *564 V*

	Measurement	Pass limit
impedance	<i>&gt; 100 MΩ</i>	>2MΩ

3.2.2.3. Insulation resistance applied parts to power supply

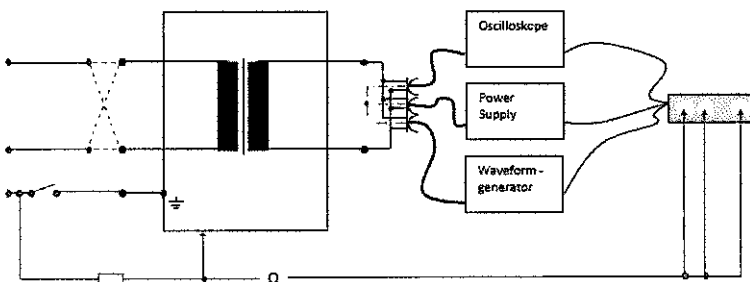


The isolation transformer is connected on the supply side to the "Equipment under Test" (EUT) socked on the measurement device. Measurement was done using the probe (connected to the applied part connector of the measurement device) linked to all three piezo-bending elements at the same time.

Applied Voltage: 564V

Measurement	Pass limit
impedance $> 100 \text{ M}\Omega$	$> 2 \text{ M}\Omega$

3.2.3. Measurement of the equipment leakage (direct) according to ÖVE/ÖNORM EN 62353

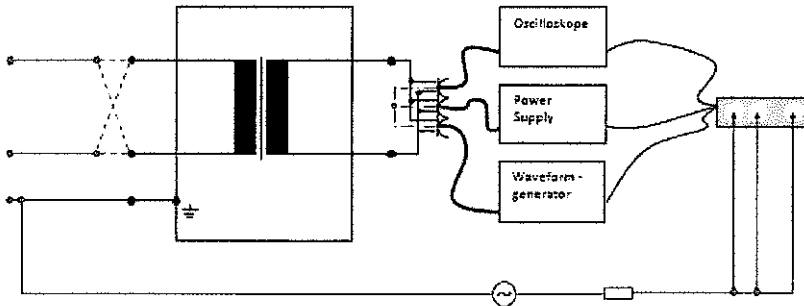


The isolation transformer is connected on the supply side to the "Equipment under Test" (EUT) socked on the measurement device. Measurement was done using the probe (connected to the applied part connector of the measurement device) linked to all three piezo-bending elements at the same time. Additionally, the test clip probe (connected to the earth bond probe socket (green)) is linked to a conducting part on the housing of the transformer.

earth bond probe socket (green)) is linked to a conducting part on the housing of the transformer.

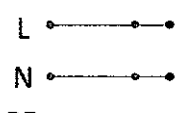
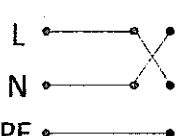
Fault condition	Measurement	Pass limit
L ————		$< 500 \mu\text{A}$
N ————	$11 \mu\text{A}$	
PE ————		
L ————		$< 500 \mu\text{A}$
N ————	$90 \mu\text{A}$	
PE ————		

### 3.2.4. Measurement of the patient leakage (direct) according to ÖVE/ÖNORM EN 62353



The isolation transformer is connected on the supply side to the "Equipment under Test" (EUT) socked on the measurement device. Measurement was done using the probe (connected to the applied part connector of the measurement device) linked to all three piezo-bending elements

at the same time.

Fault condition	Measurement	Pass limit
	123 $\mu A$	<5000 $\mu A$
	198 $\mu A$	<5000 $\mu A$

### 3.2.5. Measurement of the earth leakage according to ÖVE/ÖNORM EN 60601-1

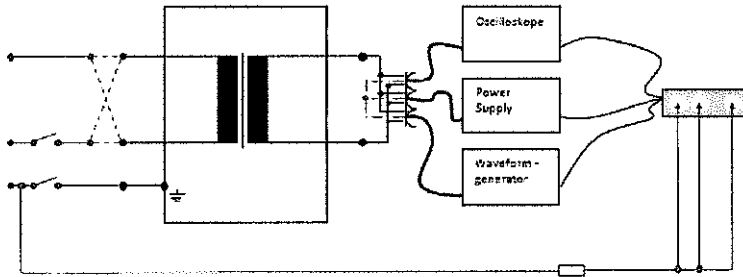
Already measured, see test certificate isolation transformer.

### 3.2.6. Measurement of the enclosure leakage according to ÖVE/ÖNORM EN 60601-1

Already measured, see test certificate isolation transformer.



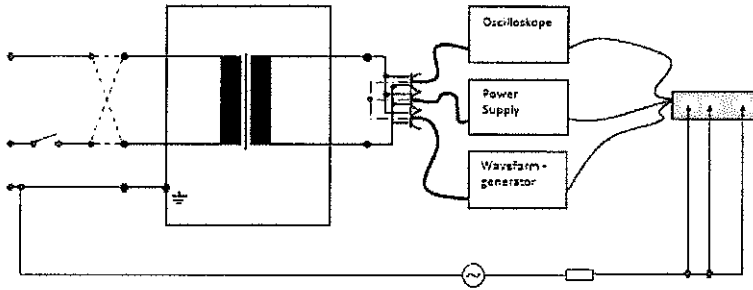
### 3.2.7. Measurement of the patient leakage (direct) according to ÖVE/ÖNORM EN 60601-1



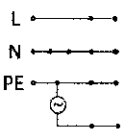
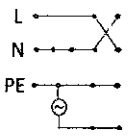
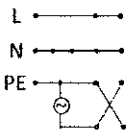
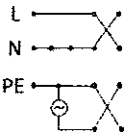
The isolation transformer is connected on the supply side to the "Equipment under Test" (EUT) socked on the measurement device. Measurement was done using the probe (connected to the applied part connector of the measurement device) linked to all three piezo-bending elements at the same time.

Fault condition	Measurement	Pass limit
L → DC	< 4 $\mu$ A	< 10 $\mu$ A
N → AC	< 4 $\mu$ A	< 100 $\mu$ A
L → DC	4 $\mu$ A	< 50 $\mu$ A
N → AC	< 4 $\mu$ A	< 500 $\mu$ A
L → DC	< 4 $\mu$ A	< 50 $\mu$ A
N → AC	84 $\mu$ A	< 500 $\mu$ A
L → DC	< 4 $\mu$ A	< 50 $\mu$ A
N → AC	84 $\mu$ A	< 500 $\mu$ A
L → DC	< 4 $\mu$ A	< 10 $\mu$ A
N → AC	39 $\mu$ A	< 100 $\mu$ A
L → DC	< 4 $\mu$ A	< 50 $\mu$ A
N → AC	34 $\mu$ A	< 500 $\mu$ A

### 3.2.8. Measurement of the patient leakage F-Type according to ÖVE/ÖNORM EN 60601-1



The isolation transformer is connected on the supply side to the "Equipment under Test" (EUT) socked on the measurement device. Measurement was done using the probe (connected to the applied part connector of the measurement device) linked to all three piezo-bending elements at the same time.

Fault condition	Measurement	Pass limit
	126 $\mu$ A	<5000 $\mu$ A
	202 $\mu$ A	<5000 $\mu$ A
	92 $\mu$ A	<5000 $\mu$ A
	<25 $\mu$ A	<5000 $\mu$ A

### 3.2.9. Measurement of the patient auxiliary current according to ÖVE/ÖNORM EN 60601-1

Measurement of the leakage current between the applied parts under normal or fault condition is useless, as a fact, that the piezo bending elements are connected to each other using the insulated ground potential.

## 4. Release

Created by:  
Konrad Leskovar

Measured by:

09.11.2018 *Konrad Leskovar*